Lehrstuhl für Steuerungs- und Regelungstechnik
Technische Universität München

Safe and Adaptive Control Approaches for Mobility Assistance Robots

Milad Geravand

Vollständiger Abdruck der von der Fakultät für Elektrotechnik und Informationstechnik der Technischen Universität München zur Erlangung des akademischen Grades eines

Doktor-Ingenieurs (Dr.-Ing.)

genehmigten Dissertation.

Vorsitzender: Prof. Gordon Cheng, PhD.

Prüfer der Dissertation:

1. Prof. Dr. Angelika Peer
2. Prof. Dongheui Lee, Ph.D.

Die Dissertation wurde am 29.06.2016 bei der Technischen Universität München eingereicht und durch die Fakultät für Elektrotechnik und Informationstechnik am 14.11.2016 angenommen.

Foreword

This dissertation summarizes my work as a research associate at the Institute of Automatic Control Engineering (LSR), Technische Universität München. This work was financially supported by the MOBOT project within the 7^{th} Framework Programme of the European Union and the Institute for Advanced Study (IAS), Technische Universität München. I gratefully acknowledge this generous support.

Firstly, I would like to express my sincere gratitude to my advisor Professor Angelika Peer for her continuous support, the numerous fruitful discussions and her high research and ethical standards. She always made plenty of time to talk about the research, was open to possibilities, and dedicated to working through the uncertainties and difficulties in pursuit of solutions to problems that are both challenging and practical. Her guidance helped me throughout the research and writing of this thesis.

In addition to my advisor, I would like to thank my thesis mentor Professor Gordon Cheng, for his insightful comments and encouragement. Moreover, my sincere thanks also goes to Dr. Marion Leibold for her useful comments on the theories developed in the third chapter of this thesis, Professor Alessandro De Luca for the fruitful collaboration on the idea proposed in the sixth chapter, and Professor Martin Buss, who provided me the opportunity to join LSR as doctoral candidate, and who gave access to the laboratory and research facilities. Without their precious support, it would not have been possible to conduct this research.

Many heartfelt thanks go to my great friend, and colleague, Christian Landsiedel who always offered me assistance, whether with research or my daily life in Munich. Special thanks go to friends and colleagues, Daniel Carton, Andreas Lawitzky, Mohammad Abu-Alqumsan for their friendship and persistent support; Ken Friedl, for all of his positive energy, as well as support on editing video and photos; Laith ALkurdi, Philine Donner, Stefan Friedrich, Stefan Kersting, Alexander Pekarovskiy, Muhammad Sheraz Khan, Annemarie Turnwald and Sotiris Apostolopoulos for all of their friendship, support, useful comments and productive discussions. To Professor Klaus Hauer, Dr Costas Tzafestas, Professor Petros Maragos, Professor Katja Mombaur, Dr.-Ing. Bartlomiej Stanczyk and all of MOBOT partners for inspiring discussions and collaboration. To my students, Tobias Blume, Wolfgang Rampeltshammeri, Andreas Lederhuber, Navid Zeinali, Erfan Shahriari, in particular, Peter Zeno Korondi, for sharing my research interests and continually assisting me. Finally, special thanks go to all of my other colleagues and LSR team-mate for giving me insights, support, and friendship throughout these years. I am also very grateful to the great administrative support I received at LSR, especially from Mrs. Schmid, who treated me with professionalism and helped in every matter I had.

I am also grateful to the following staff at Fraunhofer IPA, Martin Hägele, Thomas Dietz, Alexander Kuss, Julian Diaz Possada, Ulrich Schneider, for their various forms of support during my last year of doctoral research, the excellent and enjoyable working atmosphere

they created and the trust they had in me. Moreover, I would like to thank Mrs. Luzia Schuhmacher and Dr. Werner Kraus, for their support on proofreading this thesis.

Last but not least, I would like to thank my parents, sisters and brother for supporting me spiritually throughout the writing of this thesis and my life in general. I am forever grateful to my dear wife, Nastaran. She was always there cheering me up and stood by me through the good and bad times. It is because of her that I have been able to successfully complete this endeavor.

Munich, June 2016 Milad Geravand

Abstract

Due to a consistent increase in the size of the elderly population and the existence of a large number of people living with disabilities, the demand for healthcare specialists or assistance devices has become critical. Robotic assistance systems can help with supporting the mobility functionality of disabled persons. These devices could provide physical, sensory, and cognitive support as required for those who have lost a portion of their capabilities. One major challenge for the above-mentioned assistive devices is their control design. It requires a high level of safety since the robot is in direct interaction with the user, and also user and environment-adaptive shared control.

This thesis introduces context-aware, user and environment-adaptive as well as safe control approaches for mobility assistance robots (MARs) that support the elderly and patients in three main operational modes of the sit-to-stand (STS) transfers from chair, walking and human fall prevention assistance. Under the assumption that the human optimizes his/her activities, this thesis focuses on understanding the human motor control models and decision-making formalisms, then formulates their mathematical principles and finally employs them into novel and human-inspired control design of MARs.

In particular for the STS assistance, this thesis formulates human unassisted and assisted STS transfers as optimal feedback control problems. These are then employed to derive assistive strategies to be provided by a MAR to its user. This approach was used to determine user-specific optimal assistive trajectories for the elderly, who were mostly not able (or hardly able) to perform unassisted STS transfers, and to implement the trajectories on a MAR. This resulted in promising achievements in terms of the user's satisfaction and success rate.

Moreover, this thesis focuses on the design of a user and environment adaptive shared control between human and robot during the user's walking. For this, an integrated control architecture to adapt the parameters of the shared control system of a MAR is presented. The control parameters are adapted based on a human decision-making mechanism aiming for human-inspired and therefore natural robot behaviors. The proposed architecture allows us to adapt the robot cognitive assistance helping the user to follow a desired path, the robot sensorial assistance to avoid collisions with obstacles, and the user-specific robot overall assistance based on user's performance and physiological state. The effectiveness of the proposed architecture is illustrated by means of experiments and an intensive user-study.

This thesis also investigates approaches to enhance user safety. To this respect, an approach for human fall prevention is introduced for a MAR equipped with a pair of actuated arms. This is proposed by an evaluation of the user's balance criteria and the formulation of an optimal control problem in order to determine the required supportive forces to be applied to the user for fall prevention as soon as a risk of fall is predicted.

Finally, the safety aspect is further emphasized by introducing a general approach for limiting of the energy and power applied to the user during the physical human-robot interaction. To this end, a safety supervisory and control system is introduced to observe the energy flowing between all components, in particular energy exchanging over the interaction ports with the human and this shapes the robot behavior, whenever a harmful energy flow or human fatigue is observed.

Contents

1 Introduction **1**
- 1.1 Challenges . . . 1
- 1.2 Main Contributions and Outline of the Thesis . . . 4

2 Review of Mobility Assistance Robots and their Functionalities **7**
- 2.1 Mobility Assistance Platforms . . . 7
  - 2.1.1 Actuation . . . 9
  - 2.1.2 Kinematics . . . 9
  - 2.1.3 Sensors . . . 10
  - 2.1.4 Human-Machine Interfaces . . . 10
- 2.2 Functionalities . . . 11
  - 2.2.1 STS Assistance . . . 11
  - 2.2.2 Walking Assistance . . . 15
  - 2.2.3 Cognitive Assistance . . . 20
  - 2.2.4 Health Monitoring . . . 23
  - 2.2.5 Extra Functionalities . . . 24
- 2.3 Summary and Discussion . . . 24

3 Biologically Inspired Sit-to-Stand Assistance **26**
- 3.1 STS Transfers formulated as Optimization Problem . . . 28
  - 3.1.1 Human-Biomechanical Model . . . 28
  - 3.1.2 Balance and Task End-Point Accuracy Criteria . . . 29
  - 3.1.3 Formulation of Optimization Problem . . . 30
  - 3.1.4 Optimal Feedback Control . . . 31
  - 3.1.5 Inverse Optimal Control to Determine Cost Function Weighting Factors 31
  - 3.1.6 User-group Optimized STS Assistance . . . 32
- 3.2 Validation of STS Model . . . 33
  - 3.2.1 Data Capturing . . . 33
  - 3.2.2 Validation Method . . . 36
  - 3.2.3 Weighting Factors . . . 36
  - 3.2.4 Validation Results . . . 39
- 3.3 Robot-Assisted STS Transfers . . . 40
  - 3.3.1 Optimization Results considering External Assistance . . . 41
  - 3.3.2 User Study . . . 43
- 3.4 Summary and Discussion . . . 47

4 User and Environment-Adaptive Walking Assistance **49**
- 4.1 Related Work . . . 50
  - 4.1.1 Adaptive Shared Control for MARs . . . 50

4.1.2 Human Decision-Making Models . . . 51
4.2 MAR Low-Level Control . . . 52
4.2.1 System Description . . . 52
4.2.2 Admittance Control . . . 52
4.3 Shared Control Architecture . . . 53
4.4 Decision-Making for MARs . . . 55
4.4.1 Decision-Making Principle based on DD Model . . . 55
4.4.2 Decision on Cognitive Assistance . . . 56
4.4.3 Decision on Sensorial Assistance . . . 59
4.4.4 Decision on Physical Assistance . . . 62
4.5 Experimental Results . . . 65
4.5.1 Technical Validation . . . 65
4.5.2 User Study . . . 70
4.6 Summary and Discussion . . . 74

5 Human Fall Prevention Assistance 76
5.1 System Description . . . 77
5.1.1 Robot Model . . . 77
5.1.2 Human Model . . . 77
5.2 Fall Prevention Control . . . 79
5.2.1 Derivation of Assistive Forces . . . 79
5.2.2 Robot Control . . . 81
5.3 Results . . . 82
5.3.1 Simulation . . . 82
5.3.2 Experiments . . . 84
5.4 Summary and Discussion . . . 86

6 Energy-Based Supervisory Control for Safety Enhancement 87
6.1 Background . . . 88
6.1.1 Port-based Modeling Framework . . . 88
6.1.2 PH Formulation . . . 89
6.1.3 Twists and Wrenches . . . 89
6.2 PH Modeling of HRC . . . 89
6.2.1 PH Modeling of the Robot . . . 90
6.2.2 PH Modeling of the Object . . . 91
6.2.3 PH Modeling of the Human . . . 92
6.2.4 Physical Contacts . . . 93
6.2.5 Overall PH Modeling . . . 93
6.3 Safety-Enhancing Energy Shaping Control . . . 95
6.3.1 Safety Metrics for HRC . . . 95
6.3.2 Control Design . . . 96
6.4 Results . . . 100
6.4.1 Simulation of the HRC Model . . . 100
6.4.2 Validation of the Safety-Enhancing Control Approach . . . 102
6.5 Summary and Discussion . . . 105

7 Conclusion and Future Work **106**
7.1 Summary and Concluding Remarks 106
7.2 Perspectives 108

A Anthropomorphic Data of Participants in STS Model Evaluations **110**

B Optimal Feedback Control **111**

Bibliography **113**
Supervised Students' Theses 131
Author's Publications 132

Notations

Abbreviations

BOS	Base of support
COG	Center of gravity
COM	Center of mass
COP	Center of pressure
DD	Drift-diffusion
DDP	Differential dynamic programming
DoF	Degree of freedom
HMI	Human-machine interface
HRC	Human-robot collaboration
HRI	Human-robot interaction
ILQG	Iterative linear-quadratic Gaussian
IMU	Inertia measurement system
IOC	Inverse optimal control
LIP	Linear inverted pendulum
MAR	Mobility assistance robot
MDP	Markov decision process
MMSE	Mini-mental state examination
OFC	Optimal feedback control
PH	Port-Hamiltonian
pHRC	Physical human-robot collaboration
pHRI	Physical human-robot interaction
ROS	Robot operating system
SQP	Sequential quadratic programming
STS	Sit-to-stand
TAFC	Two-alternative forced-choice
XCOM	Extrapolated center of mass
ZMP	Zero moment point

Conventions

Scalars, Vectors, and Matrices

Scalars are denoted by upper and lower case letters in italic type. *Vectors* are denoted by underlined lower case letters in boldface type, as the vector $\boldsymbol{x}$ is composed of elements x_i. *Matrices* are denoted by upper case letters in boldface type, as the matrix $\boldsymbol{M}$ is composed

of elements M_{ij} (i^{th} row, j^{th} column).

a or A	Scalar
$\boldsymbol{a}$	Vector
$\boldsymbol{A}$	Matrix

Subscripts and superscripts

$\boldsymbol{A}^T$	Transposed of $\boldsymbol{A}$
$\boldsymbol{A}^{-1}$	Inverse of $\boldsymbol{A}$
$\boldsymbol{A}^+$	Pseudoinverse of $\boldsymbol{A}$
$\nabla \boldsymbol{A}$	Gradient of $\boldsymbol{A}$
$f(\cdot)$	Scalar function
$\dot{a}$, $\ddot{a}$	First and second derivative of variable a
a^*	Optimal or desired value of variable a
a_0	Initial value of variable a
a_{max}	Maximum value of variable a
a_{min}	Minimum value of variable a
$\boldsymbol{a}_\perp$	Vector $\boldsymbol{a}$ perpendicular to a path
$\boldsymbol{a}_\parallel$	Vector $\boldsymbol{a}$ tangential to a path

Symbols and functions

General

b, $\boldsymbol{B}$	Scalar damping and damping matrix
$diag(.)$	Diagonal matrix
$\boldsymbol{f}$, $\boldsymbol{F}$	Force vector or matrix
$\boldsymbol{g}$	Gravitation vector
k, $\boldsymbol{K}$	Scalar stiffness and stiffness matrix
K_i	User defined gains
m, $\boldsymbol{M}$	Scalar mass and mass matrix
T	Time interval or sample time
t	Time
$\boldsymbol{\tau}$	Torque vector
$\boldsymbol{x}$	State vector

Sit-to-stand assistance

$\boldsymbol{C}(\boldsymbol{\theta}, \dot{\boldsymbol{\theta}})$	Vector of Coriolis and centripetal forces
$\boldsymbol{c}_i$	Position vector for center of gravity of segment
$e_{\tau a}, e_{\tau k}, e_{\tau h}$	Variables for ankle, knee and hip joint torques
e_{com_x}, e_{com_y}	Variables corresponding to error on the x and y components of the COM position
F_x, F_y	Variables for vertical and horizontal components of external force
$\boldsymbol{F}$	External generalized force vector

$\boldsymbol{G}(\boldsymbol{\theta})$	Gravitational force vector applied to the human model
$\boldsymbol{J}_k(\boldsymbol{\theta})$	Jacobian matrix
l_i	Variable for the length of center of gravity of each segment
M_z	External angular momentum
$\boldsymbol{M}(\boldsymbol{\theta})$	Positive definite symmetric inertia matrix
$\boldsymbol{m}_i$	Mass vector of the i^{th} segment
$\boldsymbol{p}_{zmp}^{min}$, $\boldsymbol{p}_{zmp}^{max}$	Vectors for boundaries of BOS
$\boldsymbol{p}_{com}^{tar}$	Desired vector of the human COM position
$\boldsymbol{p}_{com}^{tar}$	Position vector of COM for the whole system
$\hat{\boldsymbol{p}}_i$	Position vector of center of gravity of segment i
$\boldsymbol{\tau}$	Joint torques
$\boldsymbol{\tau}_{ext}$	Torque vector due to external force
$\boldsymbol{\tau}_{min}, \boldsymbol{\tau}_{max}$	Vector of human's joint torque constraints
$\boldsymbol{\theta}_{min}, \boldsymbol{\theta}_{max}$	Vector of human joint angle boundaries
$\boldsymbol{T}$	Vector of horizontal components of contact force $\boldsymbol{F}$
v_{exp}, v_{sim}	Variables corresponding to data in experiments and simulation
w_{2a}, w_{2k}, w_{2h}	Variables for ankle, knee and hip in $\boldsymbol{W}_2$ matrix
w_{3a}, w_{3k}, w_{3h}	Factors for ankle, knee and hip in $\boldsymbol{W}_3$ matrix
w_{4a}, w_{4k}, w_{4h}	Factors for ankle, knee and hip in $\boldsymbol{W}_4$ matrix
$\boldsymbol{W}_1$	Weighting matrix for the human balance term
$\boldsymbol{W}_2$	Weighting matrix for the minimum jerk
$\boldsymbol{W}_3$	Weighting matrix for the minimum torque change
$\boldsymbol{W}_4$	Weighting matrix for the human effort
$\boldsymbol{W}_5$	Weighting matrix for the human joint angel and velocity
$\boldsymbol{W}_6$	Weighting matrix for interaction forces
$\boldsymbol{W}_{f1}$, $\boldsymbol{W}_{f2}$	Weighting matrices for the terminal costs
$v_{exp,max}$, $v_{exp,min}$	Variables corresponding to maximum and minimum value of experiments
$\theta_1, \theta_2, \theta_3, \theta_4, \theta_5$	Ankle, knee, hip, shoulder and elbow joint variables
$\boldsymbol{\theta}$	Joint angle vector
$\dot{\boldsymbol{\theta}}_{min}, \dot{\boldsymbol{\theta}}_{max}$	Vector of human joint velocity boundaries

Walking assistance

$d_{\theta,min}$, $d_{\theta,max}$	Variables for minimum and maximum values of the damping factor
D_{handle}, K_{handle}	Damping and stiffness variables for control of handle's position
$\boldsymbol{D}_d$	Desired damping matrix
$\boldsymbol{d}_{obs,max}$	Shortest distance in which the potential field becomes active
$\boldsymbol{d}_{obs}$	Distance vector from nearest obstacle to the robot
$f_{\parallel}$	Human force variable along the reference path
$f_{\perp}$	Human force variable perpendicular to the reference path
$\boldsymbol{F}(\boldsymbol{q})$	Artificial force vector
$\boldsymbol{f_b}$	Brake force vector
$\boldsymbol{f}_{applied}$	Interaction force vector between human and robot
$\boldsymbol{f}_{int}$	Internal force vector
$\boldsymbol{f}_{obs}, \boldsymbol{\tau}_{obs}$	Virtual forces and moments vectors due to obstacle

$\boldsymbol{f}_{support}$	Desired support force vector
k	Positive constant gain
$k_{C,e}$, k_{C,θ_e}	User-defined variables
K_h, K_r	Force gain variables
$\boldsymbol{K}$	Stiffness matrix
$\boldsymbol{M}_d$	Desired mass matrix
$\boldsymbol{M}_{env}$, $\boldsymbol{D}_{env}$	Mass and damping matrices for environment situation
$\mathbb{P}_A(t+1)$	Variable for probability of the human preference for choice A at time $t+1$
$p_{T,C}$	Variable for normalized task performance
$r_z(t)$	Variable for obtained reward for choice z
$\boldsymbol{T}_h$	Transformation matrix
$\boldsymbol{T}_h$, $\boldsymbol{T}_b$	Geometrical transformation matrices
$\boldsymbol{U}(\boldsymbol{q})$	Vector of artificial potential field
$w_A(t)$, $w_B(t)$	Variable for accumulated evidences for choosing option A or B
λ	Variable for forgetting factor
μ	Variable related to slope of the sigmoid function
θ_e	Variable for orientation error between the reference path and the global x-axis
θ_{ref}	Desired orientation variable

Fall prevention assistance

$\boldsymbol{D}_{d,arm,i}$	Desired damping matrix for either left or right arms
$\boldsymbol{F}_{tot}$, $\boldsymbol{T}_{tot}$	Vectors of total interaction forces and moments
$\boldsymbol{h}_i$	Distance vector between the robot handles and the center of robot handles
$\boldsymbol{M}_{d,arm,i}$	Desired inertia matrix for either left or right arms
$x_{COM}, y_{COM}, z_{COM}$	Variables of COM position vector
v, ω	Variables for control inputs for linear and angular velocities

Supervision-based safety control

$\bar{\boldsymbol{D}}_t$	Damping coefficient for the contact point t
$\boldsymbol{D}_r$	Robot's dissipation matrix
$\boldsymbol{D}_i$	Dissipation matrix for the robot(s) or human
$\boldsymbol{e}_{R,r}$	Robot's effort vector
$\boldsymbol{f}_{R,r}$	Dissipative robot's joint torques
(f_I, e_I)	Interaction port variables
(f_R, e_R)	Resistive port variables for energy dissipation
(f_S, e_S)	Energy storage port variables
(f_C, e_C)	Control port variables
$\mathcal{F}$	Variables for linear space of flows
$\mathcal{F}^*$	Variables for dual linear space of efforts
f, e	Variables for power-conjugate port variables: *flow* and *effort*
$\boldsymbol{I}_{n_r}$	Identity matrix of order n_r
$\boldsymbol{I}_o$	Inertia matrix of object
$\boldsymbol{G}$	Mapping matrix
H	Hamiltonian function

H_{tot}	Total energy of the system
H_{max}	Maximum limit of the total energy of the system
H_T	Hamiltonian of the energy tank
$\boldsymbol{J}_r$	Jacobian matrix of robot r
M_o	Total mass of object
$\boldsymbol{M}_r$	Inertia matrix of robot r
m	Total number of collaborative robots
n_r	Number of DoFs of robot r
$P_{c,r}$	Power injected by the controller of robot r
P_h	Power passing through the HRI port
P_{max}	Maximum power passing through the HRI port
$\boldsymbol{R}$	Symmetric dissipation matrix
$\boldsymbol{R}_l^0$	Rotation matrix
r	Robot r
s_T	State variable of energy tank
$U_r(\boldsymbol{q}_r)$	Robot gravitational energy
$\boldsymbol{u}$, $\boldsymbol{y}$	Input and output variables
$W_{h,max}$	Total performed work
$\boldsymbol{x}_{des,r}$	Desired robot configuration
z_t	Binary variables for interconnection of subsystems to manipulate
z	Modulating factor
Ψ_i Ψ_j	Reference frames

1 Introduction

Due to demographic changes in the world, the number of elderly persons will dramatically increase. In 2015, twelve percent of the global population (900 million) was aged 60 or over, and this is growing at a rate of 3.26 per cent per year. This group will represent nearly a quarter of the world's population by 2050 [1]. As chronic age-associated diseases such as dementia and adverse clinical events such as falls with high impact on motor performance increase exponentially with age, mobility associated disability will also increase exponentially. In addition to basic activities relating to individual hygiene and basic needs such as eating, key motor features such as walking and transfer situations are affected.

Mobility is known to be a crucial ability as ambulation and transfers are required for many activities of daily living. Mobility disabilities endanger independence and have negative consequences on quality of life and self-esteem. Physical activity was found to have a positive effect, especially if performed long-term [2, 3], while low physical activity and motor performance is known to be a risk factor for age-associated health decline with clinical consequences such as risk of falling [4, 5].

The rising demand for mobility assistance is endangered by an increasing lack of qualified care workers, decrease in social support systems (family members) and the immense costs for care. Thus, part of the requests have to be covered by assistance technologies. The development of mobility assistance robots (MARs) became of great interest in the last two decades. A series of devices have been developed by various groups, see [6] for an overview. These devices can provide physical, sensory, and cognitive support as required for those who have lost a portion of their capabilities.

How to safely and efficiently control such devices to satisfy the user's need is a challenge that is the main focus of this thesis.

1.1 Challenges

The presented work focuses on supporting human mobility and thus enforcing fitness and vitality by developing proper assistive approaches for intelligent MARs designed to provide user-centred and natural support for ambulating in indoor environments. This thesis envisions the design of cognitive and biologically-inspired approaches that can interpret specific forms of human activity or decision making in order to deduce what the human needs are, in terms of mobility and to provide user and context-adaptive assistance to elderly users, and generally to individuals with specific forms of moderate to mild walking impairment. A big challenge raised in this respect, and therefore focused in this thesis, is on safe, intuitive, and user and environment-adaptive control designs of MARs as detailed as follows:

Intuitiveness: The human-robot shared controller should be designed in order to result in intuitive and natural support to the human user. From our point of view,

"intuitive and natural" means that the robot behavior is compatible with the support provided by another person (e.g. a nurse). Such design of the robot shared control is a challenging task, since an assistance robot under full user's authority can have difficulties guaranteeing acceptable performance and safety due to cognitive, sensorial and physical weaknesses down to target users being either elderly or disabled persons. On the other hand, a fully autonomous system that ignores the user's intention can result in an overall non intuitive behavior and therefore user's dissatisfaction and even dangerous situations in case of human and robot disagreement. Therefore, a shared control approach which takes the user's intention into account, but at the same time exploits all benefits of robotic systems should be considered for assistance robots. However, how to adapt the behavior of the shared control system based on environment conditions, history of user's performances, and the user's physiological state is still considered a major research challenge. An intuitive and natural behavior can be achieved if the robot can similarly mimic the human's motion or if it can decide on the provided level of assistance in a similar way to humans. Thus, human motor control models and decision-making formalisms are considered in the formulation of the robot control design in order to improve the intuitiveness of the robot's behavior.

User and environment adaptation: The robot's behavior should enhance the overall human-robot interaction behavior by being aware of the context of the operation. The robot should reason and adapt its operational behavior based on the environment state as well as the user's behavior and his/her physiological state, postural stability or intentions. Such adaptations are critical requirements in the design of a context-aware robot control resulting in improvement of the quality of interaction between the MAR and human.

Safety: The MARs should behave safely since they have to operate in close interaction with humans, more specifically elderly or patients with cognitive and/or physical impairments. Safety is one of the most important features of MARs since any hardware or software failure may put users at risk. Therefore, as a basic requirement, the MARs control architecture should guarantee the user's safety.

A possible technical realization of the above mentioned features within the control system of MARs can consist of components shown in Fig. 1.1. At the lowest level of the architecture a series of mode-dependent control modules can be found that drive the mobility assistant and parametrize its low-level controller. To guarantee safety, a safety supervision module ensures that certain velocity, force and energy limits are not exceeded and the robot stays within a given workspace required for the specific mode of control used. Furthermore, the architecture can include a series of modules for online sensor data recording and pre-processing for determination of the environment state as well as human behavior analysis. An example can be data coming from Kinect or laser scanners employed on the robot to detect obstacles and to refine the environment information. Multimodal sensor data streams can be further passed to a larger group of modules dealing with human behavior analysis as well as action, plan and intention recognition. In this context modules can be foreseen for the human performance and stability analysis, the physiological state recognition, speech recognition, and gesture recognition as well as action, plan, and

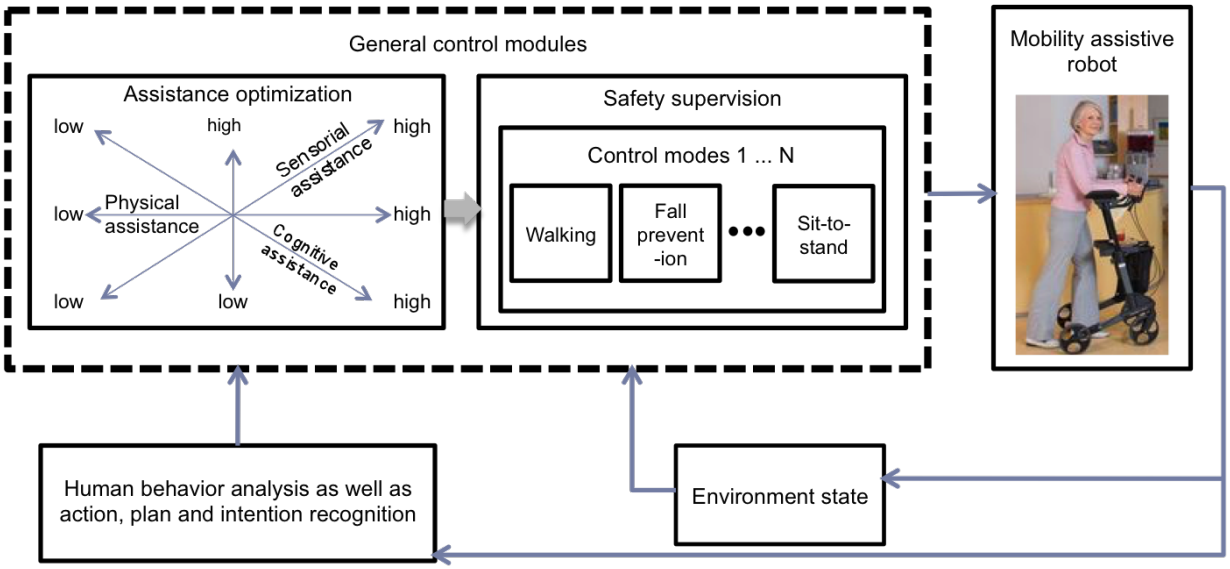

Figure 1.1: A general control architecture for mobility assistance robots.

intention recognition. These modules provide required information for the controllers that aims for intuitive and user and environment-adaptive robot's behavior. The core of the architecture is represented by an agent for assistance optimization. The main idea is that this agent optimizes the level of physical, cognitive and sensorial assistance provided to the user in each specific control mode of robot operation, depending on the status of the human behavior and environment state.

This thesis is dedicated to the design of the modules indicated in dashed in Fig. 1.1 (referred as "General control modules"), with specific focus on proposing solutions related to three already-reviewed challenges and therefore realizing *safe, intuitive and natural* as well as *human and environment-adaptive* robot's behavior during interaction with human users. To this aim, control approaches are designed for three main operational modes of sit-to-stand (STS), walking and human's fall prevention. Safety aspects are firstly taken care of in the control design for each mode of operation. Moreover, it is further emphasized by the realizing of a general safety supervisory controller. The latter supervises the behavior of the specific control unit in the specified mode of operation and reshapes the robot's behavior to enhance the user's safety if an unsafe situation is about to happen. In respect of the goal of intuitive and adaptive robot reaction, an analysis of human motions, human to human assistance as well as human decision-making policies are presented to help better understand the underlying principles, and therefore to mathematically formulate and employ them in the robot control design. These principles are used within the assistance optimization to decide on the optimal level of provided robot support. This thesis also aims for practical validation of the proposed approaches with real end-users. The major parts and contributions of this thesis are described hereafter in more detail.

1.2 Main Contributions and Outline of the Thesis

The goal of this thesis is the development of controllers for mobility assistance robots in three main modes of operation including sit-to-stand transfer, walking and fall-prevention. As graphically shown in Fig. 1.2, a key component of the techniques discussed throughout this thesis is assistance optimization, which is considered in the design and evaluation phases of the assistance approaches for each mode of operation. Assistance optimization is investigated through development of natural, user and environment-adaptive control concepts, that incorporate online gained knowledge about environment, user, or task in the control law. Chapters 3-5 present how the above-mentioned control concepts are realized for the main three operational modes. Moreover, in chapter 6, energy-based safety-enhancing approaches are realized to monitor and improve the behavior of the robot in order to enhance the human's safety during human-robot collaboration.

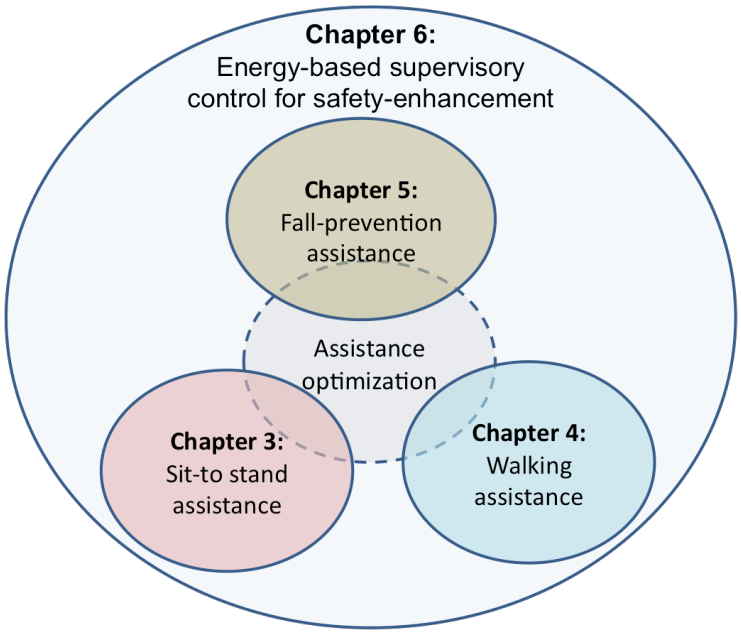

Figure 1.2: Outline of the thesis.

The main contributions of this work as well as further details of the developed approaches are presented as follows:

- **Comprehensive study of rollator-type mobility assistance robots**: Over the years, several MARs have been developed, however a complete review of their employed hardware and functional capabilities was missing in literature. Chapter 2 focuses on MARs of rollator type and provides a detailed review of their systems and implementations of functionalities. The systems are grouped according to their actuation, kinematic structure as well as employed sensors and human-machine interfaces. Functionalities consider mainly sit-to-stand and stand-to-sit assistance, walking assistance, cognitive assistance, and health monitoring. Different implementations of these functionalities are reviewed followed by individual discussions about the current state of the art in this field and possible future directions.

- **Biologically-inspired robot control for human sit-to-stand transfers**: Sit-to-stand (STS) transfers are a common human task which involves complex sensorimotor processes to control the highly nonlinear musculoskeletal system. Understanding and imitating the human behavior during STS transfers provides a powerful tool to control assistance robots towards an intuitive and natural behavior of the coupled system of human and robot. Previous works on human STS transfer assistance hardly incorporate computational models of the motions, and STS transfers were mainly studied and analyzed in explorative and hypothesis-driven experiments. Chapter 3 goes beyond the state of the art and formulates typical unassisted and assisted human STS transfers as optimal feedback control problem that finds a compromise between task end-point accuracy, human balance, energy consumption and smoothness of the motion and takes human biomechanical control constraints into account. Accuracy of the proposed modelling approach is evaluated for different healthy and elderly subjects by comparing simulations and experimentally collected data. Finally, the proposed STS model is used to determine optimal assistive strategies suitable for a person either with weakness in specific part of the body or more general weakness. These strategies are implemented on a robotic mobility assistant and are intensively evaluated by 33 elderly subjects who are mostly not able to perform unassisted STS transfers. The validation results show a promising STS transfer success rate and user satisfaction.

- **Adaptive shared control for walking assistance**: A main application of MARs is to provide support to elderly or patients during walking. The design of a safe and intuitive assistance behavior is one of the major challenges in this context. Chapter 4 presents an integrated approach for the context-specific and on-line adaptation of the assistance level of a rollator-type MAR by the gain-scheduling of low-level robot control parameters. For the first time, a human-inspired decision-making model, the Drift-Diffusion Model, is introduced as the key principle for gain-scheduling parameters and to adapt the provided robot assistance in order to achieve a human-like assistive behavior. The shared control approach is designed to provide a) cognitive assistance to help the user following a desired path towards a predefined destination as well as b) sensorial assistance to avoid collisions with obstacles while allowing for an intentional approach of them. Further, the robot observes the user's long-term performance and fatigue to adapt the overall level of c) physical assistance provided. For each type of assistance, a decision-making problem is formulated that affects different low-level control parameters. The effectiveness of the proposed approach is demonstrated in technical validation experiments. Moreover, the proposed approach is evaluated in an intensive user study with elderly persons. Obtained results indicate that the proposed gain-scheduling technique incorporating the ideas of human decision-making models shows a general high potential for the application in adaptive shared control of mobility assistance robots.

- **Robot control for human fall prevention**: Mobility assistance robots with actuated arms can provide physical and balance support preventing falls of elderly people or patients. In chapter 5, for the first time a fall prevention approach is

proposed for a MAR equipped with a pair of actuated arms. The algorithm evaluates the user's balance criteria and determines required supportive forces to be provided to the user in order to prevent user falls. This chapter further presents how the required forces are realized by the robot. Performance of the proposed approach is tested in experiments by a mobility assistance robot supporting subjects provoking falls in different directions.

- **Supervisory control for safe human-robot collaboration**: Safety is a major challenge on control design of not only MARs, but also any robotic system having physical interaction with humans. While collision detection and contact-related injury reduction in physical human-robot interaction has been studied intensively in literature, safety issues in physical human-robot collaboration (pHRC) with continuous coupling of human and robot(s) (that is the common case of assistance robotic applications) has received little attention so far. In chapter 6, an energy monitoring control system is developed that observes energy flows among the different sub-systems involved in pHRC, shaping them to improve human safety according to selected metrics. The Port-Hamiltonian formalism is used to model each sub-system and their interconnection. An energy-based compliance controller that enhances safety by adapting the robot's behavior is proposed and validated through extensive simulations.

Finally chapter 7 summarizes the contributions and main results of the thesis and highlights future research directions.

2 Review of Mobility Assistance Robots and their Functionalities

The development of MARs has become of great interest in the last two decades. A series of devices have been developed by various groups, see [6] for an overview and [7] for an application-oriented view. The two main categories of mobility assistants are robotic wheelchairs and robotic walkers [8]. The latter can again be divided into three main groups [9]: the *Standard Walking Frames* (aka Zimmer Frame), designed to provide support to a person with lower limb weakness, the *Rollators* which are a standard frame with attached wheels used where balance is the major problem, and the *Reciprocal Frames* which are similar to the Standard Frames except that the frame is hinged on either side allowing the sides of the frame to be moved alternately. Reciprocal Frames are designed to accommodate a normal walking pattern with opposite arm and leg moving together.

Although several MARs have been developed over the years, a comprehensive review of their employed hardware and functional capabilities was missing from literature. This chapter provides a detailed and complete review of the MARs' system and implementations of functionalities. Different systems are compared by their kinematics, actuation system, sensors, and human-machine interfaces (HMI), see section 2.1. We discuss different implementations of provided functionalities like sit-to-stand and stand-to-sit (STS) assistance (section 2.2.1), walking assistance (section 2.2.2), cognitive assistance (section 2.2.3), health monitoring (section 2.2.4) as well as extra functionalities realized for very few systems (section 2.2.5). After having reviewed platforms and realized functionalities along with their various implementations we conclude with a summary. It should be noted that the intention of this chapter is to review functionalities from an engineering perspective and not from a human factors or clinical point of view as available literature shows a lack of formal evaluation studies with patients and thus, does not allow us to make strong conclusions about the benefits of developed systems and functionalities from a clinical and users' perspective. We summarized our findings and recommendations for future evaluation studies in a separate survey paper, see [10].

2.1 Mobility Assistance Platforms

In the following sections we review kinematics and actuation systems, sensors as well as interfaces used for a total number of 27 mobility assistance robots of rollator type, see Table 2.1 for a summary.

Table 2.1: Comparison of hardware and sensing systems of different rollator-type mobility assistants

	Actuation		Kinematics				Sensors									Interfaces	
Mobility assistant	active	passive	three wheels	four wheels	holonomic	non-holonomic	LRF	sonar	cameras	GPS	Kinect	F/T	tactile	slope detectors	heart rate	touch screen	speech interface
Kosuge walkers [11–22]	○	√	–	√	√	○	√	√	√	–	√	√	–	√	–	–	–
MARC [23–27]	–	√	√	–	–	√	√	√	–	–	–	√	–	–	–	–	–
iWalker (US) [28]	–	√	–	√	–	√	–	√	–	–	–	–	–	–	–	–	–
i-Walker (EU)[29]	–	√	–	√	–	√	–	–	–	–	–	√	–	–	–	–	–
i-Walker (Japan) [30]	–	√	–	√	–	√	–	–	√	–	–	–	–	–	–	–	–
COOL Aide [31]	–	√	√	–	–	√	√	–	–	–	–	√	–	–	–	–	–
Care-O-bot I-II [32–36]	√	–	–	√	√	–	–	√	√	–	–	√	–	–	–	√	√
Guido [37–39]	√	–	–	√	–	√	√	√	–	–	–	√	–	–	–	–	√
CMU walker [40, 41]	√	–	–	√	√	–	√	√	–	–	–	√	–	–	–	–	–
Pearl and FLO [42–44]	√	–	–	√	–	√	√	√	√	–	–	–	–	–	–	√	√
PAMM [45–47]	√	–	–	√	√	–	–	√	√	–	–	√	–	–	√	–	–
i-go [48, 49]	√	–	–	√	√	–	–	–	–	–	–	√	–	√	–	–	–
Johnnie - CAIROW [50, 51]	√	–	–	√	–	√	√	√	–	–	–	√	–	–	–	√	–
Walkmate [52]	√	–	–	√	–	√	√	–	√	–	–	√	–	–	–	–	–
walbot [53, 54]	√	–	–	√	√	–	√	–	–	–	–	–	–	–	–	–	–
JARoW [55–57]	√	–	√	–	√	–	√	–	–	–	–	–	–	–	–	–	–
UTS [58]	√	–	–	√	–	√	√	–	–	–	–	√	–	–	–	–	–
HITOMI [59]	√	–	–	√	–	√	–	√	√	○	–	–	√	–	–	–	–
NeoASAS [60–62]	√	–	–	√	–	√	–	√	–	–	–	√	–	–	–	–	–
MONIMAD- robuwalker [63–68]	√	–	–	√	–	√	√	–	–	–	–	√	–	–	–	–	–
Chugo group walker [69–74]	√	–	–	√	–	√	√	–	–	–	–	√	–	–	–	–	–
WAR [75, 76]	√	–	–	√	–	√	√	√	–	√	–	√	–	√	–	√	–
SMW [77, 78]	√	–	–	√	–	√	–	–	–	–	–	√	–	–	–	–	–
MOBIL [79, 80]	√	–	–	√	–	√	–	√	–	–	–	√	–	–	–	–	–
MOBOT [81–83]	√	–	–	√	–	√	√	–	√	–	–	√	–	–	–	√	√

√: full support, ○: partial support, –: no support

2.1.1 Actuation

Literature distinguishes between mobility assistants that are passive or active. *Passive* mobility assistants are considered systems that can not accelerate by themselves and rely on applied user's forces, while *active* mobility assistants are considered to have motors to drive the system and thus, their motion and interaction behavior can be actively controlled. Passive systems provide passive support by guiding or decelerating the user with the help of brakes when needed, e.g. to avoid collisions. Safety is inherently guaranteed for passively assisting robots because of their dependency on external forces that have to be applied by the user. On the other hand, poor maneuvering capabilities and rather high inertia are considered disadvantages of passive systems as the whole robot load needs to be pushed by the human applying forces onto it. In contrast, active-type robots can be featured with many components since their active mobile base carries their weight. A manual or automated (motorized) brake system is typically used in both passive and active systems.

Among the overall 26 mobility assistant robots reviewed, only 6 devices were found to belong to the passive category, while 21 devices belong to the active category, see Table 2.1.

2.1.2 Kinematics

Mobility assistants can be mainly categorized into devices with locomotion support and with STS support. In the following subsections we report typical kinematic features of systems belonging to each of these categories.

Rollator-type Devices with Locomotion Support

Rollator-type devices with locomotion support typically consist of three or four wheel systems. Four wheel devices typically consist of a support frame, two castors at the front, and two actuated rear wheels. Only few prototypes are equipped with motorized wheels at the front and non-motorized wheels at the rear (e.g.[84]), motors on all four wheels (e.g. [40]), or represent passive systems without motors at any wheel (e.g. [12, 28]). Three-wheel-systems are typically based on commercially available frames equipped with sensors and handles. They often employ an automated braking and steering system for the front wheel (e.g. [24, 31]).

Four wheel configurations have been used in 24 platforms, while three wheel configurations have only been used in 3 systems.

Mobility assistance robots can employ holonomic or non-holonomic mobile bases. Most of the available prototypes (17 systems) use non-holonomic mobile bases, while the rest (8 systems) use holonomic bases either with four omni-directional wheels (see CMU walker[41] and 'walbot' [53, 54]), two omnidirectional wheels plus castors (see PAMM, [46, 47]), or even three omnidirectional wheels (see JAIST Active Robotic Walker ('JARoW') [55–57]).

More versatile kinematic structures have been investigated only in very few prototypes. Examples found in literature include the test of a handrail instead of handles in an early version of the 'walbot' [53, 54], a re-configurable structure from a walking support system into a chair [52], as well as the mounting of an additional manipulator arm for manipulation of objects [85].

Rollator-type Devices with STS Support

In total 6 mobility assistance robots include STS assistance mechanisms in their kinematic structures. Different kinematic structures were realized for each of the systems. Parallel actuated arms with 2 DoFs mounted on an active mobile base are proposed in "MONIMAD" and its predecessor "robuWalker" [63–68]. The same concept, but with independently controlled spindle drives for each arm is followed for the Mobot platform [81, 82]. For both aforementioned devices the handles are designed to keep the same orientation while moving. A 3 DoF support pad manipulated by four parallel linkages mounted on an active mobile base was developed by the group of Chugo [69–74]. A prerequisite for this platform though is that the patient must lean on the pad (by his/her chest), place the arms on the two arm holders and grip the two handles during sit-to-stand transfers. The supporting pad assures the patient's postural stability while performing a STS transfer. Finally, a concept for adjusting the height of the handles or arm support by reconfiguring either the base mechanism is proposed in three more systems, see[75, 76], [86], and [77, 78].

2.1.3 Sensors

Most developed prototypes are equipped with laser range finders, sonar, and force torque sensors, while cameras are less used. GPS, Kinect, and tactile sensors are so far only rarely employed. More specific sensors such as a slope detection sensor was found in [48, 49], heart-rate sensors in [46, 47], and tactile sensors in [59].

Laser range finders or sonar sensors are mainly used for the purpose of navigation or obstacle avoidance, see e.g. [46, 47, 84]. Only some groups use laser range finders to distinguish different user's states (walking, stopped, and emergency) [87], or to detect the user's lower limb positions and speed [55–57]. Force torque sensors are mainly employed for the evaluation of interaction forces applied by the user. Only in [29] force sensors are used at the rear wheels to measure ground reaction forces. Cameras are employed for localization [28, 46, 47, 59], obstacle avoidance [75, 76], or documentation of the user's behavior for rehabilitation purposes [30]. Self localization by means of GPS/GIS is only studied in [75, 76].

2.1.4 Human-Machine Interfaces

A series of human machine interfaces (HMI) have been investigated in the context of mobility assistant robots. Manual switches or buttons to receive control inputs from the user and speakers to provide information about the robot states are the most basic HMIs used [40, 84]. A hand-held remote control is being used in [40] to send signals to the robot from distance. More advanced systems using displays and touchscreens are employed in [42, 51, 75, 88] to provide a graphical interface for switching between different robot control modes [88], walking characteristics [51] or to set a destination [42, 75]. Further information in form of a front camera-view of the robot, the current location, and guidance messages is displayed in [42, 75]. Speakers and microphones are also used for verbal communication, see e.g. [88, 89]. Since elderly people often have difficulties interacting through keyboards and computer screens, verbal communication has been tested as alternative. Care-O-Bot 3 is equipped with

a simple speech synthesis function to process user's verbal commands as well as to provide speech feedback to the user during task execution [88, 89]. Advanced real-time speech recognition and synthesis functionalities are implemented in Pearl and Flo ([42, 43, 90]) based on CMU's SPHINX II system [91].

In the following sections we will provide details about the specific functionalities realized with the various hardware platforms.

2.2 Functionalities

Functionalities of robotic mobility assistants are reviewed and classified into STS assistance, walking assistance, cognitive assistance, health monitoring, and some extra functionalities that don't fall into these categories and that were realized only for few systems. In general, walking and cognitive assistance are implemented in most mobility assistants, while the rest of functionalities have been less focused on so far.[1] Table 2.2 provides an overview of available functionalities in all reviewed prototypes.

2.2.1 STS Assistance

Different robot control approaches have been investigated to provide STS assistance. As some controllers differentiate between different STS phases we also report on approaches to estimate postural states during STS transfers.

Estimation of Postural State

Only very few manuscripts could be found that consider the detection of different postural phases during STS movements for providing STS transfer assistance. Pasqui presents a fuzzy logic to distinguish between seven different phases in STS transfers: seated, returned, pre-acceleration, acceleration, start rising, and rise [67]. In [98] the same type of fuzzy logic estimator is presented, but with a reduced number of phases. In [69] authors distinguish between four phases: still sitting and inclining the trunk forwards, lifting off from the chair, lifting the body and extending the knee completely. Phase three is detected by observation of the interaction force and its comparison with a predefined threshold. The other phases are not detected explicitly. It is remarkable though that no evaluation could be found that aimed at determining how many and which of the phases are essential for control and beneficial for realizing an STS functionality.

Human Balance Criteria

Human balance is a critical issue to be considered in STS transfers. The most used balance criterion applied in the context of mobility assistants was found to be the Zero Moment Point (ZMP), which is defined as the point at which the net moment has no component along the horizontal axes. If the ZMP lies within the support polygon, the configuration can be considered stable [103].

[1] Please note that the length of the following sections varies depending on the available material found in literature.

Table 2.2: Comparison of developed functionalities by different rollator-type MARs

Mobility assistant	Functionality									
		Walking assistance				Cognitive assistance				
	STS assistance	Maneuverability improvement	Human fall prevention	Gravity compensation on slopes	Obstacle/step avoidance	Assisted localization	Assisted navigation	Orthotic functions	Health monitoring	Extra functionalities
Kosuge walkers [11–22, 87, 92]	∘	√	√	√	√	–	–	–	–	–
MARC [23–27]	–	√	–	–	∘	–	–	–	–	–
iWalker (US) [28]	–	–	–	–	–	√	√		–	–
i-Walker (EU)[29]	–	–	–	–	–	∘	∘	–	–	–
i-Walker (Japan) [30]	–	√	√	–	–	–	–	–	–	–
COOL Aide [31]	–	√	–	–	√	–	–		–	–
Care-O-bot I-II [32–36, 93–95]	–	–	–	–	–	–	√		–	–
Guido [37–39, 84]	–	√	–	–	√	√	√		–	–
CMU walker [40, 41]	–	–	–	–	√	√	√	–	–	–
Pearl and FLO [42–44, 90]	–	–	–	–	√	–	√	√	√	√
PAMM [45–47]	–	√	√	–	√	–	√	–	√	–
i-go [48, 49, 96]	–	√	–	√	–	–	√	–	–	–
Johnnie - CAIROW [50, 51]	–	–	√	–	√	–	–	–	√	√
Walkmate [52]	–	√	–	–	–	–	–	–	–	–
walbot [53, 54]	–	√	–	–	√	–	√	–	–	–
JARoW [55–57]	–	√	–	–	√	–	–	–	–	–
UTS [58]	–	–	–	–	√	–	–	–	–	–
HITOMI [59]	–	–	–	–	√	√	√	–	–	–
NeoASAS [60–62]	–	√	–	–	–	–	–	–	–	–
PAM-AID [97]	–	√	–	–	–	–	–	–	–	–
MONIMAD - robuwalker [63–68, 98, 99]	√	–	–	–	–	–	–	–	–	–
Chugo group walker [69–74]	√	–	–	–	–	–	–	–	–	–
WAR [75, 76]	√	–	–	–	√	–	√	–	–	–
SMW [77, 78]	√	–	–	–	–	–	–	–	–	–
MOBIL [79, 80]	√	–	–	–	√	–	–	–	–	–
MOBOT [81–83, 100–102]	√	√	√	–	√	√	√	–	–	–

√: full support, ∘: partial support or just sketched support, –: no support

It should be mentioned though that the ZMP has been mainly applied and studied in robotic applications, but it is unknown whether humans follow similar balance-keeping principles. Thus, a future research direction may target the investigation of human stability criteria that can also be implemented for mobility assistants.

Robot Control for STS Transfers

Surveying implementations for assisted STS transfers we found that different control approaches were realized that can be grouped into three categories: force control, motion control, and switching control.

STS Support by Robot Force Control: In terms of robot force control very basic interaction-force-minimizing optimization-based approaches were found with posture stability criteria used as side criterion. Médéric and Pasqui evaluate the Zero Moment Point (ZMP) for a simplified human model [65] and control the interaction force between user and robot to stabilize the configuration. Their model considers a 7 link mechanism studied in the sagittal plane.They evaluate the ZMP position and formulate an optimization problem that determines appropriate interaction forces to be applied to the user during a STS transfer by means of force control to stabilize the configuration of the ZMP within its support polygon.

STS Support by Robot Motion Control: An alternative approach to realize STS transfers is to command the motion of the platform or arms.

The simplest form is studied in [16] where the authors use a very basic, passive approach to assist in STS transfers that positions the support system in a fixed position in front of the user and activates the brakes of the system, while the user grasps the handles to perform a STS transfer by using the weight of the support system to assist in STS transfers.

A more sophisticated approach is studied in [77, 78] where STS transfers are guided by the trajectory of a support plate mounted on the developed robot called SMW. The support plate is designed to balance the user as well as to support specified portions of the patient's weight during the STS transfers. The desired trajectory is implemented by controlling the linear actuator guiding the angle and height of the support plate. The authors propose two predefined trajectories and compare their characteristics using the force/torque data measured by sensors at the top plate.

Pasqui and Médéric investigate least effort user-centered natural trajectories in order to effectively assist a patient in STS transfers. They define *natural* trajectories as paths that are "compatible with hand movements when the STS transfer is assisted by someone/something else" as well as paths leading to a "smooth and continuous motion". Based on the biomechanical data analysis of recorded STS transfers, the authors approximate the recorded hand paths with cubic splines [64]. The global trajectory shape was found to be highly related to the initial and final point of the handle rather than other factors such as patient's age, height or pathology. In [66, 99] authors achieve smoothness of trajectories by minimizing jerk along the path [104]. In [64] they finally present very preliminary results towards the optimization of parameters defining an S-shaped curve in order to reduce human effort. They implement 5 trajectories with different parametrization using impedance control and ask patients to interact with the device while guiding them on the predefined compliant trajectory. The implementation with least deviation from the controlled trajectory is selected as the best for a specific subject. More formal optimization

methods are mentioned in the authors future work.

A more advanced approach for the determination of optimal assistive strategies to be performed by a mobility assistant is presented in [83, 100]. Typical unassisted and assisted human STS transfers are formulated as an optimal feedback control problem that finds a compromise between task end-point accuracy, human balance, jerk, effort, and torque change and takes further human biomechanical control constraints and external forces provided by the robot handles into account. Optimal handle trajectories to be controlled during STS transfers are determined by offline dynamic optimization for either a person with specific body segment weakness or more general weakness.

Finally, in [21] the authors present an online approach that takes over parts of the required knee torque. Instead of pre-calculating the whole trajectory, they introduce a motion control algorithm that moves the support system following an admittance control law based on the currently measured interaction force and the desired support knee torque, which is calculated as the scalar product of the applied force at the handle and the distance of the handle to the human knee. Three accelerometers are attached to shank, thigh and trunk of the user to determine joint angles. Using these joint angles in combination with the human model joint torques are calculated [105, 106]. In order to simplify the implementation, only gravity effects are considered and no inertia, which is acceptable for slow STS transfers. The same simplification has been also made in [105].

STS Support by Switching Control: Again another approach for providing assistance during STS transfers is to switch between different controllers depending on the actual human postural state.

The Chugo group initially proposed a switching position/damping control for their stationary STS assistance system [69] consisting of a support bar with two degrees of freedom and a bed system which can move up and down. Their approach assists in sit-to-stand and stand-to-sit transfers by exploiting the remaining physical strength of a patient in order to not decrease the force generating capacity of the patient. Inspired by [107], they divide the standing up motion into four phases: *i*) still sitting and inclining the trunk forwards, *ii*) lifting off from the chair, *iii*) lifting the body and *iv*) extending the knee completely. Analyzing these four phases by means of multi-body computer simulations and assuming a Kamiya motion strategy to perform the STS transfer, they conclude that assistance is mainly required in the third phase in order to reduce the required knee torque, while in the other phases maintaining stability of the body is sufficient. Based on these considerations they realize compliant impedance control for phase $1, 2, 4$ and an admittance controller with force reference implementing damping control for phase 3. Force sensor readings and a predefined force threshold are used to switch between the phases. In early versions [108], the authors adopt this approach for the bed system only, while they implement a force control approach for the support bar.

Later, authors adapted their approach of the initial stationary system to their mobile mobility assistant. This system foresees a force sensor attached to the support pad to switch between position and damping control. Recent improvements of their system include further the real-time estimation of the patient's pelvis, knee and ankle load based on a biomechanical model of the human and the switching between control modes depending on predefined thresholds in these loads [74] as well as the real-time estimation of the center of

gravity (COG) of the user based on force sensor measurements [71] and its PID control by changing the position of the mobile base of the assistance robot. Finally, the assisting approach was also extended to stand-to-sit transfers by changing the reference trajectories [73] and by including sensor readings to adjust the seating position [72].

Instead of switching based on predefined thresholds, Pasqui presents a fuzzy controller to ensure stability of the patient during assisted STS transfers [67, 98]. They subdivide the STS transfer into several phases and define fuzzy rules to evaluate these phases as well as to evaluate the center of pressure and the horizontal component of the handle force to guarantee stability for the patient by switching between different controllers named "normal", "admittance", "stabilization", and "return", basically implementing different variations of admittance control.

More control-theoretic considerations investigating stability of the resulting hybrid and switched systems are currently lacking in literature. Also the optimal number of phases needed for achieving best STS support can be considered still an open research question.

2.2.2 Walking Assistance

Walking assistance is the functionality, which is present in almost all mobility assistant robots reviewed in this thesis and means the human-adaptive or environment-adaptive manipulation of robot control inputs or control parameters to ease the steering of the mobility assistant or to avoid safety-critical situations like collisions with obstacles or falls, some of them requiring the estimation of the human postural state as reviewed next.

Estimation of Postural State

User postural state estimation in the context of walking assistance has been studied in [13, 14, 16, 22, 23, 26]. States like *walking*, *stopped* and *emergency* are considered. As key feature to distinguish between these states the Kosuge group used the distance between the user and the rollator which is measured by means of a laser range finder. Differentiating this distance and knowing about the velocity of the rollator allows them to calculate the user velocity. *Stopped* state estimation of the user is realized by simply comparing the velocities of the user and the rollator along the heading direction. *Walking* and *emergency* states are distinguished by analyzing the distance between the user and the rollator during walking without tumbling or falling, and comparing the current user position to the histogram of his/her position in x- and y-axis (ellipsoids) with respect to the position of the rollator [14]. If the relative position of the user is found within the ellipsoid, the user state is detected as *walking*. If the relative position of the user is found outside of the ellipsoid, the user is considered to be in *emergency* state. Recently, the same group presented a very similar approach to estimate user states, but using a depth vision sensor instead of a laser range finder and analyzing the centroid of the user's upper body [18]. Doing so, a $2D$ probabilistic model of the human location is constructed during normal walking. The centroid of the upper body is used to judge whether the user is walking normally or is in an emergency state. Please note that the state-specific parameters were found to vary significantly depending on the user's size, physical capability, operational characteristics and disabilities. They also vary depending on the daily or environment conditions. Thus,

Hirata and Kosuge propose a continuous update of the estimation based on the actual user or environment conditions.

Following a slightly different approach, Huang et al.proposes a fall detection scheme based on simultaneous monitoring of the user head position by a CCD camera mounted above the user and leg positions measured by a laser range finder directed towards the user legs [109]. Possible falling states are categorized into "forward falling", "backward falling" and "sideward falling". Probability distributions of the distance between head position and the center of the two legs for the normal walking and falling state are the key features in the proposed fall detection scheme. If the head position lies outside a given distribution for the normal walking situation a falling state is detected.

In [14, 101] the authors propose a method for estimating user falls by evaluating the relative distance between the robot and user's legs measured by a laser range finder. In [12] an extended approach proposed for modelling the user with a solid body-link model, online tracking its configuration with the help of two laser range finders mounted at different heights, determining the user center of gravity and finally checking whether this center of gravity lies within the defined support polygon formed by the area of both feet. The risk of falling increases if the projection of the COG leaves the support polygon. Human falls have been characterized into falls along the horizontal direction caused for example by stumbling and leading to legs that are far apart from the walker, and falls along the vertical direction caused for example by weak legs. Evaluation of the human's extrapolated center of mass (XCOM) for faster fall detection was proposed by [82].

Summarizing, mainly walking, stopped, and emergency states have been determined by processing features like human-robot distance and human COG position. Falls as critical emergency situations have been studied by monitoring the user's head, upper body or leg positions during walking. Full-body articulated tracking of the user, however, is hardly realized, most likely due to the lack of adequate sensor systems at the time the studies were performed.

Human and Environment-adaptive Motion Control

When it comes to providing assistance during walking, human and environment-adaptive motion control has been intensively studied in literature.

One of the most often adopted approaches in this context is variable admittance control. In case of an *active* mobility assistant variable admittance control allows reacting to estimated user intentions and user states with a corresponding motion behavior of the mobility assistant. An admittance model with the human force $\boldsymbol{f}_h$ as input and the system reference velocity $\dot{\boldsymbol{x}}$ as output defines the sensitivity of the device to applied human forces. Further, the desired admittance dynamics is extended by additional forces/torques $\boldsymbol{f}_r$ generated based on environment information and applied by the motors on the system

$$\boldsymbol{M}_d\dot{\boldsymbol{u}} + \boldsymbol{D}_d\boldsymbol{u} = K_h\boldsymbol{T}_h\boldsymbol{f}_h + K_r\boldsymbol{T}_r\boldsymbol{f}_r \tag{2.1}$$

with $\boldsymbol{M_d}$ and $\boldsymbol{D_d}$ to be specified desired mass and damping matrices, $\boldsymbol{T}_h$, $\boldsymbol{T}_r$ geometrical transformations and K_h and K_r weighting factors. A low-level velocity controller finally guarantees that the device follows the calculated reference velocity $\boldsymbol{u}$. By online adapting

the admittance parameters for mass and damping, changing the transformation matrices $\boldsymbol{T}_h$, $\boldsymbol{T}_r$, weighting factors K_h and K_r or additional forces/torques $\boldsymbol{f}_r$ generated based on environment information, the behavior of the system can be modified.

For *passive* mobility assistants in contrary, the desired admittance model (2.1) can not be realized anymore actively, but only passively by dynamically activating brakes resulting in

$$\boldsymbol{M}_d\dot{\boldsymbol{u}} + \boldsymbol{D}_d\boldsymbol{u} = K_h\boldsymbol{T}_h\boldsymbol{f}_h - K_r\boldsymbol{T}_b\boldsymbol{f}_b \tag{2.2}$$

with $\boldsymbol{f_b}$ the brake force and torque.

Alternative approaches to variable admittance control consider a direct commanding of the position or velocity of the platform, using approaches that allow determining the human intention either directly from input devices or indirectly via estimation from sensor signals and context.

In the following paragraphs we detail implementations found that are based on the aforementioned concepts and that aim at maneuverability improvement, fall prevention, gravity compensation on slopes or obstacle avoidance.

Maneuverability Improvement: Basic concepts of maneuverability improvement to reduce the inertia of the overall system are realized for many active mobility assistants. Variable admittance control as defined in (2.1) is implemented to reduce the apparent inertia compared to the uncontrolled system, see e.g. [102]. In [52] authors compare a force-velocity mode and a force-acceleration mode and conclude that the force-acceleration mode has better stability and maneuverability, but the force-velocity mode has a faster response. Depending on the location of the force sensors and the type of interaction points, further different force components need to be distinguished. In [61, 62] the user is e.g. provided physical support on the lower arms rather than by gripping handles with his/her hands and thus, authors identify three force components: vibrations introduced by the floor/walker wheels imperfections, oscillations due to user's trunk motion during gait, and the voluntary components related to the user's navigational intention. They develop adaptive filtering techniques to separate the different force components and use them to control the device by means of a Fuzzy-logic-based controller.

In [17, 22] authors further improved maneuverability by applying a transformation $\boldsymbol{T}_h$ in (2.1) that allows to online modify the center of rotation of the mobility assistant.

For the PAMM robot [45] the transfer from the *stopped* to *walking* state and vice versa was supported by slowly fading from high/low to low/high damping parameters by implementing a velocity-dependent damping. A similar approach is proposed by Song [53], but using a force observer instead of a force/torque sensor in order to reduce the costs of the device.

Finally, artificial potential fields are employed in [11, 15, 92, 110] to derive force components in (2.2) for passive path following by activating brakes accordingly. In [30] they implement a line following behavior with their passive-type robot using similar principles. Authors in [39, 84] and [54] study an active type robot, but limit active robot behavior for path and wall following to the angular velocity and activate it only in case the human applies intentional forces on the robot.

In contrary, authors in [55–57] don't apply a variable admittance approach, but estimate user's lower limb and body locations using a Kalman-filter-based tracking scheme and use this information as input to the platform low-level controller that adjusts the motion corresponding to the user's walking behavior.

Also in [26] authors directly command a reference trajectory. This trajectory is derived by estimating the user's intended path from a combination of sensory data, user's input, history and device position and orientation by means of a dynamical path weighting scheme that weights a series of possible arcs starting at the current position of the mobility assistant and pointing into different directions. The arc with the highest probability is used to set the front wheel steering angle.

In [31] the authors use forces and moments a user applies to a walker's handle in addition to information on the local environment and the walker's state to derive the most likely human intention, respectively path to follow. Depending on the identified intention, the angle of the front wheel is set by the mobility assistant, leaving the user the freedom to decide on the velocity to move on the identified path. Dempster-Shafer theory is adopted to extract the user's navigational intention from historical observations and evidences. Interaction forces are evaluated to identify conflict situations based on a defined "conflict index", which influences the selection of the most likely human intention.

Also in [97] authors combine user's and environment's input for maneuverability improvement. The PAM-AID mobility assistant, which was designed for frail and elderly blind, is equipped with a user-interface with three buttons for moving forward, turning left or right and that activate respective autonomous robot behavior. To avoid erroneous inputs to the system caused by the reduced sight of the patients, the authors propose a Bayesian network that combines user's input with high-level environment information derived from sensors to provide a context-aware estimate of the human navigational intention, which is finally realized by means of a local potential field navigation scheme.

Fall Prevention: Another crucial assistance function provided by mobility assistants is fall prevention. For the active-type robot PAMM [45] high damping values were abruptly set in (2.1) to quickly stop the walker in case of emergency.

In [50] the gait of Parkinson Desease patients is analyzed with the help of a Hidden Markov Model and auditory cues are provided when abnormal gaits are recognized. Further, the walker is locked with the help of motors when sudden forward pushing is detected to avoid falls.

For the i-Walker (Japan) system, authors control the platform velocity for fall prevention triggering braking torques of the passive-type platform if its velocity exceeds certain predefined limits [30].

In [12, 14], varying admittance control on a passive mobility assistant is used for fall prevention by increasing the damping in the desired admittance if the user was found to be in a "falling" state activating the brakes accordingly, while in the "stopped" state, large brake torques were applied to each of the wheels independently of the user's applied force to the system.

More sophisticated fall prevention controllers that actively move the robotic platform or arms to stabilize the human posture are rarely studied. One exception was found in [101]

where a supervision-based safe motion control based on invariance control for forward fall and human-robot collision avoidance is presented. Human-robot distance is used as safety feature to formulate safety-constraint-admissible state space regions that are kept invariant by proper switching between a nominal (admittance) and a corrective controller, whenever one of the predefined safety constraints are about to be in violation.

Finally, authors in [82] propose an approach for a mobility assistance robot with actuated arms. They evaluate the human XCOM and present a control system for the articulated arms to apply required forces on the human for fall prevention and for recovering balance.

Gravity Compensation: Gravity compensation on slopes is a further assistance function provided by mobility assistance robots. To realize gravity compensation for downhill walk, authors in [15] derived the brake torques in (2.2) using measurements of two tilt angle sensors added to their passive mobility assistance robot.

A motion control algorithm implementing an active mode that realizes gravity compensation on slopes for uphill walking is realized in [96], whereby a model-predictive controller is employed to provide an estimate of the slope height.

Obstacle Avoidance: Finally, obstacle avoidance is a typically implemented assistance function for mobility assistance robots. In [11, 15, 92, 110] artificial potential fields are employed to derive force components f_b in (2.2) for passive obstacle avoidance. In contrary, in [20] force/torque components f_r in (2.1) are employed for active obstacle avoidance. The latter, however, can result in dangerous situations, for example in case the human releases the handles and the robot continuous to move or the human plans to walk on a straight path, while the system accidently turns to circumvent an obstacle. Thus, in [31] authors directly influence the angular velocity of the front wheel in the vicinity of obstacles and activate the obstacle avoidance behavior only in case the calculated repulsive virtual moment exceeds a certain limit. A "conflict index" evaluating the interaction moment between user and robot is used to decide on conflicting situations, e.g. when the user intends to approach an object identified as obstacle by the autonomous robot agent. When the conflict index exceeds a certain predefined value, the robot returns the full control to the user. In [111] authors compare the potential field approach to an approach based on the definition of state-based constraints in situations of static and dynamic obstacles as well as workspace constraints. They conclude that the selection of the appropriate method depends on the particular application as both methods have advantages in specific settings.

While approaches mentioned so far mainly implement fixed scheduling strategies for K_r, K_h in (2.1) or (2.2) to combine user's and autonomous robot's inputs or switch between extremes of fully autonomous or fully human control, the adaptive shared control with varying force gains K_h and K_r investigated in [45] evaluates among others the proximity to obstacles and shifts authority between computer and human by online adjusting the force gains in (2.1) as a function of a defined performance metrics. Further, in [102] authors propose an approach for the context-specific, on-line adaptation of the assistance level of a rollator-type mobility assistance robot by gain-scheduling of low-level robot control parameters in (2.1) by means of a human-inspired decision-making model, the Drift-Diffusion Model. Among other assistances, authors also implement a sensorial assistance allowing to

avoid collisions with obstacles, but also the intentional approach of them. Finally, in [25] the authors propose to shift authority from the human user to the robotic system or vice versa depending on the specific context, allowing for the implementation of a no assist mode, an assist mode, a safety mode and an override mode. In the no assist mode the rollator is under full control of the user. In the assist mode the robotic walker software senses obstacles in the current path, and provides assistance so that neither the human nor the walker frame finally collide with one or more of the obstacles by still taking the human navigational intention into account. In the safety mode, the walker software has detected an obstacle within a distance threshold that requires an immediate response and thus, the system takes over the control of the platform by paying less attention to the human intention. Finally, the override mode allows the user for the intentional approach of an obstacle by overriding the autonomous functions of the walker software. Unfortunately, authors only sketch the general capabilities of their architecture, but do not provide mathematical implementation details about the reasoning and logic unit used, nor do they provide experimental results.

Alternative approaches to variable admittance control, e.g. adjust the mapping between user's lower limb and body locations and the velocity of the platform as a function of the distance to obstacles (e.g. in case the platform lacks a force sensor, see e.g. [55–57]). Similarly, in [50] the velocity of the platform is adapted as a function of the measured distance of the human user to the platform trying to keep this distance constant, while adjusting the maximum angular and translational velocity in the vicinity of obstacles. In [58] authors implement an obstacle avoidance and local path planning functionality based on the Vector Field Histogram algorithm and fuse human and autonomous agent velocity inputs by means of a fuzzy logic module as decision making unit. Finally, in [54] authors adapt only the angular velocity of the platform as a function of the distance to obstacles, while the human decides on the translational velocity leading to a pure passive approach. The Guido system again realizes a fully autonomous mode in which laser scanner data is used to create a local point map to detect obstacles and to elastically deform the originally planned path to avoid collisions [39, 84].

2.2.3 Cognitive Assistance

Frequent relocations between hospital, rehabilitation centre and nursing home can lead to confusion and disorientation. Thus, cognitive assistance in terms of localization and navigation has frequently been implemented for mobility assistants. In addition cognitive orthotic assistance may become important, which means the reminding of people about routine activities.

Localization and Navigation

The implementation of assistance functionalities like localization and navigation require solving technical issues like map building, localization, and path planning. In the following paragraphs we fist review methods that have been tested in the context of mobility assistant robots before we introduce assistance functionalities of localization and navigation that use these techniques in the context of mobility assistance robots.

Early methods, considered the combination of local methods for robot localization based on odometry and gyroscopes with global localization methods that compare laser scan data and natural features observed in the environment with a given map and features, see [93]. Later, map-based navigation and more recently simultaneous localization and mapping (SLAM) algorithms are implemented. In the Guido systems [39, 84] for example the most sophisticated approach solves the SLAM problem with an extended Kalman filter (EKF) for estimating a feature-based map, composed of the walls of the environment. The Guido system is featured to build the map of an environment in a few minutes by either manually or autonomously driving around. Another robot navigation system for assistive walkers has been built using the Carnegie Mellon's Navigation Toolkit (Carmen), a probabilistic software system, which has been developed in the context of different robot guidance projects. It contains software modules for collision avoidance, localization, mapping, path planning, navigation, and people tracking and uses metric environment maps at its core. Localization is realized with the help of conditional particle filters. In [44] authors further present advanced localization techniques for highly populated areas like the cafeteria.

In terms of path planning, the Guido system plans the shortest path to the target with respect to its nonholonomic constraints of the mobile platform using a graph-based method [39, 84]. As the generated path does not take dynamic obstacles into account, laser scanner data is used to create a local point map to detect obstacles and to elastically deform the original path to avoid collisions. No path modifications by the user are possible in the Guido framework. In [33] authors suggest different types of path planning methods including rapidly exploring random trees, potential grids with wavefront expansion, quad trees, and visibility graphs [93, 95] as well as variants, which have been extended for non-holonomic platforms [95] based on a static map and a target in this map. To allow for dynamic obstacles and planning of smooth paths as well as path modifications according to user's inputs, advanced methods for dynamic path planning (e.g. elastic bands [112]) are employed as presented in [34, 94, 95]. In the context of the Carnegie Mellon's Navigation Toolkit (Carmen), the navigation module integrates collision avoidance and global path planning methods based on dynamic via point calculation.

In the following paragraphs we report on found assistance functionalities of localization and navigation that take advantage of introduced methods for mapping, localization, and path planning.

Assisted Localization: While a series of mobility assistance robots have an embedded functionality for localizing themselves, only few also use this information and implement a localization assistance functionality for the user. In [28] and [40, 41] the user's position is visually marked on a map displayed on the platform. In contrary, in [59] information on landmarks is provided via Braille, while automatic verbal feedback about the current location, navigation events or selected goals is provided in [39, 84].

Assisted Navigation: Realized functionalities for assisted navigation typically foresee that users either manually mark desired target locations in a given map [102], select from a given list on a screen using buttons ([40, 41] and [76]), use switches to select a specific

labelled target location [39, 84], send orders via voice or via a remote like a Bluetooth or Wi-fi device [47], or the system interacts with the user via a dialogue system to determine the desired target location [44].

In terms of guiding behaviors, guidance can either be provided by controlling the robot motion, providing visual or auditory cues, or by mixed versions of the above.

Most platforms provide assisted navigation by controlling the robot motion behavior. Examples can be found e.g. in [44], where the Pearl robot guides people to desired target locations by estimating the person's velocity to properly online adjust the guiding speed.

In [45] an adaptive shared control with varying force gains evaluates the user's performance by combining multiple criteria like the proximity to obstacles, the deviation from the planned trajectory and human stability criteria to finally online shift the control authority between computer and human and with this to determine the robot motion behavior.

In [33] authors study three different navigation assistances under the assumption of a given static map and target in this map. The first implementation guides the user at constant speed with activated automatic path planning and obstacle avoidance. The second implementation uses automatic path planning and obstacle avoidance, but lets the user decides on the velocity. Finally, the third implementation advances the second one by the possibility of modifying the path by the user.

In [54] a goal seeking behavior is designed for an omni-directional mobile robot by evaluating laser sensor data and by fusing this assistive behaviors with further behaviors like obstacle avoidance and wall following by means of a Fuzzy Kohonen Clustering Network. The goal seeking behaviour is designed to redirect the mobile robot so that it moves again towards a desired goal direction, which comes from a path planning algorithm. The active robot behavior is limited to the angular velocity and is activated only in case the human applies intentional forces on the mobility assistant. The translational motion is commanded by the user by applying translational interaction forces to the mobility assistant.

The motion control algorithm proposed by the Ko group and implemented on the robot walking helper called "i-go" combines passive and active control modes [96]. The passive mode implements a braking control law to differentially steer the vehicle and guide the user, while the active mode realizes gravity compensation on slopes. The gain that controls the brakes is online adapted using the theory of differential flatness depending on the current user force and speed of the mobility assistant as well as the planned path of the robot to a given target destination.

Finally, in [102] authors propose an integrated approach for the context-specific, on-line adaptation of the assistance level of a rollator-type mobility assistance robot by gain-scheduling of low-level robot control parameters. A human-inspired decision-making model, the Drift-Diffusion Model, is introduced as the key principle to gain-schedule parameters and with this to adapt the provided robot assistance in order to achieve a human-like assistive behavior. Among context-aware sensorial and physical assistances, also cognitive assistance is provided to help the user following a desired path towards a predefined, pre-selected destination.

In contrary to these implementations that define the robot motion behavior to provide navigation assistance, authors in [28] developed a navigation assistance system that provides verbal and visual instructions and interfaces with a smart world with embedded RFID tags

for localization.

In [40] again arrows overlaid on a map are tested to guide users from a given start to a desired target point on a given map. In a slightly different implementation authors investigate a mixed mode of providing user assistance in form of controlled robot motion and visual cues. A passive, active and forced robot control mode are implemented on the platform [41]. The passive mode leaves full control over the trajectory by the user focusing only on obstacle avoidance, the active control shifts to full autonomous control and compares the user's estimated trajectory with the desired one and if a deviation greater than a certain given angle is detected the robot slows down and eventually halts if the user does not realign with the desired robot path. An additional user interface showing arrows that point into the direction of the next waypoint has been tested in this mode to communicate the robot intention to the user. In the forced mode the robot has full control over the platform motion and the user input is only used to switch the robot motion on and off.

Orthotic Functions

Cognitive orthotic functions that remind the user about routine activities and guide her/him to desired locations are rarely incorporated in today's mobility assistance robots. In [43, 90] authors develop a higher level reasoning software that provides cognitive orthotic assistance by reminding people about routine activities such as eating, drinking, taking medicine and using the bathroom. Three modules, a Plan Manager, a Client Modeler and a Personal Cognitive Orthotic are combined into the so called Autominder architecture. The plan manager models client plans as disjunctive temporal problems. The Client Modeler uses a reasoning formalism in form of a Quantitative Temporal Bayes Net. The Personal Cognitive Orthotic finally uses a Planning-by-Rewriting approach to create a high-quality reminder plan that satisfies the caregiver and client.

2.2.4 Health Monitoring

Health monitoring functionalities are among the more rarely implemented functionalities in mobility assistance robots.

In the PAMM system a continuous health monitoring system is installed that supervises the user's speed and applied forces as well as heart rate. Further, force/torque sensor data is used along with odometry information to study the user's gait and to analyze the stride-to-stride variability derived from the velocity power spectrum density [47].

The CAIROW walker records the statics of the user gait as basic health evaluation and monitoring function [50]. Gait analysis is specifically performed for patients with Parkinson disease by monitoring the step length, velocity, and acceleration of each leg for each step. As a result, the gait analyzer specifies the type of the gait as Festinating Gait (i.e. patient walks with small steps), Freezing of Gait (i.e. patient normally grips the handle tightly and their leg muscles become stiff), and Normal Gait (i.e. in other conditions). This statics of the patient's gait is aimed to be either used in the platform motion control or to help therapists in the rehabilitation process.

The mobility assistance robots Pearl and Flo are designed to collect statistical data on medication, daily living activities and even factors related to prediction of specific medical risks based on e.g. blood sugar and leg diameter, but this system has only been partially implemented [43, 90].

Summarizing, health monitoring functionalities have only rarely been combined with mobility assistance robots and are limited to basic functions like the analysis of heart rate and gait. More advanced and long-term health monitoring functionalities have not been explored yet. Similarly the implementation of training functions to gradually improve or maintain the current health status are not considered so far.

2.2.5 Extra Functionalities

Extra functionalities can be found in few of the surveyed mobility assistance robots. Occasionally basic functionalities for phone and Skype call, entertainment and social interaction as well as telepresence have been realized.

In [51] phone and Skype call possibilities for fast contact of the patient to a doctor are provided.

Flo and Pearl's speech recognition system is capable to understand a variety of questions related to daily living activities such as inquiries for the television program and the weather forecast ([42, 43, 90]). Thanks to wireless internet connection, the dialog manager can connect to a number of online external sources of information to provide answers to questions on a number of topics [42].

Emotional feedback as a higher level human-robot interaction is implemented in the Flo system, which is equipped with an actuated face and allows showing different facial expressions by modifying the angle of its mouth, eyebrows, and eyes [42].

Moreover, Flo allows for virtual visits of doctors or nurses using its telepresence interface consisting of an onboard camera and microphone that transmit the video and audio signals to a remote station, and a joystick on the remote side, which allows a health care giver, friend or relative to drive the robot around the user's rooms, and also direct the robot's gaze by controlling the head configuration [42].

Finally, in order to reduce the boredom of the exercise, authors in [51] developed an online music player for their walker. The platform is connected to the Internet, and allows users to select their preferred music.

2.3 Summary and Discussion

In this chapter a total number of 5 passive and 20 active rollator-type mobility assistance robots were reviewed from a perspective of system design and functionalities. Most reviewed systems were found to be active, based on four wheels and to have a non-holonomic kinematics, which is the same as the considered system for control development in this thesis. Main functionalities were identified as sit-to-stand and stand-to-sit transfer assistance, walking assistance, cognitive assistance as well as health monitoring.

In terms of sit-to-stand and stand-to-sit transfer assistance, three categories of robot control have been implemented: position control, force control and switching control. These

approaches mainly rely on results from hypothesis-driven experiments in which researchers investigated chair, subject and strategy-related determinants of STS-transfers to find best STS trajectories to be realized by the mobility assistance robot. However, concerning robot control, analysis of human STS transfers and posture stability mechanisms (both during unassisted and assisted STS transfers) could help to better understand underlying principles, to mathematically formulate them and to develop proper robot assistive controllers. To this end, chapter 3 goes beyond the state of the art and proposes computational models for unassisted and assisted STS transfers.

Concerning the walking assistance, performance of the system was found to be enhanced mainly by the tuning of control parameters that change the apparent impedance of the system based on high-level environment or user information. This approach was successfully realized to actively avoid obstacles and steps and compensate for gravity on slopes. So far, however, mainly fixed scheduling strategies have been employed in the tuning laws. In this respect, chapter 4 investigates context-dependent and dynamic authority sharing mechanisms involving methods for decision making, to determine adaptation laws for the MAR controller.

For human fall prevention, approaches were found that mainly aimed to determine the states like walking, stopped, and emergency. Moreover, the braking strategy when an emergency state is detected was found as the only available approach for human fall prevention in literature. The states of the human were also mainly identified by looking at the user's head and leg positions. These indeed can be improved by considering a MAR with actuated arms, and more sophisticated human fall detection and assistive approaches. The latter is investigated in chapter 5.

Furthermore, safety for MARs have received little attentions so far. It was considered in terms of posture stability measures, which are typically considered in the offline design phase (e.g. the robot force profiles and trajectories in STS assistances). However, a more elaborate safety analysis that goes beyond classical posture stability measures and includes the definition of posture-dependent safe states and safe robot behaviors considering for example the allowed energy exchange between user and robot is so far missing in current literature, but is of crucial importance because of the tight physical coupling of human and robot. Solutions for the user's safety are introduced in this thesis, especially in chapter 6 where an energy-based modeling and control approach is presented for reshaping the robot's behavior to enhance the user's safety if an unsafe situation is about to happen.

3 Biologically Inspired Sit-to-Stand Assistance

Human sit-to-stand (STS) transfers are a frequently exercised daily activity, which highly influence the quality of life for people who are no longer able to accomplish normal STS transfers due to either a specific or a more general muscle weakness.

Development of a proper STS assistance strategy to be provided by a MAR is one of the main goals of this thesis, and is discussed in this chapter. As reviewed in chapter 2, only a few assistance robotic devices are focused on supporting human STS transfers so far and their control can be grouped into three categories: motion control, force control and switching control (see section 2.2.1 for more details). These approaches barely incorporate computational models of natural STS transfer motions into the development of assisitive strategies. However, understanding and imitating the human behavior during STS transfers can provide a powerful tool to control assistance robots towards an intuitive and natural behavior of the coupled system of human and robot.

STS transfers have been mainly studied and analyzed in hypothesis-driven experiments, which led to a considerable amount of findings. Authors in [113] for example developed a correlation formula to derive power from body weight and standing up duration. Authors in [114] studied different phases and their duration for standing up and sitting down motions and [115] divided STS transfers into 4 phases and discussed characteristics of these phases. STS characteristics such as high torque and large range of motion in the lower limb joints during a normal STS were reported by [113, 114, 116]. Further, studies on the categorisation of different seat, subject and strategy-related classes were performed by [117]. In [118–121] authors studied average time, maximal hip flexion, knee extension angle and velocities for completion of a STS transfer. Modifications of CoM trajectories during STS transfers by lowering the horizontal and vertical CoM displacements were found to lead to a significant reduction of joint moments on the knee and hip, see [122]. Shifting the chair height from 65 to 115% of knee height resulted in a large change of moments in hip and knee joints, see [123]. Moreover, minimum peak joint moments and their relation to movement time were determined by studying a large set of experimentally collected kinematic data in [124, 125]. More findings about STS transfers are presented in reviews like [126] and [117].

While this way a huge variety of data has been analyzed by various researchers, only few computational models to study human STS transfers have been presented so far. In [127] and [128] authors investigated an optimal LQR formalism in the context of an optimal tracking controller combined with a fuzzy biomechanical model, which interpolates between two linearized models of the nonlinear four segment/bipedal dynamics around the sitting and standing position. They optimized physiological costs when tracking a predefined ankle, knee, hip, and pelvis reference trajectory [127, 129–132].

In [133] the author employed a cost function combining joint torques squared with absolute head orientation. The author argues that the first term increases efficiency of the motion, while the second term results in a stabilization of the head, but no comparison with

human data is performed allowing to judge whether this model is sufficient or appropriate to model human behavior in STS transfers. The same cost function has been adopted in [134] for the design of a STS mechanism.

In [135] authors employed dynamic optimization to determine optimal STS trajectories by considering a cost function that minimizes joint torques, torque change and the difference between left and right ground reaction forces based on sequential quadratic programming (SQP). They determined different weights of the single criteria for unassisted STS transfers of healthy subjects as well as amputees, but did not study assisted STS transfers. Moreover, critical balance criteria were not considered in their approach. Further, from an optimization point of view, SQP is considered a method of local optimization and thus, may lead to suboptimal solutions, while global methods based on the Hamilton-Jacobi-Bellmann equations and dynamic programming typically suffer from the curse of dimensionality. Both is problematic when considering biomechanical problems, as they are typically high-dimensional and involve model uncertainties [136]. Differential Dynamic Programming (DDP) and Iterative Linear-Quadratic Gaussian (ILQG) have been proposed in literature to overcome aforementioned limitations. They solve the optimization problem by dynamic programming, and lead to feedback control laws. Both are methods based on Optimal Feedback Control (OFC) that have shown to be a powerful tool to study biological movements and interpreting human motor behavior [136].

This chapter proposes biologically-inspired and optimal assistance approaches to be provided by MARs. It extends the state of the art on STS assistance with respect to the following aspects: i) mathematical modeling of the human's STS transfers and exploiting their underlying principles, ii) extension of the obtained models to derive the optimal and biologically-inspired assistive strategies to be provided to the users, and iii) intensive evaluation by real end-users. Unassisted and assisted STS transfers are formulated as optimal feedback control problems and are solved using an iterative optimal control approach to derive optimal assistive strategies to be provided by an assistance robot. Optimal assistive strategies for subjects characterized by a specific or more general muscle weakness are studied, and optimal trajectories are derived. We employ DDP that iterativelly quadratically approximates the nonlinear system dynamics and the optimal cost-to-go function around the current trajectory. It takes physical control constraints like torque limitations into account, while human balance-related criteria are considered in the cost function. The modelling approach for unassisted STS transfer is validated for 3 different human healthy subjects and 9 elderly/patient subjects by comparing simulations and experimentally collected data. Finally, the STS model has been used to determine user-specific optimal assistive trajectories for 33 elderly, mostly not able (or hardly able) to perform unassisted STS transfers. The obtained trajectories have been implemented on a robotic mobility assistant and intensively tested by the same subjects in a formal user study. The validation results show a promising success rate of achieved STS transfers.

This chapter is organized as follows: STS transfer modeling is formulated as an optimal feedback control problem in section 3.1. Section 3.2 reports on capturing of experimental data, evaluates the model and compares simulation with experimental results. Section 3.3 presents obtained optimal STS assistive trajectories for different subject classes as well as results of the performed user study with the mobility assistance robot. Section 3.4 finally

concludes the chapter and presents some final remarks.

3.1 STS Transfers formulated as Optimization Problem

In the following subsections the STS transfer task is formulated as an optimal feedback control problem with a nonlinear cost function subject to control constraints. An approximative optimal control approach based on DDP (firstly introduced by [137] and recently reformulated by [138]) is employed to allow for an efficient solving of this optimization problem.

3.1.1 Human-Biomechanical Model

While a triple inverted pendulum has been widely studied as a simplified biomechanical model of the human in biomechanics and biomedical literature (e.g. [139]), in this thesis a model consisting of five joints and six rigid bodies [1] involving foot, lower leg (shank), upper leg (thigh), trunk (torso and head), lower and upper hand is considered, which moves in the sagittal plane as shown in Fig. 3.1. The ankle, knee, hip, shoulder and elbow joint torques are used to control the motion of the model. The equations of motion are derived using the Euler-Lagrange method. The nonlinear dynamics of the biomechanical model is given by

$$\boldsymbol{M}(\boldsymbol{\theta})\ddot{\boldsymbol{\theta}} + \boldsymbol{C}(\boldsymbol{\theta}, \dot{\boldsymbol{\theta}}) + \boldsymbol{G}(\boldsymbol{\theta}) = \boldsymbol{\tau} + \boldsymbol{\tau}_{ext} = \boldsymbol{\tau}_{tot} \tag{3.1}$$

where $\boldsymbol{M}(\boldsymbol{\theta}) \in R^{5\times5}$ is the positive definite symmetric inertia matrix, $\boldsymbol{C}(\boldsymbol{\theta}, \dot{\boldsymbol{\theta}}) \in R^5$ the vector of Coriolis and centripetal forces, and $\boldsymbol{G}(\boldsymbol{\theta}) \in R^5$ the gravitational force vector, while $\boldsymbol{\theta} \in R^5$ refers to the joint angle vector with ankle ($\boldsymbol{\theta}_1$), knee ($\boldsymbol{\theta}_2$), hip ($\boldsymbol{\theta}_3$), shoulder ($\boldsymbol{\theta}_4$) and elbow ($\boldsymbol{\theta}_5$) angles, $\boldsymbol{\tau} \in R^5$ the joint torques and $\boldsymbol{\tau}_{ext} \in R^5$ the torque due to external assistive generalized forces applied to the human.

The equations can be written as first order dynamic system with $\boldsymbol{x} = [\boldsymbol{\theta}, \dot{\boldsymbol{\theta}}]^T \in R^{10}$

$$\dot{\boldsymbol{x}} = \boldsymbol{f}(\boldsymbol{x}, \boldsymbol{\tau}) = \begin{pmatrix} \dot{\boldsymbol{\theta}} \\ -\boldsymbol{M}(\boldsymbol{\theta})^{-1}(\boldsymbol{C}(\boldsymbol{\theta}, \dot{\boldsymbol{\theta}}) + \boldsymbol{G}(\boldsymbol{\theta}) - \boldsymbol{\tau}_{tot}) \end{pmatrix}. \tag{3.2}$$

Considering $\boldsymbol{F} \in R^m$ external generalized forces applied to a specific point on the human model, and $\boldsymbol{J}_k(\boldsymbol{\theta}) \in R^{m\times5}$ the Jacobian associated to this point, then $\boldsymbol{\tau}_{ext}$ is given by

$$\boldsymbol{\tau}_{ext} = {\boldsymbol{J}_k}^T(\boldsymbol{\theta})\boldsymbol{F}. \tag{3.3}$$

Please note that in the unassisted case, we adopt a simplified version of this model controlled by three joint torques (hand segments not actuated). Moreover, in case of assisted STS transfers we study two different supporting points based on the level of the patient's demand advised by nurse specialists: i) on the upper body under the patient's shoulders and ii) at the hands.

[1] Stiffness of the human segments, specially arms, is neglected in the model assuming that the human willingly accomplishes the STS task and thus, reacts very stiff to external forces.

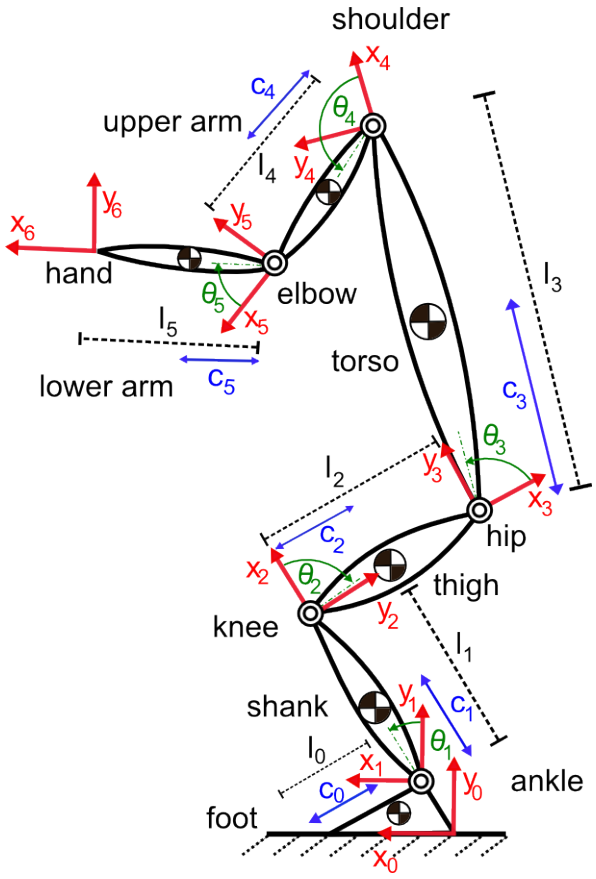

Figure 3.1: Rigid body biomechanical model of the human, l_i and c_i represent the length and center of gravity of the segments while x_i,y_i are the reference frames attached to each joint.

3.1.2 Balance and Task End-Point Accuracy Criteria

To determine human balance and postural stability during STS transfers, the virtual zero moment point (for abbreviation ZMP) is evaluated. As summerized by [140], the ZMP is a point on ground level where the pressure between the foot and ground is replaced by a force which can balance active forces acting on the human dynamics during the motion. ZMP can be computed from the vertical component of contact moment $\boldsymbol{T}$ and the horizontal component of contact force $\boldsymbol{F}$ as follows:

$$\boldsymbol{p}_{zmp} = \frac{\boldsymbol{T}}{\boldsymbol{F}}. \tag{3.4}$$

Task end-point accuracy is determined using the center of mass (COM):

$$\boldsymbol{p}_{com} = \frac{\sum_{i=1}^{6} \boldsymbol{m}_i \hat{\boldsymbol{p}}_i}{\sum_{i=1}^{6} \boldsymbol{m}_i}, \tag{3.5}$$

where $\boldsymbol{m}_i$ is the mass of the i^{th} segment and $\hat{\boldsymbol{p}}_i$ the position of its center of gravity.

3.1.3 Formulation of Optimization Problem

The STS optimal control problem is formulated as follows: The human sitting position with zero joint velocities is considered the initial state at time $t = 0$ and the position of the COM in the steady-state standing position is considered the desired final state of the system at time $t = T$. The main goal is to find a control law $\boldsymbol{\tau}^* = \pi(x, t)$ that stays within joint torque limits and that drives the system states smoothly from the initial to the final configuration while minimizing a given cost function.

We consider three main features when defining the cost function of the optimization problem: user's *energy* consumption, *smoothness* of motion and control as well as user's *balance*. Minimization of energy is achieved by the effort term C_4 in (3.6) that tries to achieve a minimum time response and thus, a minimization of energy as joint torques are much lower in the standing than in the sitting configuration (when neglecting the interaction forces with the chair). Smooth control is achieved by the torque change term C_3, while the jerk term C_2 improves smoothness of the resulting motion. As humans automatically try to stabilize their movement patterns, human balance criteria C_1 based on the ZMP are included as well [2]. The following combination of criteria is used to model the STS transfer task:

$$\boldsymbol{\phi}_{total} = \boldsymbol{\phi}_{final}(\boldsymbol{x}) + \int_0^T \Big(\sum_{i=1}^{6} \boldsymbol{C}_i \Big) dt \tag{3.6}$$

with

$$\begin{aligned}
\boldsymbol{\phi}_{final} &= \boldsymbol{\phi}_{f1} + \boldsymbol{\phi}_{f2} \\
\boldsymbol{\phi}_{f1}(\boldsymbol{x}(T)) &= |\boldsymbol{p}_{com}(\boldsymbol{x}(T)) - \boldsymbol{p}_{com}^{tar}|^2_{\boldsymbol{W}_{f1}} \\
\boldsymbol{\phi}_{f2}(\boldsymbol{x}(T)) &= |\dot{\boldsymbol{\theta}}(T)|^2_{\boldsymbol{W}_{f2}} \\
\boldsymbol{C}_1(\boldsymbol{x}(t), \boldsymbol{\tau}(t)) &= |\boldsymbol{p}_{zmp}(\boldsymbol{x}(t), \boldsymbol{\tau}(t)) - \boldsymbol{p}_{zmp}^{max}|^2_{\boldsymbol{W}_1} \\
&\quad + |\boldsymbol{p}_{zmp}^{min} - \boldsymbol{p}_{zmp}(\boldsymbol{x}(t), \boldsymbol{\tau}(t))|^2_{\boldsymbol{W}_1} \\
\boldsymbol{C}_2(\boldsymbol{x}(t)) &= |\ddot{\boldsymbol{\theta}}(t)|^2_{\boldsymbol{W}_2} \\
\boldsymbol{C}_3(\boldsymbol{\tau}(t)) &= |\dot{\boldsymbol{\tau}}(t)|^2_{\boldsymbol{W}_3} \\
\boldsymbol{C}_4(\boldsymbol{\tau}(t)) &= |\boldsymbol{\tau}(t)|^2_{\boldsymbol{W}_4} \\
\boldsymbol{C}_5(\boldsymbol{x}(t)) &= |\max(0, \boldsymbol{x}(t) - \boldsymbol{x}_{max})|^2_{\boldsymbol{W}_5} \\
&\quad + |\max(0, \boldsymbol{x}_{min} - \boldsymbol{x}(t))|^2_{\boldsymbol{W}_5} \\
\boldsymbol{C}_6(\boldsymbol{F}(t)) &= |\boldsymbol{F}(t)|^2_{\boldsymbol{W}_6}
\end{aligned}$$

and $\boldsymbol{W}_{f1}$, $\boldsymbol{W}_{f2}$ weighting matrices for the terminal costs evaluated at the desired human COM position $\boldsymbol{p}_{com}^{tar}$ in a standing position at time T with zero joint velocities, $\boldsymbol{W}_1$ the weighting matrix for the human balance term that aims to satisfy $\boldsymbol{p}_{zmp}^{min} \leq \boldsymbol{p}_{zmp}(\boldsymbol{x}, \boldsymbol{\tau}) \leq \boldsymbol{p}_{zmp}^{max}$

[2] Please note that a precise study of the human balance behavior during a STS is out of focus of this thesis, but is a very interesting biomechanical research question. Currently no study focusing on the balance criteria used during a human STS transfer that could inform the selection of these criteria could be found in literature and therefore regulation of the human ZMP position has been considered as a postural regulator as proposed by [141].

[3], and $\boldsymbol{W}_2 = diag(w_{2a}, w_{2k}, w_{2h})$, $\boldsymbol{W}_3 = diag(w_{3a}, w_{3k}, w_{3h})$, $\boldsymbol{W}_4 = diag(w_{4a}, w_{4k}, w_{4h})$ the weighting matrices for the human jerk, minimum torque change and effort terms respectively, where the term $diag(.)$ represents a diagonal matrix[4] and $|\mathtt{v}|^2_{\boldsymbol{W}} = \mathtt{v}^T \boldsymbol{W} \mathtt{v}$. The weighting matrix $\boldsymbol{W}_5$ is responsible for the human joint angle and velocity boundaries $\boldsymbol{\theta}_{min} \leq \boldsymbol{\theta}(\boldsymbol{t}) \leq \boldsymbol{\theta}_{max}$ and $\dot{\boldsymbol{\theta}}_{min} \leq \dot{\boldsymbol{\theta}}(\boldsymbol{t}) \leq \dot{\boldsymbol{\theta}}_{max}$. The weighting matrix $\boldsymbol{W}_6$ is considered to minimize the interaction forces exchanged between assistance robot and human and therefore is considered equal to zero for the case of unassisted human STS modeling. The cost function is finally considered subject to constraints of the system dynamics formulated in (3.2) and control constraints, i.e. $\boldsymbol{\tau}_{min} \leq \boldsymbol{\tau}(\boldsymbol{x}, \boldsymbol{t}) \leq \boldsymbol{\tau}_{max}$.

3.1.4 Optimal Feedback Control

We solve this optimal control problem using Differential dynamic programming (DDP) first proposed in [137] and recently reformulated by [138]. This approach iteratively, quadratically approximates the costs and the nonlinear system dynamics around the current trajectory. Then, an approximately optimal control law is found by designing an affine controller for the approximated system that enforces formulated control constraints. More details to the algorithm is presented in Appendix B.

For our specific STS transfer problem we consider pure gravity compensating forces as an initial guess of the control sequence, which is then iteratively improved by the algorithm with respect to the formulated cost function.

The algorithm shows quadratic convergence in the vicinity of a local minimum, similar to Newton's method as presented by [142] and returns the optimal control and the corresponding state sequences.

3.1.5 Inverse Optimal Control to Determine Cost Function Weighting Factors

Deriving a proper set of weighting factors for the cost function is crucial to properly model human STS transfers. We employ an Inverse Optimal Control (IOC) approach to identify underlying optimality criteria of STS motions either for healthy subjects or patients. Inverse Optimal Control allows to identify unknown parameters in the cost function (in our case the weighting factors as defined in section 3.1.3) for a set of recorded human STS trajectories. We adapt the methodology proposed by [143] to our specific problem of human STS motions.

Given a set of recorded user's STS motions, a cost function for the bilevel optimization

[3] The base of support (BOS), which determines the values of $\boldsymbol{p}^{min}_{zmp}$ and $\boldsymbol{p}^{max}_{zmp}$), typically includes the size of the feet and the room between them for a human without external support, respectively unassisted STS. For the assisted case, when the human firmly grasps the robot handles a larger BOS area can be considered. Since this, however, requires detecting whether the human stably grasps the handles, we decided to simplify the problem and to consider the most restrictive case defined by the BOS of the human user only.

[4] Please note that same values on diagonal elements are considered for each weighting matrix.

problem is formulated as follows,

$$\min_{\boldsymbol{W}} \quad \sum_{j=1}^{m} ||\boldsymbol{x}^*(\boldsymbol{W}, t_j) - \boldsymbol{x}_M(t_j)||^2 \tag{3.7}$$

where the sum of the Euclidean distance between experimentally recorded states $\boldsymbol{x}_M(t_j)$ and the results of the optimal control model $\boldsymbol{x}^*(\boldsymbol{W}, t_j)$ is used to determine optimal values for the weighting factors $\boldsymbol{W}$. The bilevel optimization handles iterations over weighting factors such that the best fit between measurements and the solution of the original optimal control problem formulated in section 3.1.3 is found. For each iteration the obtained solution of weighting factors resulting from the bilevel optimization problem is passed to the lower level where the original optimal control problem is solved and obtained results are reported back to the bilevel where (3.7) is evaluated for the next iteration.

We employed the Matlab *fmincon Trust Region Reflective Algorithm* solver to solve the bilevel optimization problem. Box constraints for each weighting factor were specified to define a search space for the solver.

3.1.6 User-group Optimized STS Assistance

Finally, we use the already introduced biomechanical model and optimization approach to calculate optimal assistive strategies for the robotic assistant that is used to support subjects in STS transfers. We implement assistive strategies that are tailored to the specific class and weakness of a certain subject.

In [144] a classification scheme for transfer assistance was proposed that considers the request for supervision, type of assistance and participation of targeted persons. Here we focus on the two classes of *maximal assist*, "the patient contributes with less than 25% of the required effort to accomplish the STS task ", and *moderate assist*, "the patient contributes with at least 50% of the required effort to accomplish the STS task". As proposed by nursing specialists, the most common techniques for assisting persons in STS transfers belonging to the maximal assist class foresee that the caregiver stands in front of the person to be assisted, locks the knees and feet of the patient, grips the patient at the upper trunk and lifts the person. Stronger patients belonging to the moderate assist class require less physical assistance, but more balance support. In this case, the caregiver stands in front of the patient, grasps the hands and applies forces to assist in the STS transfer, while simultaneously assisting in keeping the patient's balance.

Moreover, the weakness may be either limited to specific segments of the body because of a certain disease or surgery (*case a*), or spread over multiple segments (*case b*).

For the *maximal assist* class, we considered that the required assistance is applied to the upper body under the patient's shoulders. For the *moderate assist* class, the interaction point is considered on the human hands. By solving the aforementioned optimization problem we determine optimal assistive strategies in form of robot motion trajectories. Doing so, we consider torque constraints in the optimal control problem, which are based on the level of the weakness in human segments (as discussed above), and constraints on the assistive forces to be applied at the contact point(s).

The accuracy and usefulness of obtained assistive strategies highly depends on the

proposed human STS model, which has to be carefully validated. Therefore, in the following sections we study the validity of the proposed model, first for healthy subjects and then for elderly and patients.

3.2 Validation of STS Model

In order to determine weighting factors and test the quality of the STS model against real measurements, we performed a set of STS transfer experiments with healthy and elderly subjects, where both cases of unassisted and assisted STS transfers were studied. In the following sections, we report on the validation methods and obtained results.

3.2.1 Data Capturing

Capturing of STS transfer motions has been performed in two sessions, first for healthy subjects and then for patients.

Healthy Subjects

We performed STS transfer experiments with three healthy male subjects to test the quality of the STS model against real measurements. Their body measurements are presented in Appendix A.

Participants were instructed to perform a few practice trials in order to find a comfortable feet placement. They were asked to keep their feet fixed to the ground, their arms crossed over the chest, and their upper body straight during the whole experiment (see Fig. 3.3). Each subject was asked to repeat five STS transfers at a natural speed while the seat heights were adjusted on an armless office chair to fit the lower leg length. Since a set of pre-performed experiments with different subjects showed that typically people leave the chair with upper-body inclination of about 30 degree (where zero represents the upright trunk position), the subjects were asked to start the STS transfer with about 30-degree initial inclination in order to reduce the effect of not-modeled chair support and therefore allow for a fairer comparison of model and experiments.

An Xsens MVN inertial motion capture system, see [145], was used for full-body human motion capture. The subjects were asked to wear the Xsens MVN motion capture suit which consists of MTx miniature inertial measurement units with 3D linear accelerometers, 3D rate gyroscopes and 3D magnetometers. These trackers are placed at strategic locations on the human body (in the suit), to measure motion of the whole body including 23 segments (22 joints). The accuracy of the Xsense system is highly dependent on the calibration procedure, where subjects are asked to keep their body in some predefined configurations. The calibration has been performed for every subject before starting recordings. In the performed experiments a very good visual observable accuracy was achieved since the healthy subjects could easily keep their body in the requested configurations, but as no ground truth with an external tracking system was available no absolute numbers for the achieved accuracy can be given. Kinematic data including segment position and orientation, velocity and acceleration were captured with a sampling rate of 120 Hz.

Every STS transfer was assumed to start from the static configuration in the sitting position and to finish when the user arrives at the fully standing position with zero joint velocities. The average STS transfer movement time for all subjects was found to be in the range of 1 to 2.5 seconds.

The experiments took place in the Chair of Automatic Control Engineering in September 2013, under ethical approval by the Etics review committee (Etikkomission, Fakultät für Medizin, Technische Universität München, Ismaninger Str. 22, 71675, Munich, Germany).

Elderly Subjects

Validation of the proposed STS model was performed using a set of recordings from 9 elderly with varying age and gender (5 male and 4 female, from 75 to 87 years old) performing unassisted and assisted STS transfers. The recruitment of the participants was decided based on their cognitive and motor status. In general we targeted subjects with mild to moderate impairment levels.

Subjects were included if they met the following criteria: (1) unable to stand up and sit down unassisted from a normal chair or 5-chair stand test ([146]) >16.7s and (2) habitual gait speed <0.6m/s. The cognitive impairment was screened with the Mini-Mental State Examination ([147]) classifying patients into no, mild to moderate, or severe cognitive impairment if MMSE provides test scores ≥26, 17–26 or <17, respectively. The participant metadata consists of information about sex, age, height, weight as well as the cognitive and motor impairment level are presented in Appendix A.

The experiments took place in the Agaplesion Bethanien Hospital/Geriatric Centre of the University of Heidelberg in November 2013, with the ethical approval by the Ethics review committee (Ethikkommission der Medizinischen Fakulteat Heidelberg, Alte Glockengießerei 11/1, 69115 Heidelberg, Germany).

Two general variations of tasks were asked to be performed by patients in order to determine optimal policies regarding STS transfers:

a. Unassisted STS transfers: 3 repetitions of STS transfers performed in the patient's own preferred way without providing any instruction for initial configuration, hand or feet positions. This was an optional task and was only performed if the patient was able to accomplish unassisted STS transfers.

b. Assisted STS transfers: 3 repetitions of STS transfers when a passive rollator was positioned in front of patients and they were asked to grasp its handles to receive physical support while performing STS transfers.

The passive rollator was equipped with two 6 DOF force/torque sensors of type JR3 45E15 mounted on the rollator's handles. Figure 3.2 presents the snapshots taken during the unassisted and assisted STS experiments by one elderly.

Motion of the subjects was captured using a Qualisys system with 8 infrared cameras mounted on tripods and placed around the recording area. A suitable marker set including 48 reflective markers was used to track the limb movements. The accuracy of the Qualisys tracking system depends on the type of camera chosen, the number of cameras used in the experiment, the size of the tracking environment, the selection of the marker sets and

Figure 3.2: Snapshots taken during the unassisted and assisted STS experiments performed by elderly.

how the markers are fixed on the moving segments: In the performed experiments, the accuracy of 0.7mm was achieved for tracking each of the markers. Markers were selected to result in least possible occlusions when tracking the whole body and based on suggested marker sets of the manufacturer of the system. However, the biggest source of inaccuracy (which should not be more than 1 cm although we have no direct possibility to measure it) comes from the installation of markers on the subjects. Tapes were used to fix the subject clothes in the vicinity of each marker to guarantee an as stable as possible marker position. Nevertheless, movements of the subject may have resulted in a slight shift of the markers with respect to the human skin. The usage of special stretch clothes with free arms and legs was unfortunately declined by most elderly subjects and thus, the usage of strips was considered as a good compromise.

The motion capture data was post-processed in two steps: cleaning of raw data and labeling of marker trajectories using the QTM-manager software [5], reconstruction of the human model and extracting the motion data using Visual3D software. We used extracted

[5]This required that the image-based 3D-recordings of the trials were cleaned from gaps, phantom markers, flickering and other inconsistencies which occurred due to occlusions, reflections, loose clothes of the patient, missing markers, and other unexpected incidences during the recordings. Moreover, marker trajectories that have been mismatched by the automatic marker identification algorithms of the software had to be identified and reassigned manually.

human joint angles, velocities and accelerations for the computation of joint torques based on the human inverse dynamics.

3.2.2 Validation Method

Captured data was preprocessed to remove noise using a low-pass filter with 5 Hz cut-off frequency. Parameters of the biomechanical model were estimated for all subjects using regression formulas provided by [148], see Table 3.1 for results of subject S1. Based on the captured motion data, human torques and the COM trajectories were estimated based on the human inverse dynamics for each STS transfer motion.

Next, the proposed optimal control approach for simulating natural STS transfers was evaluated by comparing simulations with measurements. For each simulation, the same experimental conditions of initial upper body inclination and chair height as well as task completion time were considered. The weighting factor was selected according to the obtained values from the inverse optimal control approach, see section 3.2.3 for more details. Moreover, simulated STS trajectories were derived using the optimization approach described in Section 3.1. Finally, simulation data was compared with captured data from the instance where subjects left the chair as we did not consider the effect of the chair support in our simulations. The joint configuration at this instance with zero velocity was used as initial condition for the optimization algorithm.

Table 3.1: Estimated anthropometric limb data for subject one

	length $[m]$	COG $[m]$	mass (half body) $[kg]$	inertia (half body) $[kg.m^2]$
foot	0.11	(0.115,0.01)	1.434	–
shank	0.414	0.257	3.346	0.0476
thigh	0.459	0.224	9.56	0.2431
trunk	0.736	0.431	22.66	2.6967

3.2.3 Weighting Factors

Deriving proper weighting factors for the cost function is one of the most critical steps in order to achieve an acceptable STS modeling performance. An inverse optimal control approach was applied for each trial and subject to determine the corresponding weighting factors best fitting to the presented cost function for replicating human STS transfers. Only joint angles were required as input data for unassisted STS transfers, performed either by healthy or elderly subjects. For assisted STS transfers additionally the measured forces at the robot handles were taken into account. In order to determine the subject's weakness, the following steps were performed: first, required joint torques were computed based on the recorded motion data to determine required torques for a successfully performed STS transfer. Then, the recorded external force profiles were transformed into joint torques.

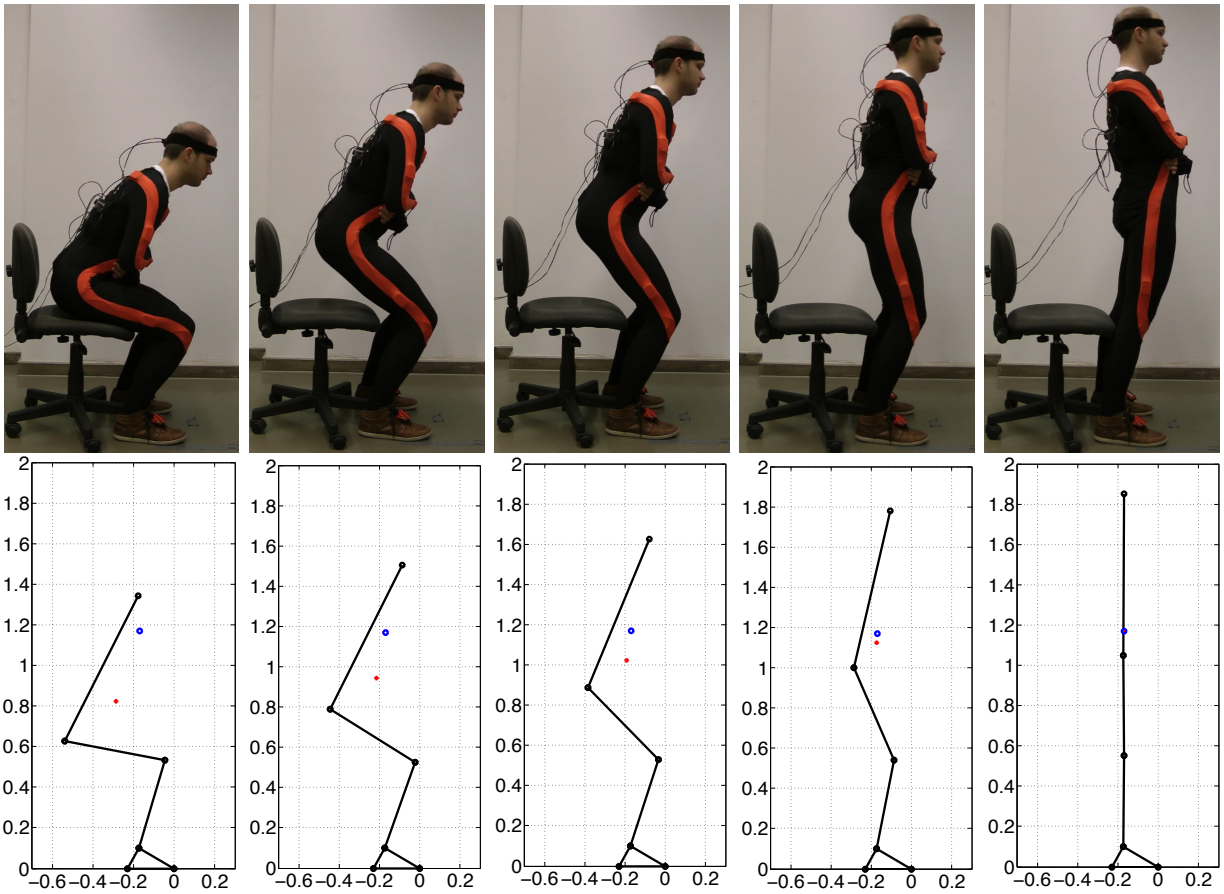

Figure 3.3: Snapshots taken during a human STS transfer (first row) and corresponding simulation results (second row). The blue and the red dots are the COM's position at the desired final and current states respectively.

Finally, the required assistance was estimated by relating joint torques from the provided assistance to the total required joint torques for a successful STS transfer.

Since a STS transfer is a complex task, in the following section we investigate the effects of each weighting factor on the overall combination of different criteria used to model the STS motion. Moreover, we report on the obtained weighting factors using the bilevel optimization approach for each group of subjects.

Qualitative Sensitivity Analysis of Weighting Factors

To get an understanding for the sensitivity of results on varying weighting factors, each weighting factor was manipulated manually and the model accuracy was checked by comparing simulation results with obtained measurement data. Generally for all cases of experiments with healthy and elderly subjects, good modeling accuracy was obtained when the largest weighting factors were specified for the joint angle and velocity limits ($\boldsymbol{W}_5$) to effectively remove unfeasible motions. To guarantee human balance (specifically for the case of assisted STS, see section 3.3), the corresponding weighting factors ($\boldsymbol{W}_1$) need a high priority too, while lower values are required for the minimum jerk, minimum effort, and minimum torque change terms. For the minimum jerk term ($\boldsymbol{W}_2$) small changes

in its weighting factor were found to result in a rather high variation of simulated STS transfers. Reducing the value resulted in a relative high velocity impulse close to the end of the STS transfer and increasing the value resulted in smoother trajectories with a comparable deceleration at the end of the motion. Regarding the minimum effort term, smaller weighting factors of ($\boldsymbol{W}_4$) for the knee compared to the hip and both smaller compared to the ankle resulted in a better modeling accuracy as the highest and lowest contribution for a STS transfer were observed to come from the knee and ankle, respectively. Concerning the minimum torque change term ($\boldsymbol{W}_3$), low values of the weighting factor resulted in smoother motions and control profiles while larger values produced non-human like behavior.

Final term conditions ($\boldsymbol{W}_{f1}$, $\boldsymbol{W}_{f2}$) in the cost function were also found to be a very important factor in the optimization. Selecting low values, no control in the sagittal plane was possible. On the other hand, very large values overruled all other factors in the cost function and thus, led to an immediate termination of the optimization as no improvement over iterations could be achieved. We found that the body weight strongly influences the final STS model performance that required to consider these weighting factors in proportion to the user's weight w.

Obtained Weighting Factors by Inverse Optimal Control

Using Inverse Optimal Control a series of weighting factors was finally determined for the cost function (3.6). Table 3.2 shows mean values of the obtained weighting factors for the three cases of healthy, unassisted elderly and assisted elderly STS transfers [6], while Fig. 3.4 also shows information on standard deviations. For the sake of presentation the values in Fig. 3.4 are normalized with the maximum values for each weighting factor found over all trials. Weightings for final terms as well as joint constraints are not shown since no variation (or only negligible variations) were found. Since the joint constraints have to be satisfied during the sit-to-stand motion, their corresponding weightings for the boundary conditions ($\boldsymbol{W}_5$) were considered as constant large value for all cases and were removed from IOC. However, the corresponding weights for the final terms ($\boldsymbol{W}_{f1}$ and $\boldsymbol{W}_{f2}$) were found to be a function of the subject's total weight w as reported in Table 3.2[7].

Focusing on the variation of the weighting factors, mean values of weighting factors $\boldsymbol{W}_1$ and $\boldsymbol{W}_2$ were found to be most similar between healthy and assisted elderly groups, while a very small variation was found for $\boldsymbol{W}_3$ for all groups. According to the obtained weighting factors healthy and assisted elderly subjects minimized more torque on the ankle than knee and hip ($W_{4,a} > W_{4,k} > W_{4,h}$), see Table 3.2. However, no such prioritization was observed for the unassisted elderly subjects. A considerable variation for different subjects was found in most of the weighting factors for assisted elderly subjects (maximum for $\boldsymbol{W}_1$ and the lowest for $\boldsymbol{W}_3$), than for the unassisted elderly.

[6] The box constraints in the bilevel optimization (eq. 3.7) were considered mostly in the range of $W_i * 10^{-2}$ to $W_i * 10^{-2}$ in order to consider a relatively large search space.

[7] Please note that no correlation analysis has been performed on other weighting factors of the cost function

Table 3.2: Mean value of the cost function weighting factors.

weights	healthy	unassisted elderly	assisted elderly
$\boldsymbol{W}_{f1}$	$w \times 10^5$	$w \times 10^5$	$w \times 10^5$
$\boldsymbol{W}_{f2}$	$w \times 10^2$	$w \times 10^2$	$w \times 10^2$
$\boldsymbol{W}_1$	188.9	57.2	236.6
$\boldsymbol{W}_2$	$18.2 \times \text{diag}(1,1,1)$	$1.012 \times \text{diag}(1,1,1)$	$26.21 \times \text{diag}(1,1,1)$
$\boldsymbol{W}_3$	$10^{-3} \times \text{diag}(1,1,1)$	$10^{-3} \times \text{diag}(1,1,1)$	$10^{-3} \times \text{diag}(1,1,1)$
$\boldsymbol{W}_4$	$10^{-3} \times \text{diag}(15,2,0.5)$	$10^{-3} \times \text{diag}(60,6,3)$	$10^{-3} \times \text{diag}(63,62,67)$
$\boldsymbol{W}_5$	10^5	10^5	10^5

3.2.4 Validation Results

Validation of the finally obtained models was performed by comparing simulations with mean values of the weighting factors (reported in Table 3.2) and experimental results. The user's COM position and joint torques observed during STS transfers and averaged over the captured trials (5 times for healthy subjects and 3 times for elderly) were chosen for comparison of simulation and experiments. A first comparison showed that similar STS strategies were selected by different subjects in each group.

To provide a measure for the overall model accuracy, for all subjects the normalized integral of the error between experiments and simulation was computed as

$$e_v = \frac{\int |v_{exp}(t) - v_{sim}(t)|dt}{\int |v_{exp,max} - v_{exp,min}|dt}$$

where v_{exp} and v_{sim} refer to data in experiments and simulation respectively, with $v_{exp,max}$, $v_{exp,min}$ the maximum and minimum value of experiments. This error was evaluated over the x and y components of the COM position (e_{comx}, e_{comy}) and the ankle, knee and hip torques ($e_{\tau a}, e_{\tau k}, e_{\tau h}$). The obtained results for all 3 cases of healthy, unassisted and assisted STS transfers are shown in Fig. 3.5. The maximum average error was obtained for unassisted elderly subjects in the ankle and hip torques. This is mainly due to the fact that most of the elderly subjects tried to benefit from external assistance using their hand to initially push their body up in unassisted STS transfers, see Fig. 3.2. This resulted in a small mismatch between the proposed STS model and experiments. Considering the complexity of the problem and the simplified assumptions for the human model, the errors in all 3 studied cases are considerably low and illustrate an overall high agreement of model and measurements.

As similar results were obtained for the performed repetitions in each group and for the sake of presentation we only present simulation and measurement trajectories for the COM position for five repetitions as well as joint angles and joint torques for one repetition in Fig. 3.6.[8] As can be seen all 3 joints as well as COM smoothly converge to their stable final

[8]Please note that although subjects were asked to minimize variation, still non-negligible differences were observed, especially for initial upper body inclination and feet positions.

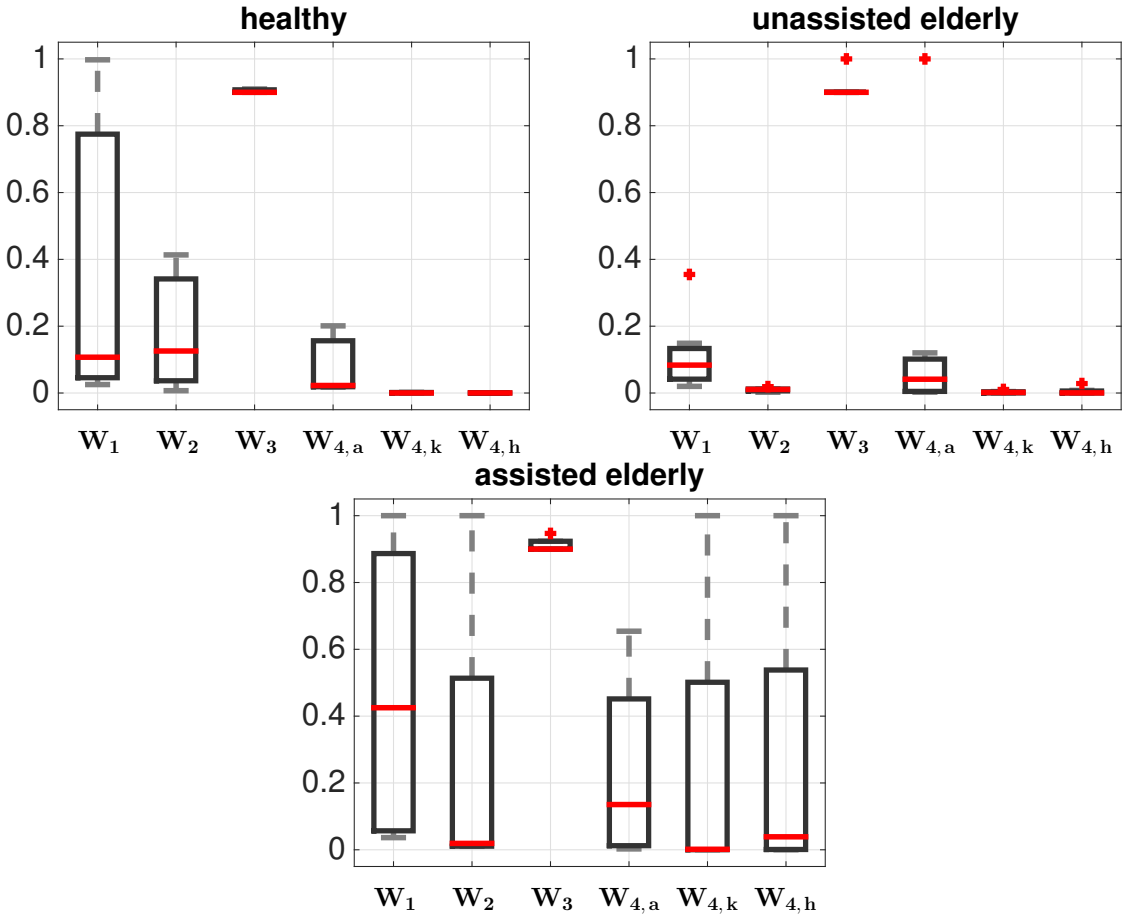

Figure 3.4: Normalized value of the obtained weighting factors for different STS transfers performed by different user-groups. Box plots represent the distribution of the weightings for different subjects in each group with respect to the mean value (red lines), while dashed gray lines present the standard deviation.

configurations, which is well captured by the model in all cases. The initial errors for the user's joint torques between simulations and corresponding experiments resulted mainly from neglecting the supportive chair effect, more specifically from neglecting initial subject velocities and accelerations at the instance of leaving the chair. A series of snapshots for above-mentioned STS transfers and corresponding simulation results are shown in Fig. 3.3 to further depict the similarity of the results. As can be observed the user leaves the chair while having almost 45 degree upper body inclination.

3.3 Robot-Assisted STS Transfers

In the following subsections we first report on optimization results obtained when taking into account external assistive forces. Then, we report on the realization of the proposed user-adapted STS transfer assistance with an assistance robot and a performed user study with elderly.

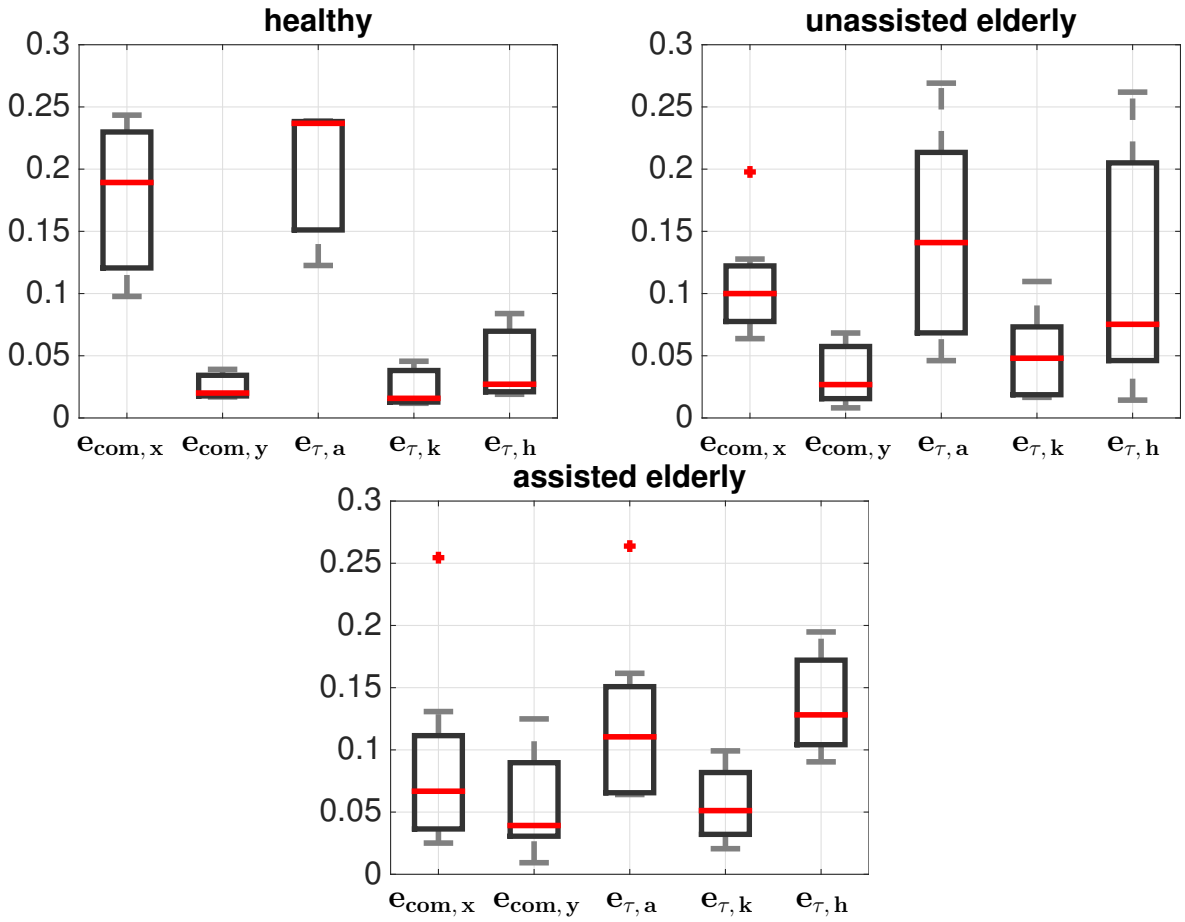

Figure 3.5: Normalized integrated error between simulation and experiments of STS transfers performed by different user-groups. Box plots show the distribution of the errors with respect to the mean value (red lines), while dashed gray lines present the standard deviation.

3.3.1 Optimization Results considering External Assistance

We implemented assistive strategies that are tailored to the specific class and weakness of a certain subject. We specifically report on simulation results for the two tailored assistive strategies of a maximal and moderate assist class as well as two patient categories with general or more specific muscle weakness (see section 3.3). The weighting factors are considered as the mean value of the assisted elderly obtained from the model validation study and reported in section 3.2.3, while the weighting for minimization of assistive forces were considered equal to $diag\,(8, 8, 8)$ for all assisted STS transfer simulations to achieve smooth force profiles.

STS Assistance for the Maximal Assist Class

For the maximal assist class the required assistance is typically applied to upper body segments under the shoulders. The independent effects of the shoulder and elbow joints were neglected in the biomechanical model. This is mainly due the fact that the patients belonging to the considered maximal assist class are expected to perform very small hand

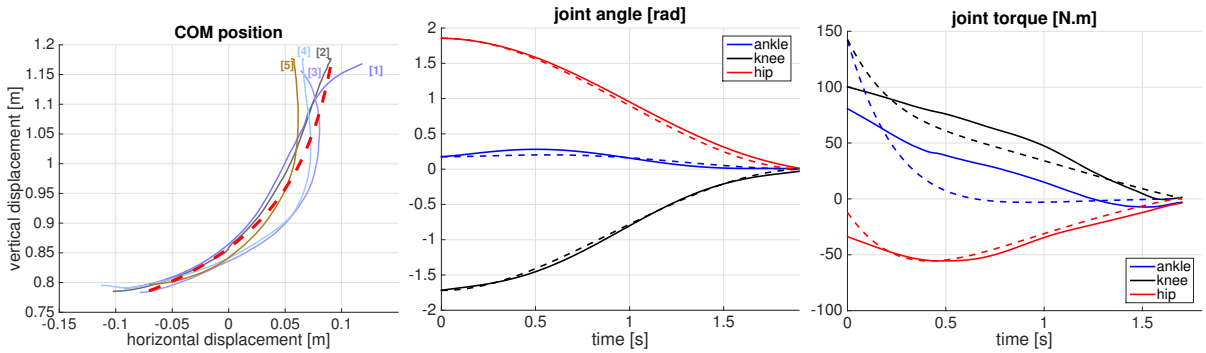

Figure 3.6: Simulation and experimental results of the human COM position (left), joint angles (mid), and joint torques (right) during STS transfers. Left: trajectories of the user's COM from five STS transfer repetitions (solid lines) and corresponding simulation result (dashed red). Middle, right: experimental results of the joint angles and torques (solid line) and simulation results (dashed).

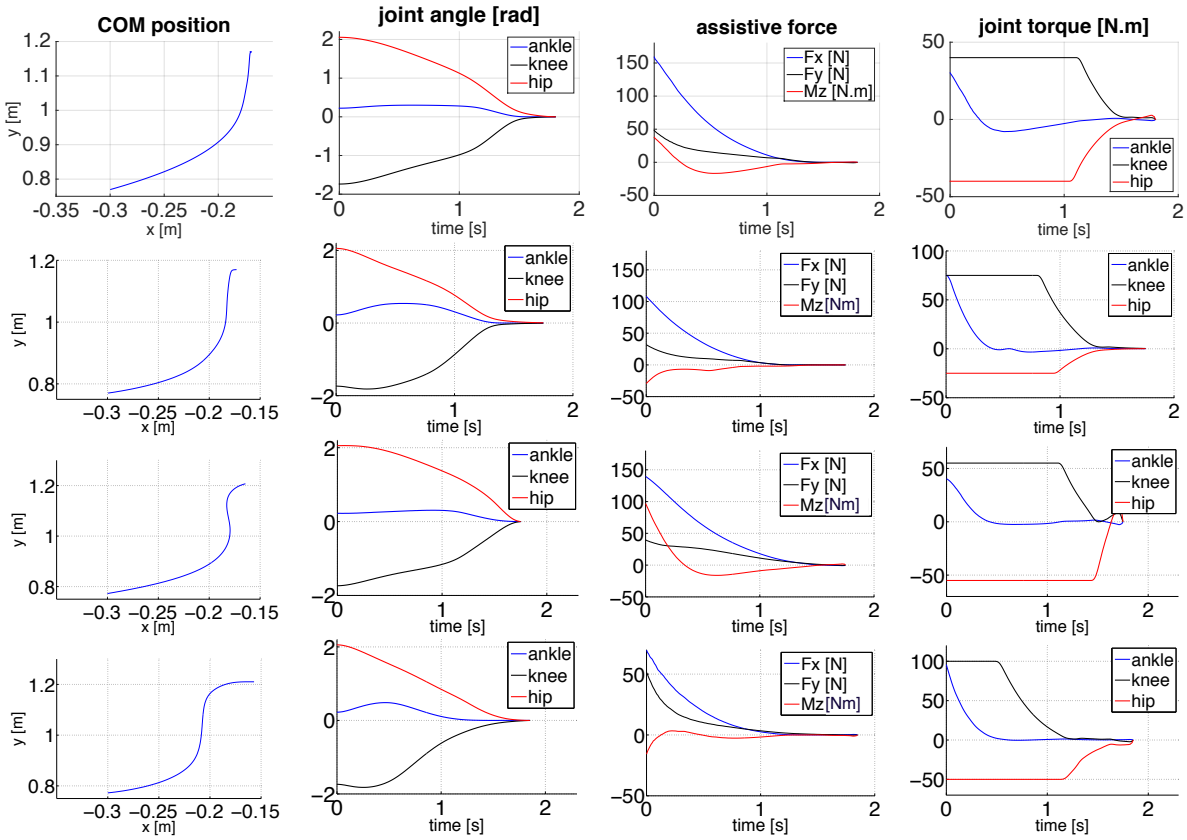

Figure 3.7: Columns from left to right: simulation results of the human COM positions, joint positions, external assistive forces and moment, and joint torques during STS transfers for patients belong to the class of maximal assistance and having equal weakness in all joints (first row) and weakness in specific joints (second row), as well as for patients belong to the class of moderate assistance and having equal weakness in all joints (third row) and weakness in specific joints (fourth row).

motions during a STS transfer. However, the inertia effects of the hands are still considered in the upper body dynamics. We restricted the shank motion by considering a lower range of motion for ankle joint (3.6) to mimic the influence of locking the patient's knees and feet during STS transfer.

Considering the minimum torques needed to rise successfully without help, see [124], joint torque constraints ($\boldsymbol{\tau}_{ankle} < 75$, $\boldsymbol{\tau}_{knee} < 75$, $\boldsymbol{\tau}_{hip} < 25$) were assumed to simulate patients of *case a* and ($\boldsymbol{\tau}_{ankle} < 40$, $\boldsymbol{\tau}_{knee} < 40$, $\boldsymbol{\tau}_{hip} < 40$) for *case b*, respectively. We considered more than 50% weakness for a person with body measurements similar to subject S1. We also activated the most effective interactive force components in the STS transfer model, namely vertical and horizontal external force components (F_x, F_y) as well as the angular momentum (M_z). Figure 3.7 shows obtained trajectories of the assistive force/moment profiles to be applied to the user as well as the user's COM, joint angles and joint torques. As can be observed human weakness is compensated through proper external assistance as the STS transfer is smoothly accomplished while the human joint torque remained lower than the considered user's capability.

STS Assistance for the Moderate Assist Class

For the moderate assist class we assumed that the patient is able to rigidly grasp a robotic device that assists in STS transfers. Thus, also the human arm has been considered in the biomechanical model. Higher joint torque limits compared to the maximum assist class and the two sorts of weaknesses were set ($\boldsymbol{\tau}_{ankle} < 100$, $\boldsymbol{\tau}_{knee} < 100$, $\boldsymbol{\tau}_{hip} < 50$) for *case a* and ($\boldsymbol{\tau}_{ankle} < 55$, $\boldsymbol{\tau}_{knee} < 55$, $\boldsymbol{\tau}_{hip} < 55$) for *case b*. Required supportive force/momentum profiles as well as the obtained user's COM, joint positions and torques during the STS accomplishment are shown in Fig. 3.7. As expected, the required external supportive force/moments are reduced in comparison to the maximal assist class while again the human weakness is well compensated.

3.3.2 User Study

An intensive evaluation by 33 elderly subjects was performed to assess the effectiveness of the proposed optimal STS transfer assistance. Thirty women and three men participated in the evaluation which took place for six weeks (from Oct. to Dec. 2014), in the Agaplesion Bethanien Hospital/Geriatric Centre of the University of Heidelberg. The average age of participants was 84.5 ±5.0, ranging from 74 to 94 years old. Subjects had on average moderate stage impairment in cognitive and motor status (MMSE score: 24.9 ±3.9; 5-chair stand: 19.6 ±3.9s; gait speed 0.47 ±0.13). Moreover, 64% of participants experienced at least one fall within the past 12 months. All the users used normal walkers in their daily life. The experiments were performed with the ethical approval of the Ethics review committee (Ethikkommission der Medizinischen Fakultät Hei-delberg, Alte Glockengießerei 11/1, 69115 Heidelberg, Germany).

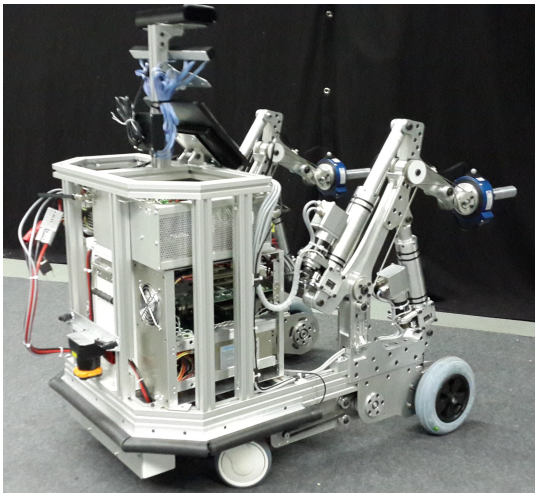

Figure 3.8: Mobot platform: an assistance robot with actuated handles that employed for the evaluation of proposed assistive STS transfers.

Experimental Setup

The assistive strategies have been implemented on our robotic mobility assistance platform equipped with two actuated rear wheels and two 2 DOF parallel actuated arms, Mobot platform in Fig. 3.8. Handle levers are designed to always keep the same orientation and are equipped with a pair of 6 DOF *JR3* force torque sensors.

The arms are actuated using spindle drives controlled independently in the sagittal plane. Each arm has 2 actuated revolute joints and 1 passive joint. The torques are applied to the actuated joints by linear actuators which are connected to the segments by the rotary joints. The torque at the passive joint is applied by a cable drive, which is rigidly connected to the first two actuated joints and keeps the handle in the horizontal position. The range of motion of each joint is as follows, $0 < \theta_1 < 49$ degree and $0 < \theta_2 < 91$ degree, resulting in a reachable handle position of $0 < x < 0.5$m and $0 < y < 0.6$m in Cartesian space.

The controller of the arms is implemented using MATLAB/Simulink Real-Time Workshop where the handle positions are controlled in Cartesian space using inverse kinematics and a high-gain low-level PID joint space position controller. Communication and sensing loop are set to run at $T = 1$ ms sampling time.

Because of workspace limitations of the used mobility assistance robot, we had to exclude very tall or small persons as the obtained optimal trajectories could not be realized.

Methods

Each subject performed a MiniMental test and its results were recorded along with body characteristics including patient's height, total weight and specific weaknesses. Anthropometric limb data for each patient was estimated based on weight and height information using regression formulas provided in [148]. Each user was assigned to a specific target group according to their level of impairment and their specific or more general weakness were recorded. Consideration of the level of subject's impairment, advice of nurse specialists and the mean value of percentage of the weakness already used in section 3.2.3 allowed the

selection of specific joint torque limits for the optimization. Finally, optimizations were performed to derive user-specific optimal robot handle trajectories taking the aforementioned joint torque limits into account. Because of robot workspace limitations, initial and final hand configurations were considered within the robot workspace to achieve optimal trajectories realizable with our assistance robot. The initial hand position was selected as close as possible to the subject hip sitting on a chair. An example of the achieved individualized robot handle trajectories is shown in Fig. 3.9.

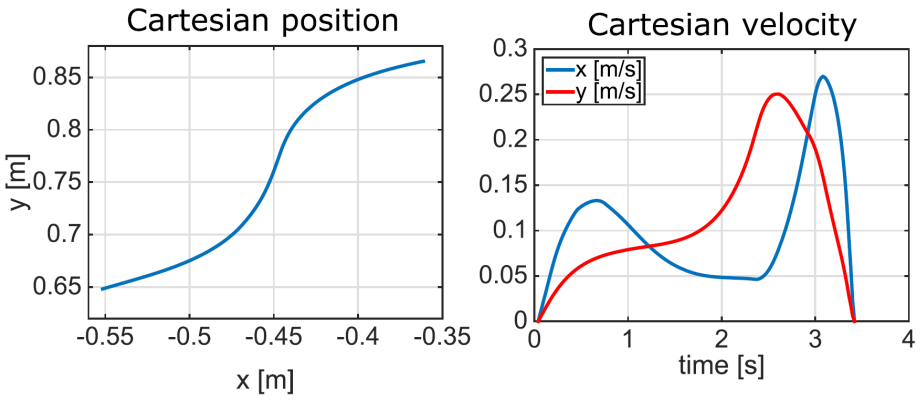

Figure 3.9: An example of the achieved individualized robot handle trajectories (left: handle position, right: handle velocities).

During the experiments the chair height was adjusted to the user's knee height. Before testing the robot STS transfer assistance, the ability of participants to perform unassisted STS transfers was assessed. The participants were instructed to stand up without receiving any support neither from the assistance robot, nor from the nurse-specialist supervising the experiments. In order to standardize experiments, each subject was orally instructed how to use the assistance robot, where to sit and how to keep the feet position. Then, the assistance robot was placed in front of the patient and the robot handles were brought to the initial configuration for the STS task. The subject was asked to grip the robot handles and to trigger the robot controller by applying a rather small downward force, whenever they felt ready for the STS transfer. Each subject performed 5 STS transfers with the help of the assistance robot considering pauses to avoid exhaustion. After finishing all 5 trials participants were asked to fill a questionnaire.

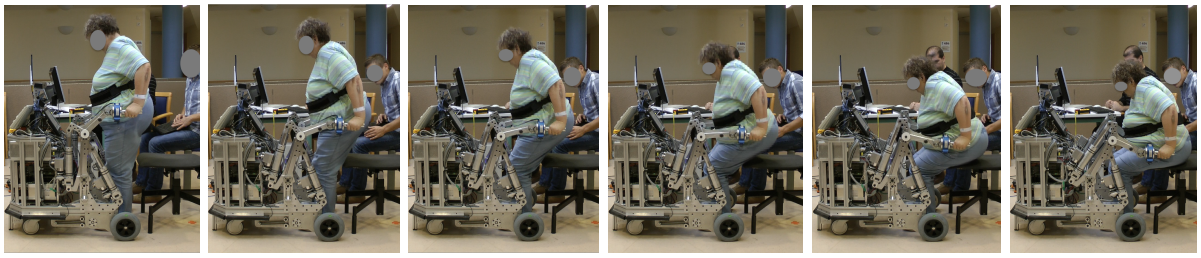

Figure 3.10: Snapshots taken during the evaluation of the STS transfer assistance.

Results

Figure 3.10 shows a sequence of the STS transfer assistance provided by the robot to an elderly subject. In total 165 STS trials were recorded from 33 participants. Apart from the results of the questionnaire (which will be reported in a different place reporting the clinical perspective), two performance metrics were considered in order to verify the effectiveness of the proposed STS transfer support: STS transfer success rates and similarity of the assistive force profiles in simulation and experiments.

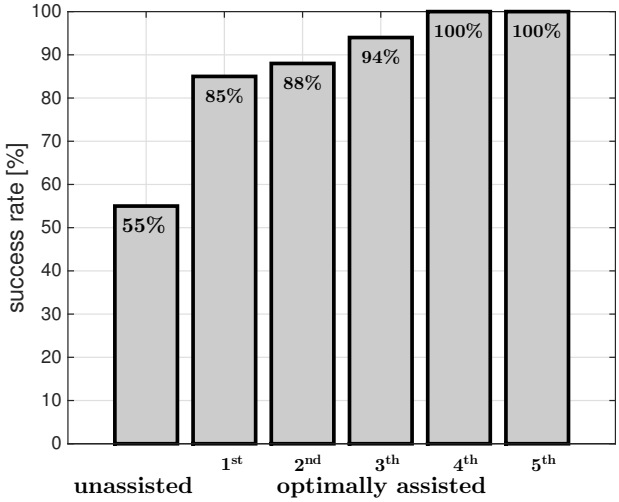

Figure 3.11: Success rate of STS transfers.

All participants were able to stand up from the chair with the help of the assistance robot at least three out of five times, where all participants successfully achieved a standing position within the 4^{th} and 5^{th} trial. Figure 3.11 shows the average success rate recorded for all patients per trials. Across all participants and trials an average success rate of 93.3% was achieved, while a success rate of 54.5% was achieved for the preliminary test assessing the STS transfer ability without support. Subjects became quickly familiar with the robot and fast motor learning took place as the success rate increased quickly with trials. The 100% success rate for the fourth and fifth trial shows a great success in providing robotic STS transfer assistance.

Apart from the success rate for STS transfers, we aimed to compare the similarity of interaction forces between human and robot obtained in simulation and experiments. The forces and moments measured at each robot handles were transferred and summed as follows to define the total interaction forces and moments ($\boldsymbol{F}_{tot}$ and $\boldsymbol{T}_{tot}$) provided to the human,

$$\begin{aligned} \boldsymbol{T}_{tot} &= \boldsymbol{h}_l \times \boldsymbol{F}_l + \boldsymbol{h}_r \times \boldsymbol{F}_r, \\ \boldsymbol{F}_{tot} &= \boldsymbol{F}_l + \boldsymbol{F}_r \end{aligned} \tag{3.8}$$

where $\boldsymbol{h}_i$ $i \in (l, r)$ are the distance between the contact points (robot handles) and the center of robot handles. We mainly compare the horizontal and vertical components of the obtained force trajectories as well as the component of the moment orthogonal to the plane

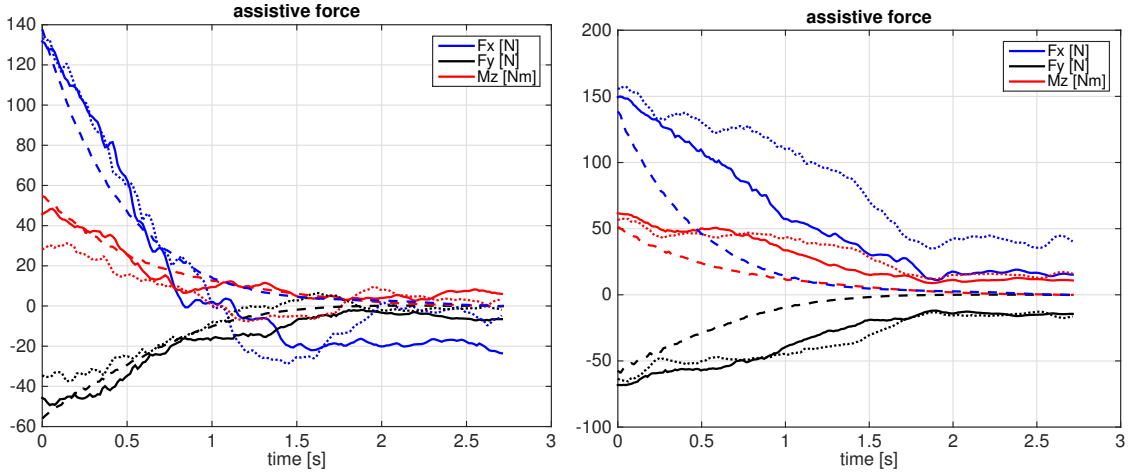

Figure 3.12: Comparison of simulation and experimental force trajectories for two elderly subjects able to fully stretch their body in the final standing configuration (left) and two elderly subjects not able to fully stretch their body in the final standing configuration (right). Solid and dotted lines are obtained measurements of the fourth and fifth STS transfer trials, while dashed lines are the expected force trajectories obtained by simulation.

of the force axis. Although for many of the patients a good similarity has been obtained, see e.g. Fig. 3.12 (left), some of the subjects could not fully stretch their body in the final configuration and therefore a considerable high amount of assistive forces was required while standing, see e.g. Fig. 3.12 (left). As this latter case was not considered in our model, clear mismatches between measurements and simulation can be observed. To incorporate this effect joint limits need to be adjusted. Further, asymmetric motions as observed for patients with one-sided impairments can not be properly replicated by our 2D model and require an extension to 3 dimensions.

After completion of all 5 STS transfers, the subjective user's perception was evaluated by means of a questionnaire adopted from [149]. High overall satisfaction with the optimal STS assistance system was observed. Details on this subjective evaluation though will be reported in a different place addressing the clinical perspective.

3.4 Summary and Discussion

Understanding the human STS motions allows us to control assistance robots in a biologically-inspired manner resulting in an intuitive and natural behavior for the coupled system of human and assistance robot. This way of control design for assistance robots has received very little attention, especially when considering STS transfer assistance.

The main contribution of this chapter is to propose a mathematical model for unassisted and assisted human STS transfers, to determine underlying principles and to further use these findings in the derivation of optimal assistive strategies. This chapter presented an optimal feedback control formulation for the modeling of assisted and unassisted human STS transfers. Compared to previous work based on SQP approaches, the presented

optimization problem is based on DDP that has been shown as a powerful tool to study biological movements. It allows us to obtain an optimal solution with respect to a defined cost function and considers the nonlinearity of human biomechanics as well as physical constraints, which are naturally incorporated into the optimization framework. It further shows the potential for future online implementations.

This chapter provided evidence that natural STS transfers could be achieved with the help of a cost function that linearly combines a series of criteria and finds a compromise between task end-point accuracy, human balance, energy consumption as well as smoothness of the motion and takes further human biomechanical control constraints into account. While we have employed the above-mentioned combination of criteria, future work can investigate other possible criteria especially considering subjects with different limitations or weaknesses. Moreover, possible adaptation of the weighting factors for each criteria over time can be investigated. This may help developing more sophisticated assistance systems, for example, to create a rehabilitation program.

The model was extended with external forces and torques and optimal assistive STS transfer strategies were determined considering two types of assistance classes and weaknesses. The resulting optimal assistive trajectories were calculated and implemented on a robotic mobility assistant. The assistive STS transfer approach was finally evaluated by 33 elderly subjects performing 165 trials. Results show a high users satisfaction as well as a 100% success rate for all participants in the fourth and fifth trial.

Further research of the presented methodology should look at the extension of the STS model by inclusion of the chair support forces, which were neglected in this chapter but will require switching the model during optimization. Moreover, online implementation of the optimal control approach for assisted sit-to-stand transfers can be an ultimate target. This is particularly important since offline computations are based on assumptions (such as human's initial joint angles) that may not correspond to the real-world situations. Apart from overcoming the latter problem, online implementation can also simplify the two steps of firstly calculating the assistance trajectories offline, and then implementing them in the real robot in one step which would be a more practical solution indeed.

The approach presented in this chapter shows how human motor control models can be employed to develop optimal assistive strategies. This human-inspired control design approach is continued in the next chapter where human-decision making mechanisms embedded into the control design of MARs to realize a user and environment-adaptive walking assistance are investigated.

4 User and Environment-Adaptive Walking Assistance

The second considered mode of operation in this thesis is walking. A sufficient walking performance that allows performing physical daily activities is a critical requirement for maintaining mobility and vitality, especially for elderly people and patients. Changes due to aging or disease may result in the limitation of human motor performance, sensory capabilities and cognitive functions, and thus reduce the ability to perform daily walking. This often leads to less autonomy and a decreased quality of life and self-esteem. Therefore, it is important that the elderly and patients are supported by MARs during walking. However, this comes with different challenges such as safety and user and environment-adaptive shared control.

A major challenge in the controller design of MARs during walking is how to adapt the provided assistance depending on the actual context of both the human and environment. An assistance robot under direct user control can have difficulties guaranteeing acceptable performance and safety due to cognitive, sensorial and physical weaknesses as a result of target users being elderly or disabled people. On the other hand, a fully autonomous system that ignores the user's intention can result in user dissatisfaction and dangerous situations in the event of human and robot disagreement. Therefore, a shared control approach allowing human and robot to share the control over resulting actions is typically employed.

Shared control has been studied for different applications of human-machine interaction: For example [150–154] investigated shared control for teleoperation, space and aviation systems, [155–158] explored similar principles for surgery applications, while [159] and [160] report on shared control for powered wheelchairs.

In literature most adaptive shared control mechanisms attempt to tune the level of assistance to improve metrics related to the task. Thus, an inherent difficulty lies in deciding on suitable metrics and adaptation strategies such that the overall robot assistance results in a natural behavior to the user. In this context *natural* refers to an intuitive cooperative control scheme that considers human and robot to collaborate as *peers*, meaning that the robot is allowed to make its own decisions to online adjust the level of assistance taking current and past information on the user and environment into account. We believe that an intuitive and natural behavior can be achieved if the robot can decide on the provided level of assistance in a similar way to humans. Thus, for the first time this chapter formulates the problem of the allocation of control authority as a decision-making problem and employs human-inspired decision-making models. We use the Drift-Diffusion (DD) model, firstly proposed by [161], that describes the decision-making mechanism in humans as a process in which decisions are based on past decisions and the decision criteria are continuously adjusted in order to maximize the reward obtained throughout task execution. Following the principles of the DD model, we propose a mathematical formulation for

an integrated control architecture to adapt the parameters of the shared control system of a rollator-type MAR. The proposed architecture allows for intuitive adaptation of the short-term a) *cognitive assistance* helping the user to follow a desired path towards a predefined destination, the robot b) *sensorial assistance* to avoid collisions with obstacles and to allow an intentional approach of them, and the more long-term adaptation of the robot c) *physical assistance* based on measured user's performance and fatigue. We illustrate the effectiveness of the proposed architecture in experiments and evaluate its performance by conducting a user-study with elderly subjects. Obtained results indicate an acceptable user's satisfaction and show a general high potential of the proposed adaptive shared control architecture for MARs.

This chapter is organized as follows: section 4.1 reviews related work. Section 4.2 introduces the MAR and the implemented admittance control approach. The integrated adaptive shared control architecture is presented in section 4.3, while section 4.4 provides details on the implementation of the adaptation policies for the sensorial, cognitive and physical assistance. Finally, section 4.5 discusses the experimental setup and reports on technical validation experiments and the performed user-study with elderly users.

4.1 Related Work

While chapter 2 provided a general review of found approaches adopted to realize walking assistance, the following section focuses specifically on reviewing approaches of adaptive shared control of MARs as well as decision-making in humans and related models.

4.1.1 Adaptive Shared Control for MARs

Variable admittance control is the most common control scheme in MARs. An admittance model defines the sensitivity of the device to the applied human forces according to a specified desired mass and damping that should be rendered by the device. The behavior of the system can be modified by adapting this admittance, or by manipulation of the force applied by the user. In [17, 22, 53] the authors for example improve maneuverability by applying a transformation on the user's force that allows to online modify the center of rotation of the mobility assistant. In [12, 14, 110] authors propose to include also a braking force to the admittance law and to achieve the robot desired behavior such as fall prevention, gravity compensation on slopes or step avoidance by proper activation of the brakes. Different environment-adaptive approaches, mainly based on the inclusion of additional forces/torques to the admittance model for obstacle avoidance and goal-seeking (generated based on environment information) can be found in [11, 15, 19, 20, 54, 92, 110]. These approaches can result in an active robot behavior which can lead to dangerous situations, for example in case the human releases the handles and the robot continuous to move or the human plans to walk on a straight path, while the system accidently turns to circumvent an obstacle.

Only few works consider the history of the human performance during the interaction with the robot in the adaptation law of the admittance controller. In [45] the author proposes a cost function with forgetting factor evaluating the user's performance by combining

multiple criteria like the proximity to obstacles, the deviation from the planned trajectory and human stability criteria. This allows to realize an adaptive shared control with varying force gains, which provides more authority to the human or the robot assistant depending on the accumulated human performance. Similarly, in [25] the authors propose to shift authority from the human user to the robotic system or vice versa depending on the specific context and logical rules allowing e.g. for the implementation of a no assist mode, an assist mode (human and robot share the execution of the task), a safety mode (robot acts fully autonomous) or an override mode (robot is under full control of the human). In [162, 163] again a logical rule-based method is proposed that evaluates the interaction force to estimate the human intentional direction which is defined as "the direction into which a person intends to move" and then select the admittance parameters among some defined values. Different admittance parameters are studied to provide the user a comfortable feeling while walking and to avoid manoeuvres in unintended directions.

Apart from the use of variable admittance control, few other approaches exist that address the problem of shared control. A Bayesian network approach that combines sensor information with user's inputs (read by an interface with three buttons for moving forward, turn left or right) and that activates respective autonomous robot behavior is proposed in [97]. An autonomous path planning and obstacle avoidance approach is discussed in [33, 34, 94, 95] that lets the user decide on the robot velocity leaving partial authority of modifying the path with the user. The author employs advanced methods for dynamic path planning (e.g. elastic bands [112]) to allow for dynamic obstacle avoidance and smooth path planning and modifications according to user's inputs. In [54] three robot guiding behaviours including obstacle avoidance, wall following, and goal seeking are designed for an omni-directional mobile robot by evaluating laser sensor data and by fusing these three behaviors by means of a Fuzzy Kohonen Clustering Network. In [31] the authors use forces and moments a user applies to a walker's handle in addition to information on the local environment and the walker's state to derive the most likely human intention, respectively path to follow. Depending on the identified intention, the angle of the robot front wheel is set by the mobility assistant, leaving the user the freedom to decide on the velocity to move on the identified path. Finally, a switching controller to avoid human forward fall and human-robot collision is proposed in [101].

Summarizing, although a series of adaptive shared control approaches for mobility assistance robots were studied in literature as listed above, to the best of the authors knowledge none of the aforementioned approaches used human-inspired decision-making models to define adaptation policies for the provided level of assistance, which is expected to result in a natural and safe human-robot interaction. Thus, for the first time we study human decision-making models as mechanism to gain-schedule low-level control parameters and with this to vary the level of assistance provided and evaluate the effectiveness of this approach for real end-users.

4.1.2 Human Decision-Making Models

In cognitive science, human decision-making has been widely studied in so called two-alternative forced-choice (TAFC) tasks. TAFC tasks require a human to make a sequence of choices between two predefined alternatives. After every choice, the subject is given a

reward based on the current choice and the previous N choices. The subject's goal is to maximize the accumulated reward over a sequence of choices. TAFC tasks were used to study optimal decision strategies, see [161, 164], or sub-optimal strategies, see [165, 166]. In human subject experiments, it was observed that for a majority of human subjects working with particular reward structures, decisions are centered around particular points, termed matching points, where the reward return curves for the two options cross.

Mathematical investigations focusing on potential underlying mechanisms of human decision-making have involved among others Markov decision processes (MDP) and drift-diffusion (DD) models. Authors in [167] consider TAFC tasks and a DD model together as a Markov process and show that, under certain assumptions, the DD model analytically exhibits matching behavior as observed in human subjects. In [168], convergence to a matching point is proven for a particular task called the matching-shoulders-type task and using the DD model with a time decay extension. In [164] and [169], a combination of a DD model and MDP is used to address empirical and analytical effects of social context (decisions and rewards of other people) on decision-making.

Although several extensions to the concept of decision-making based on the DD model in TAFC tasks exist, see for example [170, 171], its application to assistance robotics has not received lots of attention. In this work we extend our previous work [172] and explore the applicability of the DD model to MARs supporting elderly and patients.

4.2 MAR Low-Level Control

4.2.1 System Description

We consider the rollator in Fig. 3.8 that is of active and non-holonomic type, meaning that the translational motion of the robot along the heading direction as well as rotational motion along its center of rotation are possible, while motions in lateral direction are restricted. With reference to Fig. 4.1, the non-holonomic constraint is given by

$$\dot{x}_r \sin\theta_r - \dot{y}_r \cos\theta_r = 0,$$

and therefore the kinematic model can be written as follows,

$$\dot{\boldsymbol{q}} = \begin{bmatrix} \dot{x}_r \\ \dot{y}_r \\ \dot{\theta}_r \end{bmatrix} = \begin{bmatrix} cos\theta_r & 0 \\ sin\theta_r & 0 \\ 0 & 1 \end{bmatrix} \begin{bmatrix} v \\ \omega \end{bmatrix} = \boldsymbol{J}\boldsymbol{u}, \tag{4.1}$$

where v and ω are two available control inputs for the linear and angular velocities around the vertical axis and $\boldsymbol{q} = [x_r,\, y_r,\, \theta_r]^T$ the states of the robot.

4.2.2 Admittance Control

Two force/torque sensors mounted at the handles of the rollator are used to drive the differential drive MAR. Force components along and around the heading direction are used

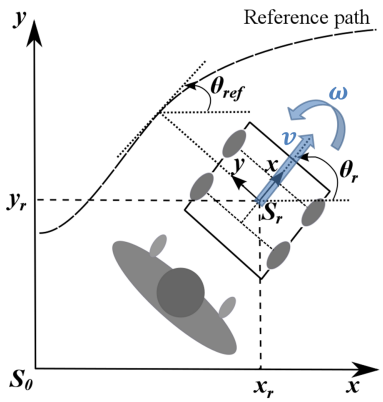

Figure 4.1: Human and MAR in the world frame.

for motion control[1]. An admittance control is implemented, which allows to design the desired dynamic behavior of the system with respect to the user's applied force by selecting proper admittance parameters. The admittance controller emulates a dynamic system and gives the user a feeling as if he/she were interacting with the system specified by the admittance model. A mass-damper system for the linear and angular motion is considered

$$\boldsymbol{M}_d\dot{\boldsymbol{u}} + \boldsymbol{D}_d\boldsymbol{u} = \boldsymbol{F}_h, \tag{4.2}$$

where $\boldsymbol{M}_d$ and $\boldsymbol{D}_d$ are the desired inertia and damping matrices, respectively, and $\boldsymbol{F}_h = [f_{h_x}, f_{h_y}, \tau_h]$ the driving forces applied by the user. Therefore, the desired reference velocity for the robot is specified by the desired admittance parameters and is based on the human input in terms of applied force. The robot reference velocity is then controlled by a low-level controller.

4.3 Shared Control Architecture

We propose an integrated architecture that allows to adapt the robot's short-term *cognitive* and *sensorial* assistance as well as the long-term *physical* assistance provided. The cognitive assistance provides required support to the user in path following situations guiding the user from an initial to a desired destination. The sensorial assistance reduces the risk of the robot colliding with obstacles and allows for the intentional approach of obstacles. The physical assistance tunes the robot contribution according to the long-term user's performance, which may be affected due to fatigue. The latter is particularly important since considerable changes in performance are observed due to user's fatigue after continuous activity, which may render performing daily activities at a desired level of performance difficult, see [173, 174].

With reference to Fig. 4.2, we propose an integrated adaptive shared control framework for MARs. Three decision-maker blocks for sensorial, cognitive and physical assistance are responsible for online adapting the parameters of the admittance controller in order to

[1]Please note that in a holonomic system also the force component in sidewards direction is used for motion control.

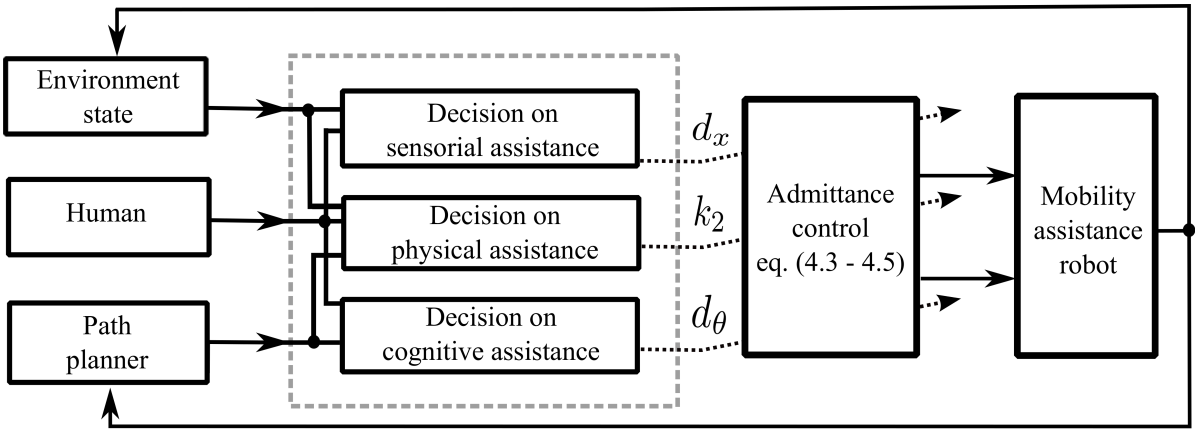

Figure 4.2: MAR adaptive shared control architecture.

achieve the desired system behavior. The *Decision on cognitive assistance* block evaluates the planned path towards the goal which is generated by the path planner block, the human navigational intention in form of force and torque applied to the robot handles as well as the actual human performance. The *Decision on sensorial assistance* block uses human input and the information provided by the *Environment state* block, which provides information on the position of obstacles around the robot. Finally, the *Decision on physical assistance* block processes all inputs and adjusts the level of active support provided accordingly.

The concept of the robot assistance is implemented by manipulating the admittance control parameters. We decompose and extend the admittance controller (4.2) as follows:

$$m_x\dot{v} + d_x v = f_{h_x}, \tag{4.3}$$

$$I_\theta\dot{\omega} + d_\theta\omega = k_1\tau_h + k_2\tau_{assis}, \tag{4.4}$$

$$k_1 + k_2 = 1, \tag{4.5}$$

where the parameters m_x, d_θ and f_{h_x} are the mass, damping and human force components along the heading direction of the robot (in alignment with the unitary vector x of the robot in Fig. 4.1). The variables I_θ, d_θ and τ_h are the inertia, damping and human torque components. The parameters d_x, d_θ and k_2 are tuned to satisfy the aforementioned sensorial, cognitive and physical assistance. Increasing the value of d_x decelerates the robot motion in heading direction and knowing that the robot is of non-holonomic nature this effect can be used for the purpose of robot sensorial assistance. Manipulation of d_θ influences the felt resistance when aiming to change the robot orientation and thus, can help preventing deviations from the desired path towards the destination. Finally, an increase of k_2 increases the robot active contribution to the control of the orientation of the robot. This effect is used for varying the physical assistance provided by the robot. The adaptation of the d_x and d_θ parameters results in a passive and thus, intrinsically safe support strategy. The advantage of active support is used to tune the parameter k_2, whenever the passive support strategy alone cannot provide the desired system behavior, e.g. when the user is exhausted and can hardly guide the robot towards his/her desired destination.

The decision-making systems that decide on the specific tuning of these parameters are discussed in the following sections.

4.4 Decision-Making for MARs

The individual decision-making policies that decide on the specific level of robot assistance provided are formulated based on the DD model to achieve an intuitive online adaptation of the robot assistance. In the following sections, we first introduce the DD model, and then detail its application for designing an adaptive robot assistance for a MAR.

4.4.1 Decision-Making Principle based on DD Model

In a two-alternative forced-choice (TAFC) task a human has to take a decision between two alternative choices and is asked to continuously choose between them. Each choice is associated with a specific reward. The human not knowing about the underlying reward structures typically explores the options and gradually optimizes the overall intake. Different reward structures have been proposed in literature to study human decision-making behavior. In this thesis, we mainly focus on the matching shoulder reward structure. The matching shoulder structure consists of two reward functions with inverse relationships as encountered for example whenever two goals are conflicting and a decision has to be taken for either improving the one or the other. The specific form of the two crossing reward functions is a design factor and allows to program different kind of behaviors allowing to favor one goal over another in some situations, while favoring the other in other situations. Thus, in general the matching shoulder structure consists of two intersecting curves that diminish with increasing/decreasing performance. Consider p_A and p_B human performance measures associated with the choices A and B and the associated rewards r_A and r_B. Further, and only assumed in the context of this thesis, the general relationship of a reward r and a performance measure p should be given by:

$$r_z = k_z(p_z - p_{offset,z})^{n_z} + r_{0,z}, \tag{4.6}$$

where $p_{offset,z}$, $r_{0,z}$, k_z, and n_z are the user and task-defined tunable variables for each specific reward structure ($z \in A,\ B$).

The Drift Diffusion (DD) model has proven to implement the optimal mechanism for TAFC decision-making tasks and accounts for an impressive amount of behavioral and neuroscientific data. The DD model characteristic can be formulated as soft-max model firstly introduced by [161] to describe human decision-making in TAFC tasks. The soft-max model as a main component in human decision-making processes was also shown by [175] and formulated using a sigmoidal function

$$\mathbb{P}_A(t+1) = \frac{1}{1 + exp^{-\mu(w_A(t) - w_B(t))}}. \tag{4.7}$$

According to this model, the probability of the human preference for choice A at time $t+1$ is $\mathbb{P}_A(t+1)$ which is computed using (4.7), where $w_A(t)$ and $w_B(t)$ are the accumulated evidences for choosing option A or B, respectively. The parameter μ is used to manipulate the slope of the sigmoid function, and therefore the level of certainty in making a decision.

The values $w_A(t)$ and $w_B(t)$ are updated with the help of a learning rule. Authors in [176] have proposed a discrete-time linear update rule. Considering the decision set $z \in$

$[A, B]$ at each time t, then

$$w_z(t+T) = (1-\lambda)w_z(t) + \lambda r_z(t) \tag{4.8}$$

where z is the decision just made, $r_z(t)$ the obtained reward for z, $\lambda \in [0\,1]$ a forgetting factor and T the sample time in the system. We consider the same initial value for the weightings w_z which implies no preference for each of the two choices.

In the following sections we employ the DDM as a key element for the gain-scheduling of low-level control parameters resulting in varying levels of physical, sensorial and cognitive assistance. Doing so, the problem of fulfilling two conflicting goals is formulated for each type of assistance studied. Then, associated performance metrics are defined and the corresponding matching shoulder reward structures are introduced. Next, the level of the provided assistance is decided upon by evaluating the DDM (4.7), which finally determines which of the two conflicting goals should be prioritized according to the accumulated evidence to improve the overall intake. Finally, a linear homotopy is applied for gain scheduling respective low-level control parameters c between a pre-defined minimum and maximum value based on the determined probabilities for deciding on either of the two choices:

$$c(t) = \mathbb{P}_A(t+1)c_{min} + (1 - \mathbb{P}_A(t+1))c_{max}. \tag{4.9}$$

4.4.2 Decision on Cognitive Assistance

In this section, we formulate the problem of providing adaptive, passive cognitive assistance as a human decision-making problem. We employ the DD model for gain-scheduling of the low-level control parameter d_θ to online adjust the level of the provided robot cognitive assistance.

Problem Formulation

An important functionality of the MAR is guiding the user from an initial to a target destination, especially for users who are cognitively impaired and have thus, difficulties in locating themselves and finding their way. An ideal robot assistance makes the user feel comfortable by giving him/her enough control over the platform, while the user is safely guided towards the desired destination. In particular, we aim at improving human-robot agreement by providing the user enough freedom in controlling the platform as long as the deviation from the desired path stays within acceptable limits and at shifting priority towards improving task performance by reducing the human control authority in case the task deviation is slowly approaching its allowed maximum, but the user performs no proper reaction to prevent this. This trade-off is formulated as decision-making problem. The assistance is realized by a passive guidance that prevents movements in directions perpendicular to the desired path and giving the user's freedom to control the robot when moving along the reference path.

Consider a task of path following from an initial to a final location where the desired path is known for the robot assistant. The human forces ($\boldsymbol{f}_h = [f_{h_x},\, f_{h_y}]^T$), represented by the linear components (two first entries) of $\boldsymbol{F}_h$ in (4.2) are used to control the linear robot

motion along the robot reference frame. They can be split into two main components, the human force along the reference path ($\boldsymbol{f}_{\parallel}$) and perpendicular to it ($\boldsymbol{f}_{\perp}$). With reference to Fig. 4.1, the magnitudes of these forces are given as follows,

$$f_{\parallel} = \parallel \boldsymbol{f}_h \parallel cos(\theta_e), \quad f_{\perp} = \parallel \boldsymbol{f}_h \parallel sin(\theta_e), \tag{4.10}$$

where $\theta_e = \theta_{ref} - \theta_r$ and θ_{ref} is the desired orientation between the reference path and the global x-axis.

We believe that the proper control of the robot orientation error is satisfactory for the purpose of providing cognitive assistance. To ensure a safe robot behavior, we propose a passive assistance by adapting the damping parameter d_θ and thus, indirect manipulation of the robot angular velocity and orientation error while giving the user the freedom to move freely along the path. This reduces the problem to the adaptation of only one parameter, namely the damping parameter d_θ. The adaptation law for this parameter is formulated as a decision-making problem using the DD model.

Performance Measures

Task performance is measured using the rotational and translational tracking error formulated with respect to the desired path over an observation windows N_C

$$p_{T,C} = \frac{\sum_{i=1}^{N_C} k_{C,e} e_i + k_{C,\theta_e} \theta_{ei}}{N_C \cdot \max(k_{C,e} e + k_{C,\theta_e} \theta_e)}, \tag{4.11}$$

where the subscript i refers to the value of the variable at the sample i and e is the robot position error given by

$$e = \sqrt{(x_{ref} - x_r)^2 + (y_{ref} - y_r)^2}, \tag{4.12}$$

and $p_{T,C}$ means the normalized task performance computed over N_C samples, and $k_{C,e}$ and k_{C,θ_e} are two user-defined factors distributing the weightings between orientation and translation. The max value is initialized with the maximum acceptable error with respect to the task and is updated if a larger value is observed during the interaction process.

Disagreement is assumed to occur when the user and robot assistant apply forces in opposite directions leading to so called internal forces. These internal forces provide important information on haptic interaction, see e.g. [177]. Minimizing disagreement can enhance the quality of human-robot interaction as the robot then behaves according to human expectations. Considering the task of providing cognitive assistance described in the previous section, we define the internal moment τ_{int} as follows

$$\tau_{int} = \begin{cases} \tau_h + l_f f_{\perp} & sign(\tau_h + l_f f_{\perp}) \neq sign(\tau_{robot}) \wedge \\ & |\tau_h + l_f f_{\perp}| \leq |\tau_{robot}|, \\ -\tau_{robot} & sign(\tau_h + l_f f_{\perp}) \neq sign(\tau_{robot}) \wedge \\ & |\tau_h + l_f f_{\perp}| > |\tau_{robot}|, \\ 0 & \text{otherwise}, \end{cases} \tag{4.13}$$

where l_f is a variable representing the Euclidean distance between the robot position and the reference point on the desired path. The value of τ_{robot} can be computed by any orientation controller, similar to the one proposed for τ_{assis} in (4.26) and is only used as virtual input to calculate a potential human-robot disagreement, but is not applied to the real robot as we aim for a fully passive cognitive assistance. The disagreement metric is then computed over N_C samples and is further normalized to define the following agreement performance $p_{A,C}$,

$$p_{A,C} = 1 - \frac{\sum_{i=1}^{N_C} |\tau_{int,i}|}{N_C \cdot \max(|\tau_{int}|)}. \tag{4.14}$$

The final performance set to be considered for each decision is $p_C \in [p_{T,C}, p_{A,C}]$.

Reward Structure and Decision-Making

Following ideas of the DD model in TAFC tasks, a reward function is associated with each performance measure. For the considered decision-making problem, we propose a matching shoulder structure with two intersecting reward functions as depicted in Fig. 4.3 and both functions expressed using (4.6).

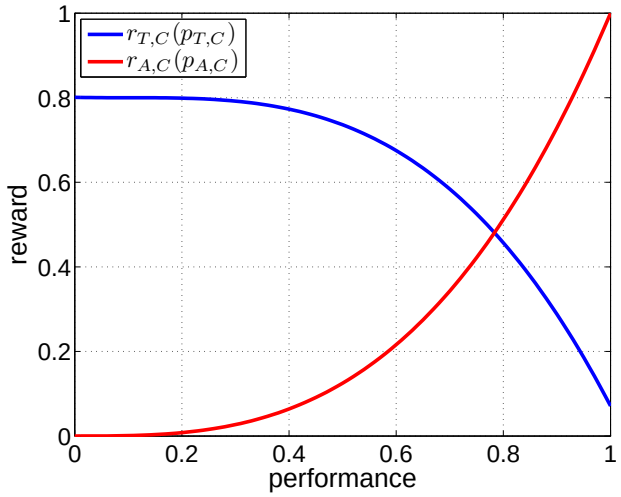

Figure 4.3: Reward structure for adapting the cognitive assistance. The blue function is the reward $r_{T,C}$ associated to the task performance measure $p_{T,C}$ and the red function is the reward $r_{A,C}$ associated to the agreement performance measure $p_{A,C}$.

The proposed reward structure is designed to fit to the requirements introduced in section 4.4.2. The assistant faces a trade-off between providing low assistance to improve human-robot agreement and providing high assistance to improve task performance. When the user is following the desired path, high agreement (agreement measure at its maximum) and high task performance (task performance measure at its minimum) are typically observed and thus, the maximum corresponding rewards are associated for both choices. The maximum reward associated to human-robot agreement is designed to be larger than the maximum reward for improving task performance. This implies an assistant's preference for improving agreement over task performance whenever the user's deviation from the reference path is acceptable. When both performances are decreasing, the reward for task

performance decreases with a slower rate than the one for human-robot agreement. This implies a change of the preference from improving agreement to task performance. On the other hand, when rewards are again improving, even a small increase of human-robot agreement results in a quick change of the preference towards improving human-robot agreement because of the higher rate of change in the reward associated to it (except phases of really low task and interaction performance, where task performance dominates).

The probability to assist the human to improve human-robot agreement at time $t+1$ is calculated using the DD model represented by (4.7) and considering $\mathbb{P}_A = \mathbb{P}_{A,C}$, $w_A = w_{A,C}$ and $w_B = w_{T,C}$ and $\mu = \mu_C$. The values of $w_{A,C}$ and $w_{T,C}$ are updated according to (4.8) considering $z \in [A_C\,, T_C]$.

Finally, the level of the provided cognitive assistance is adapted with the help of a linear homotopy defined as follows

$$d_\theta(t) = \mathbb{P}_{A,C}(t+1)d_{\theta,min} + (1 - \mathbb{P}_{A,C}(t+1))d_{\theta,max} \tag{4.15}$$

where $d_{\theta,min}$ and $d_{\theta,max}$ are the minimum and maximum considered values of the damping factor.

4.4.3 Decision on Sensorial Assistance

The formulation of the sensorial assistance problem and the proposed adaptation policy for gain-scheduling of the low-level control parameter d_x based on the described decision-making approach is discussed in the following sections.

Problem Formulation

Although typically a collision-free path is planned for robot assistants, reducing the risk of colliding with dynamic obstacles unknown at the time of planning the path has to be considered in the design of the robot control architecture. Further, an intentional approach to objects (detected as obstacle by the robot) can be desirable, e.g, when aiming to approach a table to grasp an object. This requires the robot to determine the user's intention and to decide on a proper support taking the specific context into account. Specifically, we aim at improving task performance in terms of collision avoidance by reducing the human control authority as well as allowing the intentional approach of objects by shifting the control authority to the human if large human-robot disagreement is detected. This is formulated as decision-making problem.

Since the most critical collisions occur between obstacles and the front part of the robot, we aim for collision avoidance by adapting the robot heading velocity towards obstacles. Considering the distance between robot and a detected obstacle, virtual forces/moments can be generated based on an artificial potential field, see [178]. We consider the following artificial potential field ($U(\boldsymbol{q})$),

$$U(\boldsymbol{q}) = \begin{cases} \frac{k}{2}\left(\frac{1}{\|\boldsymbol{d}_{obs}(\boldsymbol{q})\|} - \frac{1}{d_{obs,max}}\right)^2 & \| \boldsymbol{d}_{obs}(\boldsymbol{q}) \| \leq d_{obs,max}, \\ 0 & \| \boldsymbol{d}_{obs}(\boldsymbol{q}) \| > d_{obs,max}, \end{cases}$$

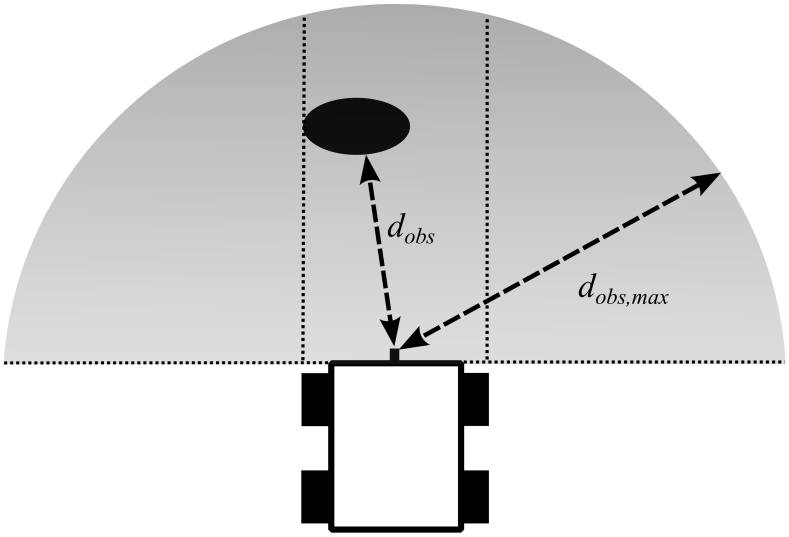

Figure 4.4: Concept of the distance definition between robot and obstacle detected by the laser range finder.

where $\boldsymbol{d}_{obs}$ is defined as the shortest distance between the nearest obstacle in front of the robot to a representative point on the robot, see Fig. 4.5, $d_{obs,max}$ the radius of the area in which the potential field becomes active and k a positive constant gain. Therefore, the value of $U(\boldsymbol{q})$ is increased whenever the robot is approaching an obstacle, and its value is zero if $\parallel \boldsymbol{d}_{obs}(\boldsymbol{q}) \parallel$ is larger than $d_{obs,max}$.

Artificial forces applied by the robot are defined as $\boldsymbol{F}(\boldsymbol{q}) = -\nabla(U(\boldsymbol{q}))$ where ∇U is the gradient vector of U. Then $\boldsymbol{F}(\boldsymbol{q})$ is transformed to the robot frame to determine virtual forces and moments $\boldsymbol{F}_{obs} = [\boldsymbol{f}_{obs}, \tau_{obs}]$ applied by the obstacle to the center of rotation of the MAR.

In a fully autonomous system, forces $\boldsymbol{F}_{obs}$ are typically used to actively drive the MAR and avoid collision with obstacles. However, in a shared control system where the robot is (at least partially) under human control and knowing that we aim for a passive support, direct usage of $\boldsymbol{F}_{obs}$ can result into an active and unsafe behavior and thus, we aim for only evaluating it and passively tuning the robot heading velocity v. Here this problem is simplified to the decision on the adaptation of d_x, which allows decelerating the robot whenever an obstacle is detected.

Performance Measures

Considering the task of collision avoidance, task performance is defined according to the distance to the nearest obstacle in front of the robot over an observation window of N_S samples

$$p_{T,S} = 1 - \frac{\sum_{i=1}^{N_S} \parallel \boldsymbol{d}_{obs,i} \parallel}{N_S \cdot d_{obs,max}} \tag{4.16}$$

where $\boldsymbol{d}_{obs,i}$ is the respective vector for sample i.

Similar to section 4.4.2, internal forces are considered to provide important information on the quality of interaction during collision avoidance. Internal forces $\boldsymbol{f}_{int}$, which represent

the level of disagreement between the force applied by a human ($\boldsymbol{f}_h$) as well as the repulsive force generated by the detected obstacle ($\boldsymbol{f}_{obs}$), are computed as follows

$$\boldsymbol{f}_{int} = \begin{cases} \boldsymbol{f}_h & \boldsymbol{f}_h \cdot \boldsymbol{f}_{obs} \leq 0 \wedge \parallel \boldsymbol{f}_h \parallel \leq \parallel \boldsymbol{f}_{obs} \parallel, \\ -\boldsymbol{f}_{obs} & \boldsymbol{f}_h \cdot \boldsymbol{f}_{obs} \leq 0 \wedge \parallel \boldsymbol{f}_h \parallel > \parallel \boldsymbol{f}_{obs} \parallel, \\ 0 & \text{otherwise}, \end{cases} \tag{4.17}$$

whereby human-robot agreement A_S is determined over N_S samples and is normalized as follows

$$p_{A,S} = 1 - \frac{\sum_{i=1}^{N_S} \parallel \boldsymbol{f}_{int,i} \parallel}{N_S \cdot \max(\parallel \boldsymbol{f}_{int} \parallel)} \tag{4.18}$$

where $\boldsymbol{f}_{int,i}$ refers to sample i. Thus, the set of performances to be considered for the sensorial assistance is $p_S \in [p_{T,S}, p_{A,S}]$.

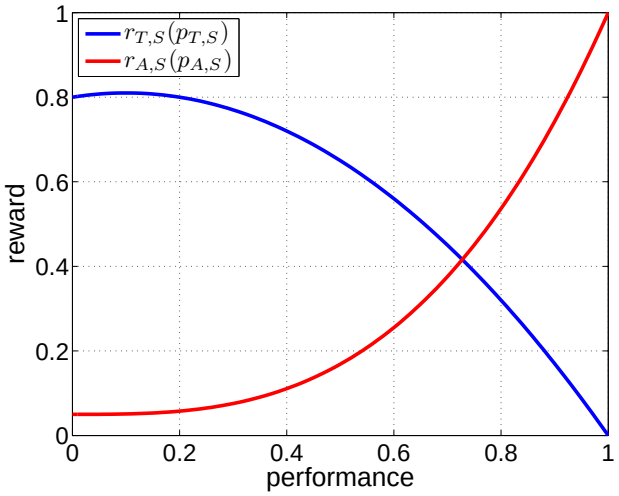

Figure 4.5: Reward structure for adapting the sensorial assistance. The blue function is the reward $r_{T,S}$ associated to the task performance measure $p_{T,S}$ and the red function is the reward $r_{A,S}$ associated to the agreement performance measure $p_{A,S}$.

Reward Structure and Decision-Making

Fig. 4.5 presents two reward functions which are defined corresponding to the two performance measures presented in section 4.4.3.

Again the DD model is adopted for decision-making. The probability to improve human-robot agreement $\mathbb{P}_{A,S}$ is calculated by (4.7) where $w_A = w_{A,S}$ and $w_B = w_{T,S}$ are the evidences for choosing to improve human-robot agreement or task performance (as defined in section 4.4.3). The evidences are calculated using (4.8) and considering the set of decisions $z \in [T_S, A_S]$ for each time t. Finally, the level of the robot sensorial assistance is modified by means of the following homotopy for the damping parameter d_x

$$d_x(t) = \mathbb{P}_{A,S}(t+1) d_{x,min} + (1 - \mathbb{P}_{A,S}(t+1)) d_{x,max} \tag{4.19}$$

where $d_{x,min}$ and $d_{x,max}$ are the minimum and maximum considered values of the damping factor.

We believe that the proposed reward structure satisfies the objectives for providing sensorial assistance as introduced in section 4.4.3. When no obstacle is detected in front of the robot, the task performance measure is at its minimum (see (4.16)) and therefore a high reward is associated to it. On the other hand, no obstacles implies no disagreement between human and robot (based on the definition of the performance measures), which results in a large value for the measure of human-robot agreement and therefore a high reward. The maximum value of the reward for human-robot agreement has been decided to be slightly larger than the maximum value of the reward for task performance, which implies a preference to improve human-robot agreement whenever no risk of collision is detected. In other words, the value of $\mathbb{P}_{A,S}$ is close to one due to the fact that the evidence $\Delta w_S = w_{A,S} - w_{T,S}$ is at its maximum according to the rewards defined.

As soon as an obstacle is detected, the reward for improving task performance decreases with a slower rate with respect to the reward for human-robot agreement. This allows a faster change from preferring human-robot agreement to task performance, the value of Δw_S decreases, which results in an increase of the level of assistance. Finally, if the human insists on continuing the motion forward despite the provided resistance of the robot (which can imply the user's interest to approach the obstacle), the task performance measure tends to its maximum value (corresponding to the lowest reward), while the human-robot agreement measure tends to its lowest value (also corresponding to a low reward). In this case the overall preference turns back again towards improving human-robot agreement since its minimum reward is larger than the minimum reward for task performance. This results in an increase of Δw_S allowing the user to approach the obstacle. However, approaching the obstacle has very low risk of collision since the robot velocity has been reduced significantly and the human remains under partial robot assistance.

4.4.4 Decision on Physical Assistance

Individualization of the robot support is considered by adapting the physical robot assistance by gain-scheduling the parameter k_2 as detailed in the following sections.

Problem Formulation

The demand for assistance of elderly and patients may increase with continuing activity due to fatigue. An assistance strategy that adapts to the current physiological state can meet the aforementioned demand and thus, can result in a higher user's satisfaction during interaction with the robot. This requires that the MAR not only evaluates the user's performance with respect to the desired task, but also estimates the physiological state of the user in order to decide on the level of the provided robot assistance. Specifically, we aim at shifting the control authority to the robot if task performance is low and human fatigue high and at gradually returning authority to the user when task performance improves and human fatigue decreases. Again, this is formulated as decision-making problem.

We propose an active support by applying an assistive torque to the admittance model. Considering (4.4) and (4.5), the input torque can be manipulated by a proper selection of

the parameter k_2.

Performance Measures

In general two different types of human fatigue are studied in literature: mental and physical. Physical fatigue, which we focus on in this thesis, presents the maximum level of exhaustion at which the human cannot exert any more work.[2] In literature, medical indicators of human fatigue are mostly discussed based on heart rate or the total performed work. Since the former requires an external monitoring system, e.g. heart rate sensor, we mainly focus on the latter. Physical fatigue is directly related to the total power consumed in the human muscles and therefore total work performed as presented by [180]. The total work performed by a person during walking is related to the user's walking velocity and the total weight of the user. Authors in [181] proposed the following formula that relates consumed calories per kilogram per hour l_{cal} to the user's velocity v_h during walking

$$l_{cal}(v_h) = 14.326\frac{v_h}{0.362 + 0.257v_h}(0.136v_h + 0.066v_h^2). \tag{4.20}$$

We use the aforementioned formula to formulate the level of the human fatigue during walking. Considering a person with total weight of M pushing a MAR with apparent mass m_x and moving with linear velocity of $v_h = v(t)$ at time t, the normalized level of human fatigue is estimated as

$$F(t+1) = F(t) + \frac{l_{cal}(v(t))(M + m_x)\Delta t}{l_{cal,fat}}, \tag{4.21}$$

where F represents the level of human fatigue, Δt the sampling time of the system and $l_{cal,fat}$ the maximum possible consumed calories resulting in human fatigue. [3] We define

$$p_{F,O} = 1 - F \tag{4.22}$$

to be the performance measure correlating with the estimated human fatigue.

The overall task performance is defined based on the tracking error of the desired path as well as the distance to the nearest obstacle in front of the robot which is computed as follows

$$p_{T,O} = \frac{\sum_{i=1}^{N_O} |\delta_i|}{N_O \delta_{max}}, \tag{4.23}$$

$$\delta = k_{O,\theta_e} \cdot \theta_e + k_{O,e} \cdot e + k_{O,obs} \cdot \frac{1}{\| \boldsymbol{d}_{obs} \|}, \tag{4.24}$$

where δ_i is defined as a measure of total task performance at sample i, δ_{max} the maximum

[2] Please note that the natural definition of mental and physical fatigue are closely related and it is commonly known that physical fatigue impairs mental fatigue. However, [179] has only recently shown that mental fatigue can also imply physical fatigue. Therefore, we just consider the effect of physical fatigue since this is the most probable cause of fatigue in a mobility assistance scenario.

[3] The work performed by a human to maneuver the platform has not been considered in the computation of human fatigue for the sake of simplicity.

value of δ, $p_{T,O}$ the observed task performance over the observation window with length N_O. We consider a larger value for N_O than N_S and N_C (defined in section 4.4.2 and 4.4.3 respectively) for a better estimation of the more long-term changes in human task performance rather than specific reactions to a given situation. The values of k_{O,θ_e}, $k_{O,e}$ and $k_{O,obs}$ are weighting factors, which can be tuned according to the importance of following the path or avoiding obstacles.

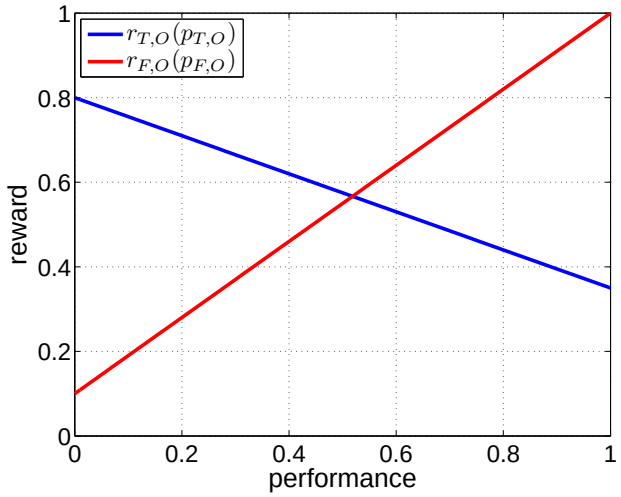

Figure 4.6: Reward structure for adapting the physical assistance. The blue function is the reward $r_{T,O}$ associated to the overall task performance measure $p_{T,O}$ and the red function is the reward $r_{F,O}$ associated to the performance measure correlating with estimated human fatigue $p_{F,O}$.

Reward Structure and Decision-Making

The reward structure for the two performance measures is shown in Fig. 4.6.

The linear structure has been chosen as there is no specific preference on improving the overall task performance or increasing the support because of human fatigue. This structure allows to change the decision (gradually) whenever human fatigue or performance changes are detected.

The level of the physical assistance is finally tuned according to the DD model. The estimated level of the robot physical assistance $\mathbb{P}_O$ is computed using (4.7) with $w_A = w_{F,O}$ and $w_B = w_{T,O}$. The evidences are computed using (4.8) and assuming the decision set $z \in [F_O, T_O]$ at each time t. Thus, the level of the robot overall assistance is adapted by tuning the weighting factor k_2 presented in (4.4) as follows,

$$k_2(t) = \mathbb{P}_O(t+1)k_{2,min} + (1 - \mathbb{P}_O(t+1))k_{2,max} \tag{4.25}$$

where $k_{2,min}$ and $k_{2,max}$ are the minimum and maximum considered values for k_2. We propose a very smooth soft-max function by considering a small value for the μ parameter in (4.7). This allows to gradually shift the preference between the human or assistant to control the robot steering velocity.

Finally, to recover the orientation error a robot assistive moment can be generated using the following control law

$$\tau_{assis} = K_{p_1} e + K_{p_2} \theta_e, \tag{4.26}$$

where K_{p1}, K_{p2} are user-specific defined gains.

4.5 Experimental Results

This section illustrates the effectiveness of the proposed approach, first by means of experiments aiming for a technical validation with a healthy user interacting with the platform and then by means of a user study involving 35 elderly persons.

4.5.1 Technical Validation

In the following sections we technically validate the proposed decision making algorithm realizing adaptive shared control in MAR.

Experimental Setup

The robotic platform as shown in Fig. 3.8 was used for validation of the presented adaptive shared control approach. The controller of the robot mobile base was implemented using MATLAB/Simulink Real-Time Workshop. The robot velocity was controlled using a low-level high gain PD controller. The control loop was set to run at $T = 1\,ms$ sampling time. The robot handles were not actuated and kept at a constant height during the whole experiments.

A static map of the experimental room was build in the Robot Operating System (ROS) using the OPENSLAM Gmapping library package based on captured laser scanner, IMU and robot's odometry data. A path planner as part of the `move_base` package in ROS was implemented that provides a fast interpolated path planning function used to create plans for the mobile base.

For determining the closest point, we used a planner that assumes a circular robot and operates on a cost map, which produces a global path from a starting robot pose to an end pose in a grid. Then, an algorithm was used that searches iteratively on the global path to find the closest points to the current robot position. To solve ambiguity in case two or more closest points are found, we implemented a look-ahead checker, which processes past closest points and returns the next closest point which is located ahead of the robot and has the maximum orientation alignment with the current robot pose.

Robot localization was performed using an Adaptive Monte Carlo Localization (amcl) approach, which was implemented in ROS as part of the `nav_stack` package and provides an estimate of the robot's pose against a known map. It continuously registers the robot pose on the map and corrects possible odometry errors.

An obstacle map based on the front laser scanner was constructed in order to provide information about the closest obstacle in defined zones around the robot. We splitted the area in front of the robot into 5 zones and computed the distance of the nearest obstacle in each zone to the robot, see Fig. 4.7 for a snapshot.

Test Scenarios

The presented approach was tested using two scenarios. In the first scenario the integration of the cognitive, sensorial and physical assistance was tested, while in the second scenario we specifically investigated the performance of the realized sensorial assistance and its ability to avoid obstacles or allow their intentional approach.

Scenario I: The user was asked to define a desired destination on the map of the experimental area shown on the screen mounted on the robot frame. According to the user's choice, a reference path was automatically generated to the final destination. The user was asked to follow the path while trying to deviate from the path at least once. At half way, another human was asked to pass in front of the robot simulating a dynamic obstacle. The user was instructed to not pay attention to this dynamic obstacle, pretending of not having noticed it. Towards the end of the path the user was asked to keep the robot orientation slightly off the reference path to test the effect of the robot physical assistance.

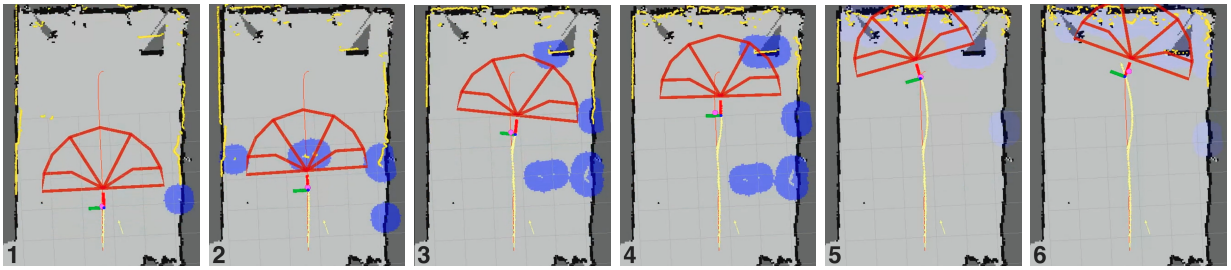

Figure 4.7: Snapshots taken during the human-robot cooperation in scenario I. The map of the area is depicted in gray, while the dark gray areas show the occupied static obstacles found during the map building. The yellow points indicate the location of observed obstacles during the experiment. The blue point clouds are clusters around each obstacle in the vicinity of the robot (this is only for presentation purposes and has no application in the presented approach). The area in front of the robot is divided into 5 zones as shown in thick red lines. The generated reference path is presented by thin red, while the path the robot passed is shown with yellow line (can be seen near the reference path behind the robot). Each snapshot presents the following information from left to right, 1: initial phase of walking where no obstacles are detected and the user is well following the path, 2: a dynamic obstacle moves in front of the robot, 3: the user is deviating from the reference path 4: increase of the user's deviation is restricted by the robot and therefore the user comes back to the path, 5: the user keeps an orientation error at the end of the experiment, and 6: the robot physical assistance recovers the orientation error.

The parameters used for realizing the cognitive assistance were as follows: $N_C = 2500$, $k_{C,e} = 5$ and $k_{C,\theta_e} = 10$. We considered $\mu_C = 0.6$ in order to increase certainty in the decision making and to avoid chattering. For the sensorial assistance functionality, we set $\boldsymbol{d}_{obs,max} = 0.85m$, $N_S = 2500$ and $\mu_S = 10$. For the physical assistance we exaggerated the value of $l_{cal,fat} = 10^4$ for the sake of presentation to be able to detect human fatigue after a short duration of walking, although the real value of $l_{cal,fat}$ is much higher and can be

Table 4.1: Defined reward structures for robot assistance.

	reward structure
cognitive asistance	$r_{T,C}(p_{T,C}) = {p_{T,C}}^3 - 0.1$ $r_{A,C}(p_{A,C}) = -{p_{A,C}}^3 + 0.8$
sensorial asistance	$r_{T,S}(p_{T,S}) = 0.95{p_{T,S}}^3 + 0.05$ $r_{A,S}(p_{A,S}) = -(p_{A,S} - 0.1)^2 + 0.81$
physical asistance	$r_{T,O}(p_{T,O}) = 0.9p_{T,O} + 0.1$ $r_{F,O}(p_{F,O}) = -0.45p_{F,O} + 0.8$

determined from literature. We mostly focused on the error of the robot orientation with respect to the reference path in order to actively point the human towards the destination. Therefore, we set $k_{O,\theta_e} = 8$, $k_{O,e} = 5$ and $k_{O,obs} = 1$. The value of forgetting factor $\lambda = 0.6$ was considered for all cases, while the value of $N_O = 10^4$ and $\mu_O = 12$ were selected in the admittance model. To fulfill the requirements of the desired robot assistance in all three cases, the reward structures were defined as presented in Table 4.1. Moreover, the parameters for the desired inertia of the admittance controller were considered to be $m_x = 15$ and $I_\theta = 5$.

Figure 4.7 shows some snapshots taken during the experiment. The map of the experimental area, the robot and defined obstacle zones, detected obstacles at the front and around the robot as well as the desired and traveled path are shown.

At the beginning of the experiment a dynamic obstacle (another person) was passing in front of the robot ($\approx 30 < t < 32$s). As depicted in Fig. 4.8, when the robot approaches the obstacle the task performance increases. Moreover, since the user was asked to not react to the obstacle, the agreement between the robot being interested in avoiding the obstacle and the human not reacting properly decreases. Taking into account the defined reward structure, the human receives a quite low reward which results in triggering the robot decision to increase the robot assistance which was achieved by automatically increasing the damping factor and therefore reducing the robot approaching velocity to the obstacle. As soon as the dynamic obstacle passed the robot and the risk of collision reduced again, the robot decided to return the authority of controlling the motion of the robot to the user, which happened quite smooth, but fast (with respect to the first decision of increasing the assistance) in order to avoid the user pushing against a blocked robot while there is no obstacle in front of it.

When trying to deviate from the path ($\approx 35 < t < 37$ s) as shown in Fig. 4.9 the task performance increases, while the agreement decreases as the robot preferred to stay on the path, while the human was deviating from it. Therefore the robot assistance hindering the user from further deviating from the path is activated and the value of the damping d_θ is increased. This notifies the user that the current direction of motion is not aligned with the desired reference path. However, as soon as the user adapts his input and aligns the robot with the desired path, the robot assistance quickly returns the authority to control

the platform to the user.

For the last part of the path when the user was simulating fatigue, we considered a low value for $l_{cal,fat} = 10^4$ in order to visualize the effect of the realized algorithm even after only 50 s of walking, see Fig. 4.10. With increasing duration of the human walking, the estimation of the human fatigue, and thus the corresponding performance measure, increased, while the overall human task performance varies according to the distance of the human to obstacles and the overall deviation from the path and orientation error [4]. By increasing the orientation error in the last phase of the experiment, the corresponding performance was influenced and therefore a lower reward was associated. This resulted in a change of the decision towards increasing the level of active assistance by increasing the robot contribution to the control of the robot's orientation. Therefore the value of k_2 was increased to its maximum which we considered to be 0.6 for the sake of safety.

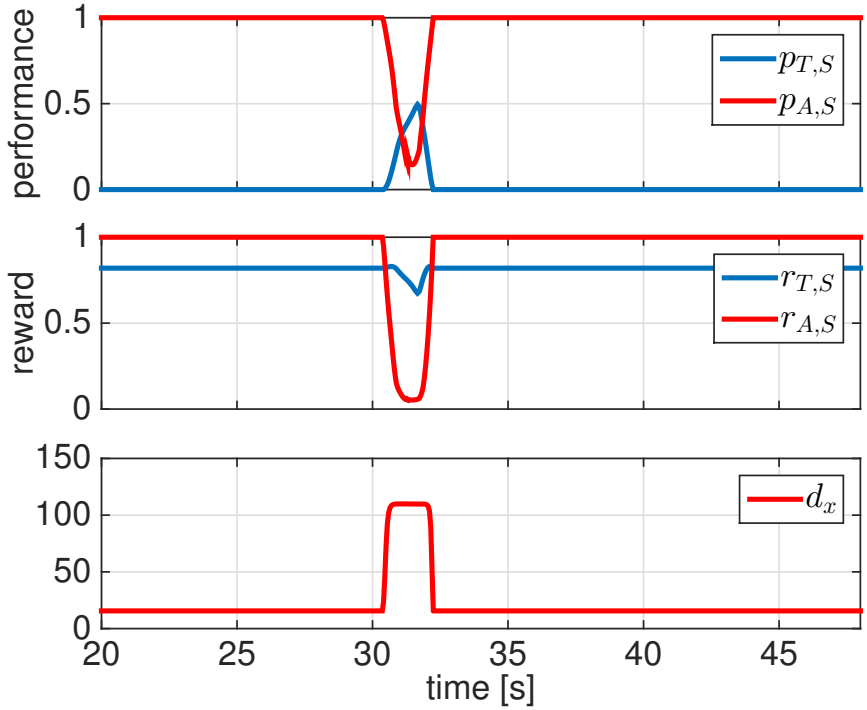

Figure 4.8: Results of the sensorial assistance during the human-robot cooperation in the scenario I.

Scenario II: In this scenario we focused on the evaluation of the robot sensorial assistance and tested the functionality of distinguishing between approaching obstacles either intentionally or accidentally. To be able to focus on the sensorial assistance functionality, the cognitive and physical assistance were deactivated to prevent the results being influenced by these other assistances. Figure 4.11 shows the snapshots taken during the experiment.

Two static obstacles were positioned in front of the robot, one after the other in heading direction. A third obstacle (table) was further considered as an intentional goal. The

[4] Please note that emphasizing mostly on the orientation error in the overall task performance was assumed only for the sake of presentation. However, one may associate different values for the contribution of each of the terms to the overall task performance.

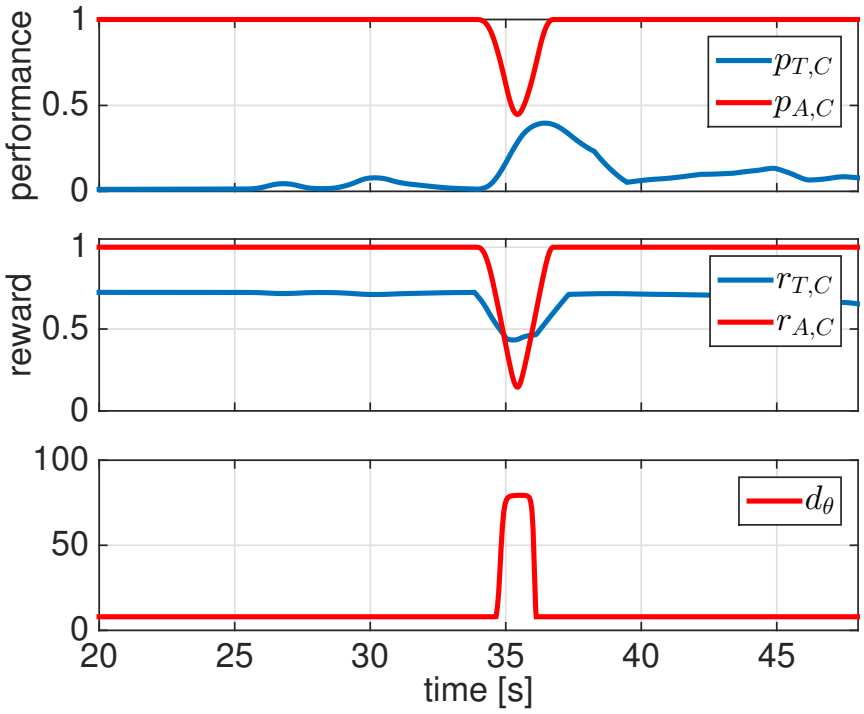

Figure 4.9: Results of the cognitive assistance during the human-robot cooperation in the scenario I.

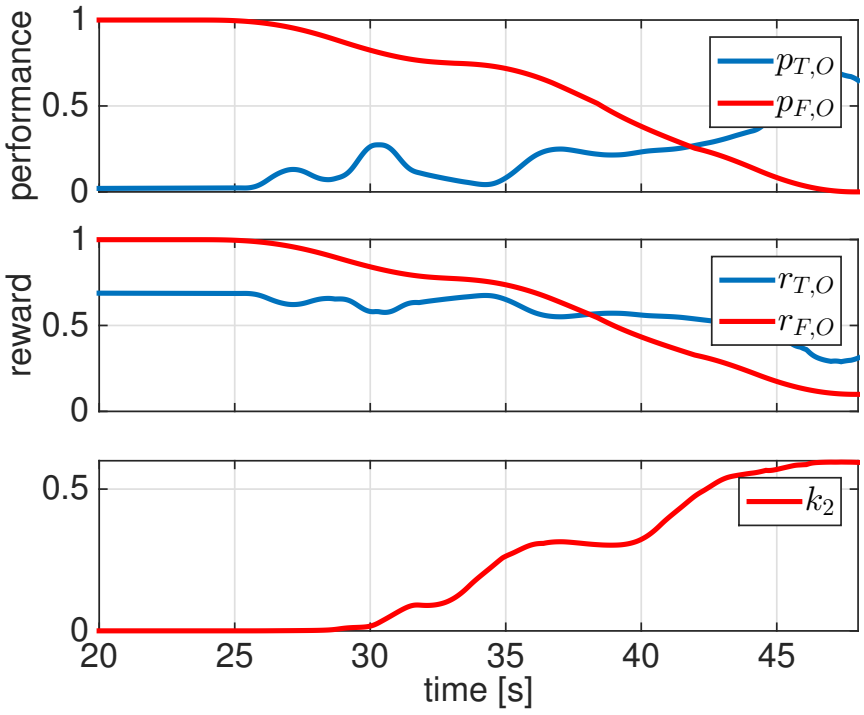

Figure 4.10: Results of the physical assistance during the human-robot cooperation in the scenario I.

user was asked to approach the table and grasp an object located on it assuming the two obstacles are initially not detected due to e.g. bad sight. As shown in Fig. 4.12, when

approaching the first two obstacles (the first at $\approx 36 < t < 37.5$ s and the second at $\approx 40 < t < 43$ s), the robot task performance is increased while the agreement is decreased, which implies a risk of collision. The robot correctly decides to prevent the collision with obstacles as the value of the damping factor d_x is increased and only returns the authority to the human once he/she changed the orientation of the robot and thus, the risk of collision decreased (damping factor d_x was decreased fast). However, in the third case where the human pushed the robot towards the intentional obstacle (at $\approx 46 < t < 52$ s), the robot initially reduced the approaching velocity (value of the damping factor d_x was increased), but then it returned the authority to the human to allow for further safe approach to the intentional obstacle (value of the damping factor d_x was reduced to 30). This change in the authority allocation happened even though task performance was low as the robot was in a very close distance to the obstacle.

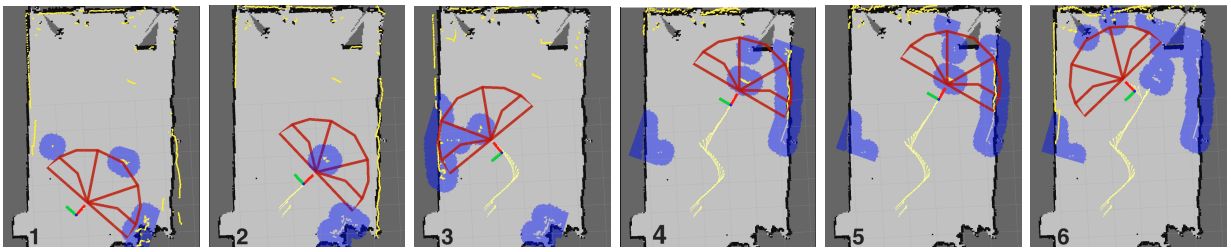

Figure 4.11: Snapshots taken during the human-robot cooperation in scenario II. The map of the area is depicted in gray, while the dark gray areas show the occupied static obstacles found during the map building. The yellow points indicate the location of observed obstacles during the experiment. The blue point clouds are clusters around each obstacle in the vicinity of the robot (this is only for presentation purposes and has no application in the presented approach). The area in front of the robot is divided into 5 zones as shown in thick red lines. The path that the robot passed is shown with yellow line behind the robot. Each snapshot presents the following information from left to right, 1: initial phase of walking where an obstacles is detected in front of the robot, 2: close distance between the robot and obstacle which increases the risk of collision resulting in the robot reaction to avoid collision, 3: the second obstacle is determined and the robot reacts to avoid collision 4: the user is guiding the robot towards a new obstacle he wants to approach intentionally, 5: the robot allows to a very close approach to the intentional obstacle, and 6: the user leaves the intentional obstacles.

4.5.2 User Study

An intensive evaluation with 35 elderly subjects was performed to assess the effectiveness of the proposed adaptive shared control approach. Thirty one women and four men participated in the evaluation which took place for six weeks at the rehabilitation centre of the Agaplesion Bethanien Hospital/Geriatric Centre at the University of Heidelberg. The average age of subjects was 84.3 $\pm$5.4, ranging from 71 to 94 years. The study sample comprised frail older persons as expressed by impaired motor status (Performance Oriented Mobility Assessment, [182]: 20.3 $\pm$5.4; gait speed, 5-chair stand test [183]: 0.48 $\pm$0.16 m/s,

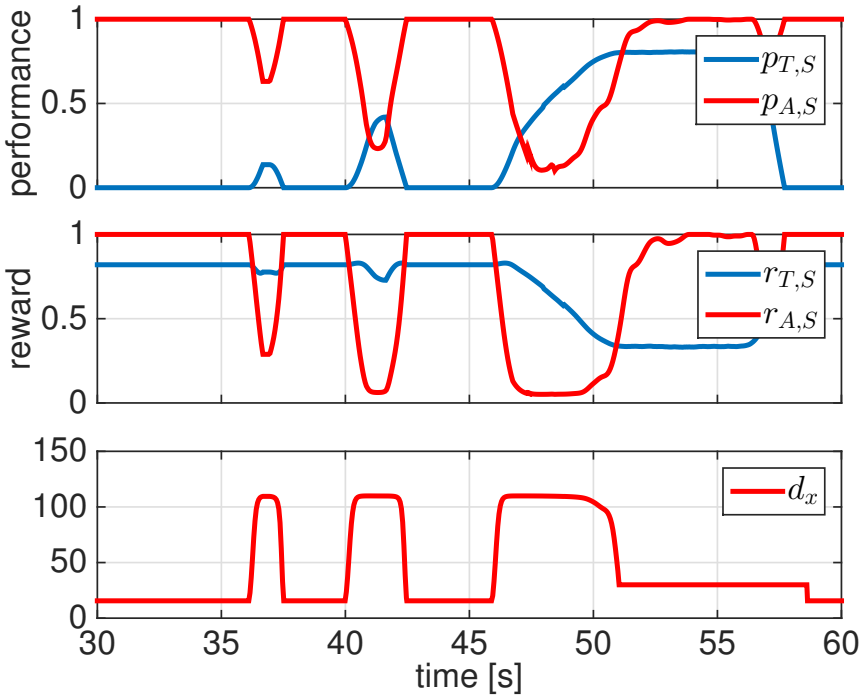

Figure 4.12: Results of the sensorial assistance during the human-robot cooperation in the scenario II.

19.2 ±7.5 s) and high risk of falling (63 % of subjects reported one or more falls in the last year). All subjects currently used conventional walkers in their daily routine. The experiments were performed under ethical approval by the ethics committee of the Medical Department of the University of Heidelberg, Alte Glockengießerei 11/1, 69115 Heidelberg, Germany. Written informed consent was obtained from all subjects participating in the study.

Test Conditions

The adaptive shared control approach for sensorial assistance has been implemented on the robotic platform and was compared with an existing approach in literature. We considered three different conditions:

- C1: Walking assistance without obstacle avoidance functionality implementing a constant virtual inertia and damping.
- C2: Walking assistance with obstacle avoidance based on the approach presented by [184].
- C3: Walking assistance with obstacle avoidance based on the decision-making algorithm presented in this manuscript.

The main reason for focusing on the evaluation of the sensorial assistance in the user study is that beside the baseline C1 there is hardly any directly comparable algorithm available for the other two modes.

For a fair comparison, base values of $m_x = 15$ kg and $I_\theta = 5$ kgm^2, and of $d_x = 10$ Ns/m and $d_\theta = 10$ Nms/rad were considered for each condition. These values were selected after discussion with rehabilitation experts. Although the above mentioned values were considered constant for condition C1, the value of d_x and d_θ were adapted up to their maximum of $d_{x,max} = 110$ Ns/m and $d_{\theta,max} = 80$ Nms/rad in C2 and C3. The maximum values were selected following discussions with rehabilitation experts as well as tests to achieve a good maneuverability of the device with respect to a standard non-motorized walker. We considered 70 cm distance between the robot and obstacles as the activation distance, i.e. the base values were considered in C2 and C3 only for distances larger than 70 cm, while the adaptation laws were applied for distances less than 70 cm.

Experimental Setup

A special test environment was prepared within the Bethanien rehabilitation center to test the proposed adaptive shared control approach. Figure 4.13 shows the map of the test environment and a representative example of a test path. The test environment covered an area of about 10×9 m with an approximate length of 40 meters of test path starting from an initial position, passing through the narrow corridor by avoiding obstacles and coming back to the same initial position. The height of obstacles varied in different sections of the area. The considered round trip allowed us to record the same number of left and right turns. Over the whole trial the user was faced to 17 obstacles, and a minimum amount of 16 turns either to avoid collisions with obstacles or to perform turns along the path. No reference path was marked on the ground during tests.

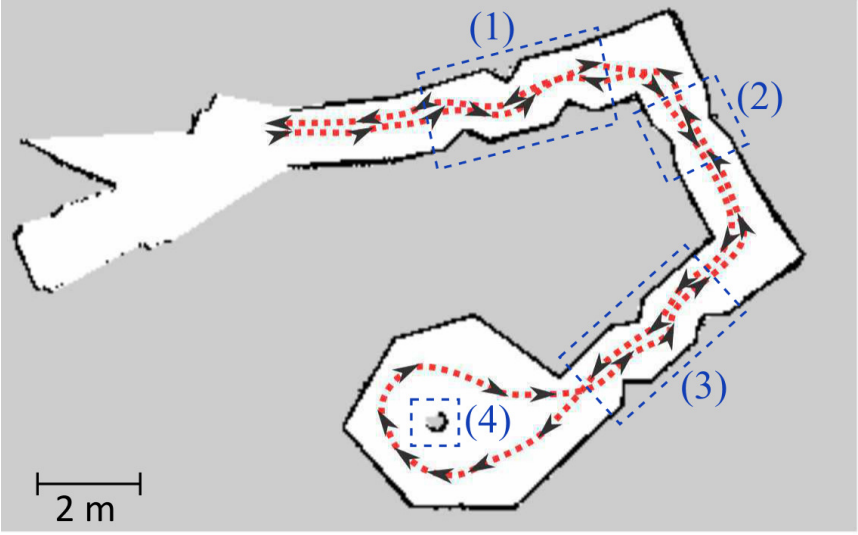

Figure 4.13: Map of the evaluation course. The main walking area has a size of about 10 x 9m. The corridor included three sections with obstacles and one turning area in which participants had to drive round a pillar (area (4)) before driving back to the very beginning of the course. The height of obstacles varied in the different sections as follows: 90 cm (1), 50 cm (2)+(3).

Evaluation Method

Before participants completed the test trials, each of them was asked to drive freely through the course. For this first run, no instructions concerning obstacle avoidance and walking speed were given by the test supervisor, and no sensorial assistance was provided by the robot platform. This trial was intended to familiarize the participants with the device and course.

Each participant then completed the obstacle course under three different conditions mentioned in section 4.5.2. The order of the conditions tested with each participant was randomized to exclude learning effects. The participants were not told which condition was used during the three different trials. Before starting each trial, the participants were instructed to complete the course as fast as possible. After each trial, a sufficient recovery phase was provided to the participants in order to prevent fatigue.

Evaluation Results

Two performance metrics were considered in order to verify the effectiveness of the proposed sensorial assistance: number of collisions (with the front of the robotic platform) and task completion time.

Differences in the number of collisions and task completion time between the three conditions were statistically analysed by a one-way analyses of variance (ANOVA) and obtained results are shown in Figs. 4.14, 4.15 and 4.16. No significant differences between conditions C1, C2 and C3 were identified in terms of task completion time. However, significant differences were found for the number of collisions and approaching velocity to obstacles. Post-hoc tests (Bonferroni corrected) showed a reduced number of collisions and reduced approaching velocity for C3 (sensorial assistance based on decision making algorithm) compared to condition C1 ($p < .05$), but no significant differences between other conditions (C2 vs. C1 / C3: $p = .07/.99$). The lowest approaching velocity to obstacles was found for C3.

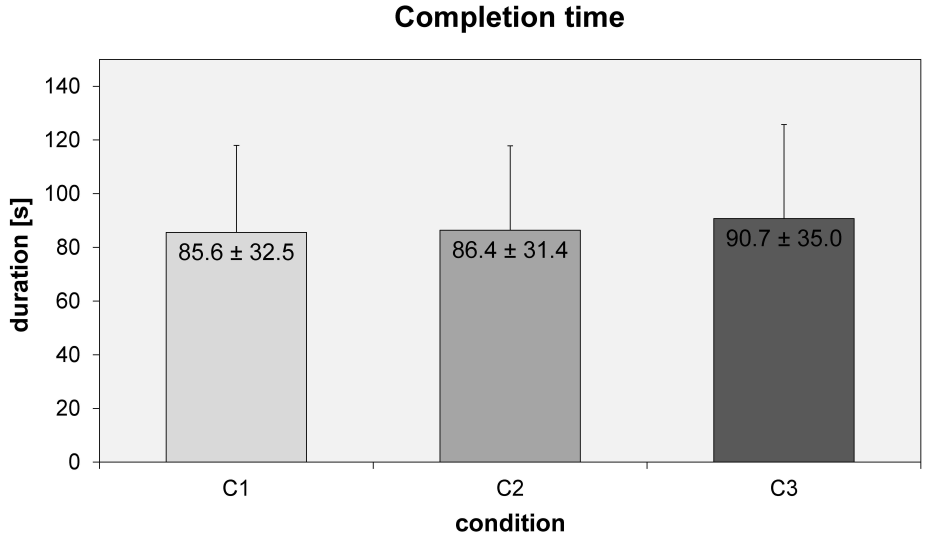

Figure 4.14: Completion time in the user study under three conditions (C1, C2 and C3).

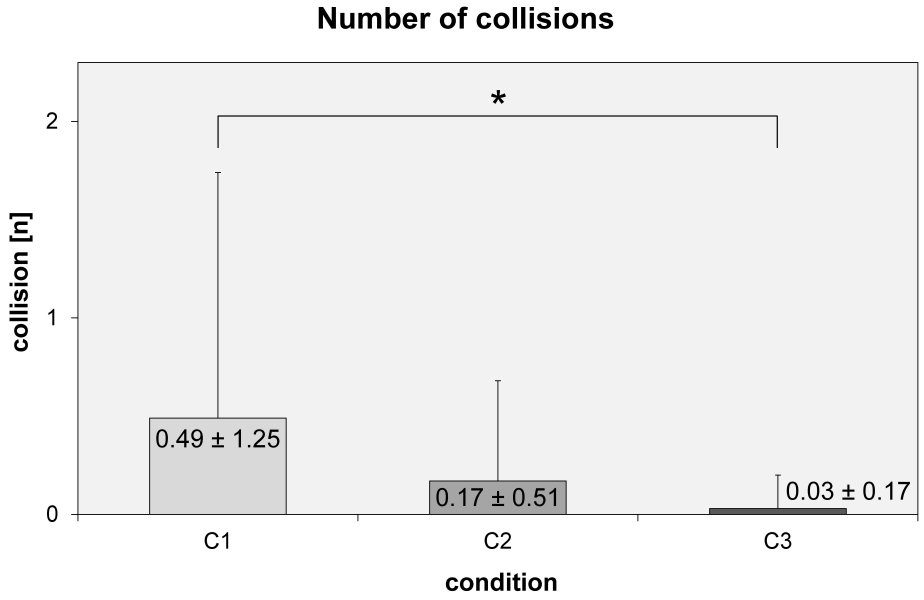

Figure 4.15: Recorded number of collisions in the user study under three conditions (C1, C2 and C3).

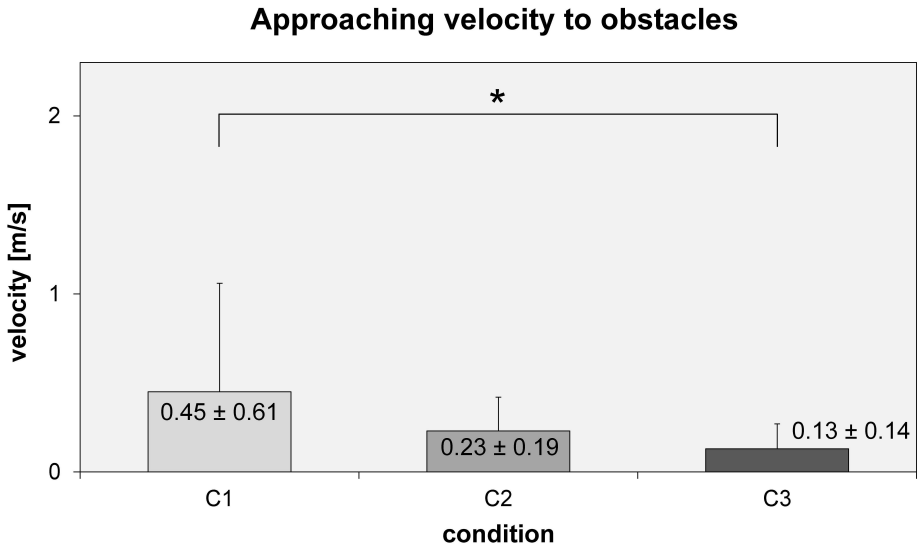

Figure 4.16: Recorded average approaching velocity to obstacles in the user study under three conditions (C1, C2 and C3).

4.6 Summary and Discussion

Mobility assistance robots are a typical example of systems, which implement shared control capabilities. So far, however, fixed scheduling strategies have mainly been employed to combine user and autonomous robot's inputs. Research into the direction of more context-dependent and dynamic authority sharing mechanism, also involving methods for decision making, have so far been little explored.

The main contribution of this chapter can thus, be summarized as follows: to develop an integrated approach for the context-specific, on-line adaptation of the assistance provided

by a rollator-type MAR, and to employ human decision-making mechanisms in the adaptation laws. The shared control architecture distinguishes between short-term adaptations providing a) cognitive assistance to support the user in following a desired path towards a predefined destination and b) sensorial assistance to avoid collisions with obstacles and to allow for an intentional approach of them. Furthermore, it considers a long-term adaptation of c) the overall assistance based on long-term user's performance and observed fatigue. To achieve an intuitive and human-like adaptation policy of the provided assistance, a decision making model explored in cognitive science, the Drift-Diffusion model, was employed.

The technical performance of the proposed approach was tested in two scenarios and resulted in the desired robot behavior as the robot's cognitive, sensorial and physical assistance were activated as needed. The effectiveness of the proposed approach was demonstrated in the performed user study with end-users. The lowest number of collisions, alongside with lowest approaching velocity to obstacles was found when the user was passing the obstacle course using our newly proposed algorithm. However, similar task completion times for all conditions indicated that the proposed sensorial assistance approach does not interfere with the normal activity of the patients and furthermore guarantees a safe intentional approach to obstacles if needed.

One of the main practical challenges in the presented work was tuning basic and maximum values of adjustable parameters. We finally agreed on the chosen values based on discussions with experts. Furthermore, the selection of suitable performance metrics and reward structures strongly affects the performance of the algorithm and a series of alternative performance metrics and related reward structures could have been chosen instead. We don't argue that our selection is the best, but that it fulfills the desired purpose of improving sensorial, cognitive and physical assistance. Further investigations of performance metrics and reward structures, possibly being time and context-dependent, can be a focus of future research. Moreover, employment of different human-decision making models for the control design of MARs can be further investigated, since only the DDM model was studied in this chapter.

While this chapter aimed to ensure safety in human-robot interaction by realizing as passive as possible robot behavior, the next chapter will further propose solutions for the prevention of possible human falls to enhance human's safety.

5 Human Fall Prevention Assistance

This thesis so far presented novel approaches for the biologically-inspired control design of MARs implementing two modes of sit-to-stand and walking assistance, while fall prevention (the last considered mode of operations in this thesis) is discussed in this chapter. For the first time, we propose an optimal control approach for human fall prevention when interacting with a MAR equipped with a pair of actuated arms.

Fall prevention is especially important since falls of elderly have a high probability to cause severe injuries that are risk factors for further disability [185].

In literature fall prevention functionalities are presented mostly for passive systems without actuated arms [186, 187]. In [186, 188] user's falls are estimated by evaluating the relative distance between the user's legs and the MAR measured using a laser range finder and averaged to estimate the projected user's Center of Mass (COM). This feature is compared to its user-specific normal distribution during walking to determine the probability of a user's fall and to activate the brakes accordingly. The risk of falling is defined to increase if the projection of the COM approached the border of the support polygon. Human falls are recognized along the horizontal direction (caused for example by stumbling and leading to legs that are far apart from the walker), and falls along the vertical direction (caused for example by weak legs). Finally, varying admittance control is realized for fall prevention by increasing the damping in the desired admittance if the user is found to be in a *falling* state achieved by activating the brakes accordingly, while in the *stopped* state large brake torques are applied to each of the wheels independently of the user's applied force to the system.

A basic challenge in designing a suitable control approach for assistance robots with fall prevention functionality is to select a proper human fall detection measure. The most sophisticated measure used in the aforementioned fall prevention algorithms is the human COM, which, however, cannot fully capture human balance [189]. The Zero Moment Point (ZMP) or Center of Pressure (CoP) determines the human balance more accurately [103, 190]. Human balance is guaranteed if the ZMP or COP stay within a support polygon that is either the area of a foot or both feet depending on the gait phase. Although these features depend on the COM position and its acceleration, their computation is very complex, especially for a human interacting with an assistance robot. In contrary, the Extrapolated Center of Mass (XCOM) (or Instantaneous Capture Point) has shown several advantages in human or humanoid balance studies [191–196]. As we will show, XCOM is easier to compute since it is related to the COM and its velocity rather than acceleration, and it can be faster in fall detection than the COM as the COM velocity provides a simple prediction of the COM future behavior.

The novelty in this chapter lies thus in the development of a fall prevention approach for a MAR equipped with a pair of actuated arms, never being exploited so far. We propose an algorithm that evaluates the user's XCOM and determines required supportive forces to

be applied to the user for fall prevention as soon as a risk of fall is predicted. Derivation of the required assistive forces are formulated as an optimization problem, while the obtained forces are realized by a MAR using a compliance controller. We further show applicability of the proposed approach by experimental evaluation using a MAR that supports subjects provoking falls in forward, backward and sideways directions.

This chapter firstly describes equations of motion of a MAR and the simplified human model in section 5.1. Then, section 5.2 presents the fall prevention control approach, while simulation and experimental results are reported in section 5.3. Finally, a summary and conclusion is given in section 5.4.

5.1 System Description

In the following section we present models for the MAR and human assuming rigid grasp conditions.

5.1.1 Robot Model

The considered MAR in section 4.2.1 is employed. We consider that both arms are independently actuated in order to transfer supportive forces to the human. Considering the kinematic model of the robot base presented as in (4.1), the kinematic model of left (l) and right (r) robotic arm is defined as $\dot{\boldsymbol{x}}_{arm,i} = \boldsymbol{J}_{arm,i}\dot{\boldsymbol{q}}_i$ where $\dot{\boldsymbol{x}}_{arm,i}$ are the Cartesian velocity of the tip of the arm $i \in (l \text{ or } r)$ with respect to its base frame and $\dot{\boldsymbol{q}}_i = \left[\dot{q}_{1,i},\ \dot{q}_{2,i},\ \ldots,\ \dot{q}_{n,i}\right]^T$ the arm joint velocities.

5.1.2 Human Model

In literature human models with different complexity have been studied. More complex models comprising a high number of human segments typically require an accurate tracking system. Simpler models such as a linear inverted pendulum (LIP) provide less accurate estimation of the human segment locations, but lead to lower complexity in computation and implementation even for real-time purposes. The LIP model has been widely used in human balance studies and gait analysis (see [191, 192, 194, 197]) and is therefore used in this thesis. The LIP model has shown a very similar behavior to the real human in balance studies, especially at the initial phase of the human movement before reaching the unbalanced state [194, 197]. This particularly justifies the use of the LIP model in the presented fall prevention approach, which has to provide a proper reaction before human falls are happening.

We employ a 3D-LIP model with finite-sized feet and no slippage at the contact points considering assistive forces applied at the interaction points as shown in Fig. 5.1. The 3D-LIP model with point foot was initially proposed by [198] for the modeling and motion generation of bipedal walking robots and was further extended to the finite-sized model in [197]. We slightly extended this model to allow for the inclusion of external interactions. Finally, the mass m of the pendulum moves under the action of the forces $\boldsymbol{F}_{assis}$ and torques $\boldsymbol{T}_{assis}$ applied by the assistance robot, the torques $\boldsymbol{\tau}$ applied at the pivot joint and the

gravity $\boldsymbol{g}$. The point mass is kept on a horizontal plane by generalized forces $\boldsymbol{f}$ in the system.

Considering the position of the COM by the vector $\boldsymbol{P}_{COM} = \begin{pmatrix} x_{COM}, & y_{COM}, & z_{COM} \end{pmatrix}^T$, the dynamic equation of motion is written as follows with respect to Fig. 5.1:

$$m\ddot{\boldsymbol{P}}_{COM} = \boldsymbol{f} + m\boldsymbol{g} + \boldsymbol{F}_{assis}, \tag{5.1}$$

$$-(\boldsymbol{P}_{COM} - \boldsymbol{P}) \times \boldsymbol{f} + \boldsymbol{\tau} - \boldsymbol{T}_{assis} = \boldsymbol{0}, \tag{5.2}$$

where $\boldsymbol{f} = \begin{pmatrix} f_x, & f_y, & f_z \end{pmatrix}^T$ are the internal forces acting on the point mass, $\boldsymbol{F}_{assis} = \begin{pmatrix} F_x, & F_y, & F_z \end{pmatrix}^T$ and $\boldsymbol{T}_{assis} = \begin{pmatrix} T_x, & T_y, & T_z \end{pmatrix}^T$ the resultant external forces and torques applied to the COM due to the external forces on the interaction point and $\boldsymbol{g} = \begin{pmatrix} 0, & 0, & -g \end{pmatrix}^T$ the gravitational acceleration. The equation 5.2 is obtained by considering moment balance for the massless link, where $\boldsymbol{P}$ is the position of the pivot point (e.g. the human's ankle), which may change when a step is taken, but is assumed to be instantaneous and therefore has no effect on the position and velocity of the point mass. Considering that the user firmly grasps the robot handles, $\boldsymbol{F}_{assis}$ and $\boldsymbol{T}_{assis}$ are computed as follows,

$$\begin{aligned} \boldsymbol{T}_{assis} &= \boldsymbol{h}_l \times \boldsymbol{F}_l + \boldsymbol{h}_r \times \boldsymbol{F}_r, \\ \boldsymbol{F}_{assis} &= \boldsymbol{F}_l + \boldsymbol{F}_r, \end{aligned} \tag{5.3}$$

where $\boldsymbol{h}_i = (h_{i,x},\, h_{i,y},\, h_{i,z})^T \; i \in (l,\, r)$ are the distances between the contact points and the position of the point mass.

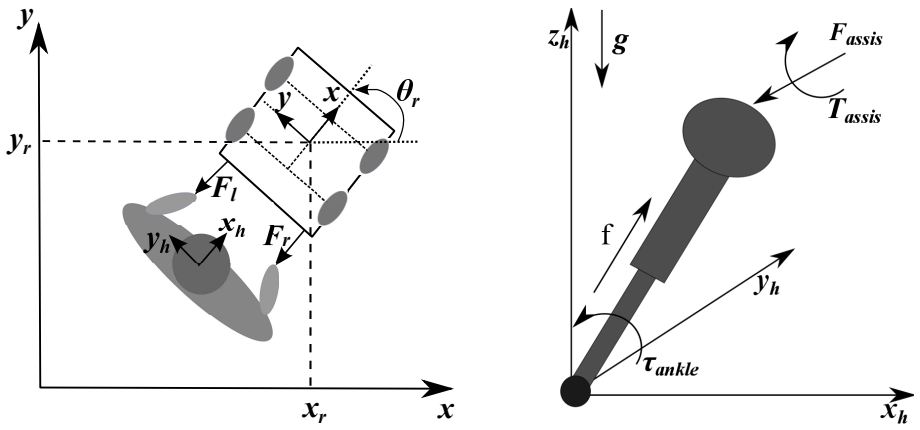

Figure 5.1: Frame representation of the human and mobility assistance robot (left) and the employed 3D Linear inverted model (3D-LIP) model.

In eq. (5.1) we obtain $f_z = mg - F_z$, which is substituted in (5.2) to compute other

components of the generalized force $\boldsymbol{f}$ as follows,

$$f_x = m x_{COM} \omega_0^2 \big(1 - \frac{F_z}{mg}\big) - \frac{\tau_y}{z_0} + \frac{T_y}{z_0}, \tag{5.4}$$
$$f_y = m y_{COM} \omega_0^2 \big(1 - \frac{F_z}{mg}\big) + \frac{\tau_x}{z_0} - \frac{T_x}{z_0},$$

where $\omega_0 = \sqrt{\frac{g}{z_0}}$ is the eigenfrequency of the pendulum. Finally, the equation of motion is given by

$$\ddot{x}_{COM} = x_{COM} \omega_0^2 \big(1 - \frac{F_z}{mg}\big) - \frac{\tau_y}{m z_0} + \frac{T_y}{m z_0} + \frac{F_x}{m}, \tag{5.5}$$
$$\ddot{y}_{COM} = y_{COM} \omega_0^2 \big(1 - \frac{F_z}{mg}\big) + \frac{\tau_x}{m z_0} - \frac{T_x}{m z_0} + \frac{F_y}{m}.$$

5.2 Fall Prevention Control

The fall prevention control approach for the considered MAR requires the i) derivation of proper assistive forces to be applied to the user, and ii) actuation of the robotic platform for a safe realization of these assistive forces.

5.2.1 Derivation of Assistive Forces

In this section we introduce an approach that evaluates human balance based on the XCOM to derive assistive forces to be applied to the user for fall prevention.

Pratt et al. [196] and Hof [191] introduced the concept of the XCOM or Capture Point. This is the point on the floor, the human or humanoid (modeled as a 3D-LIP) has to step on such that their COM is located over the ankle with zero horizontal velocity. Given the dynamics of the 3D-LIP in (5.5), the XCOM can be expressed as [196, 197]

$$\boldsymbol{P}_{XCOM} = \boldsymbol{P}_{COM} + \frac{\dot{\boldsymbol{P}}_{COM}}{\omega_0}, \tag{5.6}$$

where $(\boldsymbol{P}_{COM}, \dot{\boldsymbol{P}}_{COM})^T$ is the state of the LIP. The human gait remains stable as long as the XCOM stays within the Base of Support (BOS). The BOS typically includes the size of the feet and the room between them [191] for a human without external support. In this chapter we consider the human gripping the robot handles, which could result in a larger BOS area. However, we still consider the smaller BOS for the case of no external support in order to have a stronger balance region for the derivation of assistive forces

$$BOS := \left\{ \boldsymbol{P}_{XCOM} : \boldsymbol{\delta}^- \leq \boldsymbol{P}_{XCOM} \leq \boldsymbol{\delta}^+ \right\}, \tag{5.7}$$

where $\boldsymbol{\delta}^- = \left[\delta_x^-, \delta_y^-\right]$ and $\boldsymbol{\delta}^+ = \left[\delta_x^+, \delta_y^+\right]$ define the boundaries of the BOS.

The above mentioned balance criterion can be combined with the constraint that the COM must be able to come to a stop over the BOS and keeping the XCOM inside the base

of support using the following analytical relationship as discussed in [196],

$$\boldsymbol{\delta}^{-} \leq \boldsymbol{P}_{XCOM} + \frac{\dot{\boldsymbol{P}}_{XCOM}}{\omega_0} \leq \boldsymbol{\delta}^{+}. \tag{5.8}$$

This constraint represents a stability region in the COM state space that includes the effect of the assistive forces on the LIP balance. More importantly, satisfaction of the above criterion assures that the LIP is balanced at least during the next $t = \frac{1}{\omega_0}$ seconds which can be used for estimating human falls and thus, to realize fall prevention strategies.

With the help of some matrix manipulations and after substituting (5.5) and (5.3) into (5.7), the following inequality constraints are obtained for balance satisfaction as a function of the applied assistive forces,

$$\boldsymbol{K}\boldsymbol{F} = \begin{bmatrix}\boldsymbol{K}_l & \boldsymbol{K}_r\end{bmatrix} \begin{bmatrix}\boldsymbol{F}_l \\ \boldsymbol{F}_r\end{bmatrix} \leq \mathbf{c}, \tag{5.9}$$

$$\boldsymbol{K}_i = \begin{pmatrix} -z_0 - h_{i,z} & 0 & x_{COM} + h_{i,x} \\ z_0 + h_{i,z} & 0 & -x_{COM} - h_{i,x} \\ 0 & -z_0 - h_{i,z} & y_{COM} + h_{i,y} \\ 0 & z_0 + h_{i,z} & -y_{COM} - h_{i,y} \end{pmatrix},$$

$$\boldsymbol{c} = mg \begin{pmatrix} 2x_{XCOM} - \delta_x^- - \frac{\tau_y}{mg} \\ \delta_x^+ + \frac{\tau_y}{mg} - 2x_{XCOM} \\ 2y_{XCOM} - \delta_y^- + \frac{\tau_x}{mg} \\ \delta_y^+ - \frac{\tau_x}{mg} - 2y_{XCOM} \end{pmatrix},$$

where x_{XCOM} and y_{XCOM} are two components of the $\boldsymbol{P}_{XCOM}$, while δ_x^+, δ_x^-, $\delta_y^+$and δ_y^- are the components of BOS boundaries defined in (5.8).

The torques applied to the pivot joint (τ_x and τ_y) provide support for the human balance when the balance criterion is satisfied [191]. However, if the user looses his or her balance, no value for $\boldsymbol{\tau}$ can be applied anymore. The supportive torque is lower for weak users and therefore we decided to neglect its effect in the derivation of supportive strategies to consider the worst case.

A valid set of desired contact forces $\hat{\boldsymbol{F}}$ is found by solving the following quadratic programming problem,

$$\hat{\boldsymbol{F}} = \arg\min_{\boldsymbol{F}} \boldsymbol{F}^T \boldsymbol{W} \boldsymbol{F} \tag{5.10}$$

$$\text{s.t. } \boldsymbol{K}\boldsymbol{F} \leq \boldsymbol{c} \tag{5.11}$$

where $\boldsymbol{W}$ is used to weigh certain forces, or to penalize large supportive forces while $\boldsymbol{K}\boldsymbol{F} \leq \boldsymbol{c}$ represent the balance inequality constraints.

An analytic solution of this optimization problem is considered for online implementation. If the problem is unconstrained, i.e. the inequality (5.11) holds, the trivial solution $\hat{\mathbf{F}} = 0$ is obtained. However, for the constraint case the active constraints are taken into account by using an active-set method [199], where the active set is composed of those constraints that are satisfied as equalities and constitute the corresponding augmented matrices $\boldsymbol{K}_a$ and

$\boldsymbol{c}_a$. The associated optimization is then solved using the weighted Moore-Penrose Inverse, $\hat{\boldsymbol{F}} = \boldsymbol{K}_a^+ \boldsymbol{c}_a$, that is a constrained active solution.

The inequality constraints (5.9) automatically divide the BOS into two phases: a phase with no required control forces necessary to guarantee balance and a second phase where a monotonically increasing force with maximum at the BOS boundary can be determined. This intrinsic property assures no robot intervention for normal human walking or activity since no assistive forces are determined.

5.2.2 Robot Control

To allow the human to drive the MAR during normal walking, the robot is equipped with two force/torque sensors mounted at the handles. Force components along and around the heading direction are used for motion control[1]. Position-based admittance control is implemented, which allows to design the desired dynamic behavior of the system with respect to the user's applied force by selecting proper admittance parameters. A mass-damper system for the linear and angular motion is considered as proposed in eq. (4.2) to determine the desired reference velocities based on the human's applied force, and then being realized by a low-level controller.

We consider an extra mass-damper system for the derivation of the desired velocity of the robot handles based on the obtained assistive forces $\boldsymbol{F}_i$ described in section 5.2.1 as follows,

$$\boldsymbol{M}_{d,arm,i}\ddot{\hat{\boldsymbol{x}}}_{arm,i} + \boldsymbol{D}_{d,arm,i}\dot{\hat{\boldsymbol{x}}}_{arm,i} + \boldsymbol{K}_{d,arm,i}\hat{\boldsymbol{x}}_{arm,i} = \boldsymbol{F}_i, \tag{5.12}$$

where $\boldsymbol{M}_{d,arm,i}$ and $\boldsymbol{D}_{d,arm,i}$ are the desired inertia and damping matrices for either left or right arms, respectively. The desired joint velocities $\dot{\boldsymbol{q}}_i$ are then computed using the Pseudoinverse of the arm Jacobian,

$$\dot{\boldsymbol{q}}_i = \boldsymbol{J}^{\#}_{arm,i}\dot{\hat{\boldsymbol{x}}}_{arm,i}. \tag{5.13}$$

For the sake of safety the robot base motion was slowed down whenever a risk of human fall was determined and a stabilization maneuver needed to be performed. For this purpose, the damping factor $\boldsymbol{D}_{d,base}$ was increased as a function of the norm of $\boldsymbol{F}_i$ considering the distance of the human XCOM to the boundary of the BOS as follows

$$\boldsymbol{D}_{d,base} = \begin{cases} \boldsymbol{D}_{d,base} & \frac{\boldsymbol{\delta}^-}{2} \leq \boldsymbol{P}_{XCOM} \leq \frac{\boldsymbol{\delta}^+}{2} \\ \boldsymbol{D}_{d,base}\exp(\parallel \boldsymbol{F}_i \parallel) & \text{else} \end{cases}. \tag{5.14}$$

In the following subsections we report on simulation and experimental results of the proposed fall prevention control algorithm. The simulation results report on the used feature for fall detection and the obtained assistive forces to prevent falls, while the experimental results evaluate the effectiveness of the proposed fall prevention algorithm on a real MAR.

[1]Please note that in a holonomic system also the force component in sidewards direction is used for motion control.

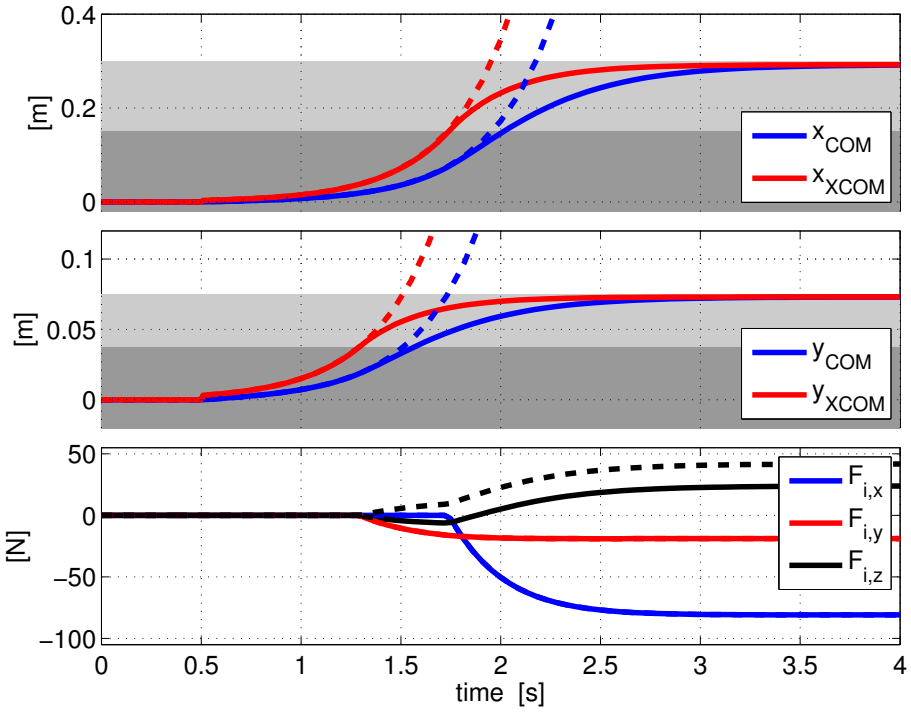

Figure 5.2: Simulation results for a provoked human fall. The balance features for unassisted (dashed-line) and assisted (solid lines) are shown in the two upper plots where two phases of the BOS boundaries are depicted by dark and light gray. The XCOM components are shown by the red line and the COM components with blue lines. Assistive forces for the left side (dashed lines) and the right side (solid lines) are presented in the lower plot (on the x and y components there is a very small difference between left and right assistive forces).

5.3 Results

In the following sections we present obtained simulation and experimental results.

5.3.1 Simulation

In a first step the proposed approach was validated in simulation where a human fall into an arbitrary direction was simulated. The human was modeled as a 3D-LIP with the length $l = 1m$, mass $m = 70kg$ and BOS boundaries $\delta^- = [-0.075, -0.075]$ and $\delta^+ = [0.3, 0.075]$. As shown in Fig. 5.2, the COM and XCOM features of the LIP were initially within their base of support, while an external force was applied at time 0.5s that resulted in loosing the LIP's balance. The simulation results clearly show that the XCOM detects the risk of fall faster than the COM. Although both balance features leave their BOS for unassisted simulation, the assistive forces which are computed according to the presented approach can well guarantee the human balance by preventing the balance features leaving their BOS. Assistive forces are determined whenever the XCOM is leaving the first phase of BOS. Both BOS phases, which are automatically defined according to the formulation presented in section 6.3, are shown in Fig. 5.2: the area where no forces are determined to

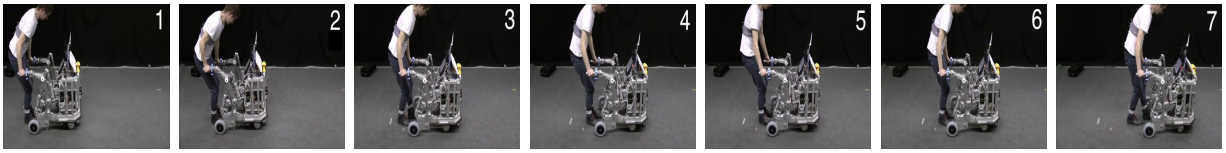

Figure 5.3: Snapshots taken during the provoked human fall experiments in sideways direction (snapshots 1 and 2) and backward direction (snapshots 4 and 5).

be applied (dark gray) and the area where forces are applied (light gray). The algorithm starts to apply forces to the LIP to slow down the fall from two interaction points located at $\boldsymbol{h}_l = -\boldsymbol{h}_r = [0, 0.25, 0]$ with respect to the $\boldsymbol{P}_{COM}$. As a result the human XCOM and COM stay within the BOS (gray area) and stabilize at the boundary of the BOS, where the COM and XCOM converge to each other. Since the fall is happening in an arbitrary direction, violation of the XCOM in both x and y directions happens independently at different time instances.

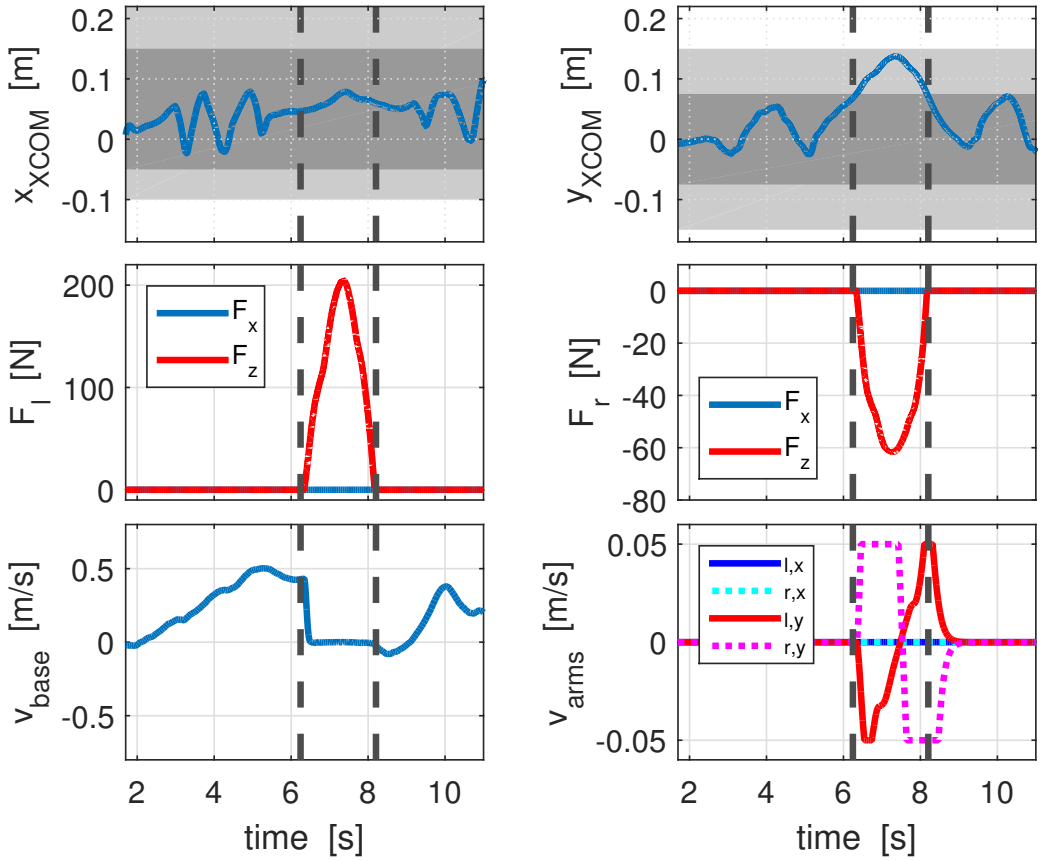

Figure 5.4: Experimental results for a provoked sideways human fall. The balance features and their corresponding two phases of the BOS boundaries are depicted by dark and light gray areas in the first row. Assistive forces for the left and right arms and the realized robot base and arm velocities are depicted in the second and third rows, respectively.

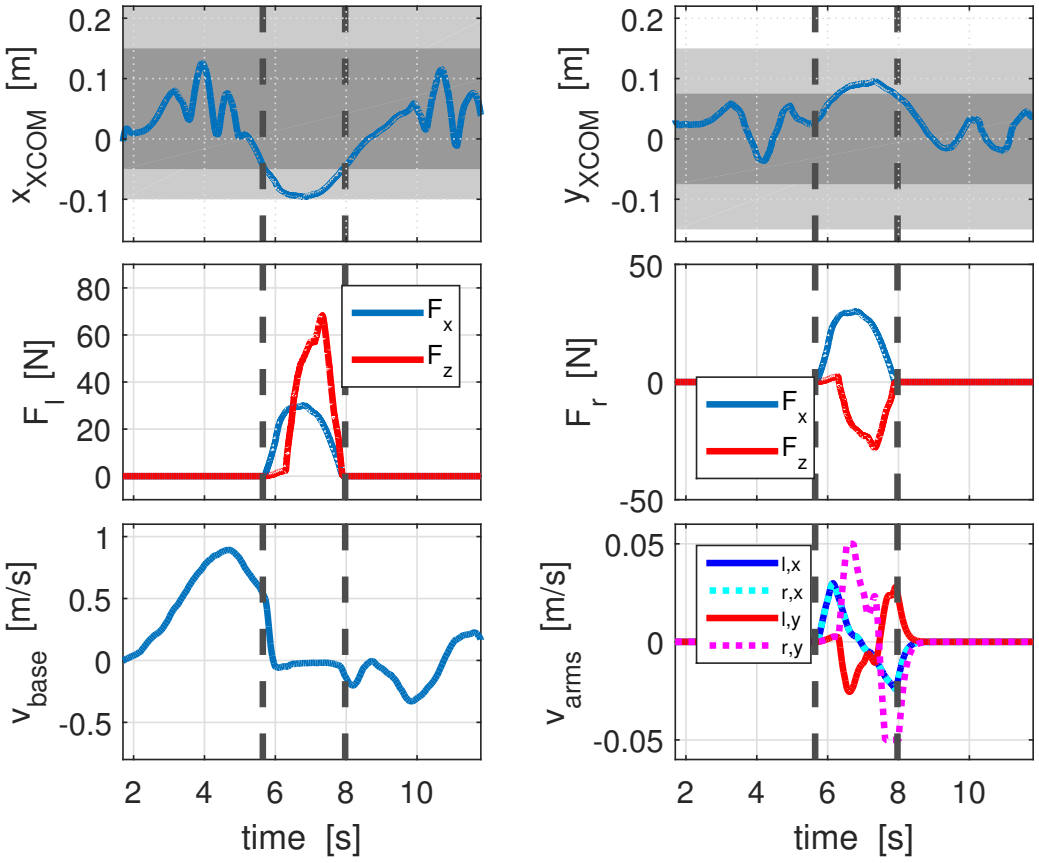

Figure 5.5: Experimental results for a provoked human fall in diagonal direction. The balance features and their corresponding two phases of the BOS boundaries are depicted by dark and light gray areas as shown in the first row. Assistive forces for the left and right arms and the realized robot base and arm velocities are depicted in the second and third rows, respectively.

5.3.2 Experiments

The assistive strategy has been implemented on the Mobot platform, presented in section 3.3.2 and Fig. 3.8. Since the derivation of the exact position of the human COM requires articulated tracking of the human body using sensors on the MAR, which is a difficult vision problem that goes beyond the scope of this thesis, we decided to estimate the COM position by the torso position, which can be tracked much easier. In this experiment we used a Qualisys motion capture system to track this torso position.

The approach was tested by a healthy fit male participant with 24 years old. In the experiment the participant was asked to provoke falls while walking by (suddenly) leaning into one direction until his feeling of balance was diminishing. After stabilization the participant was asked to continue walking. The participant provoked falls in sideways, diagonal, backward and forward directions during the interaction with the robotic platform. In sideways fall experiments as shown in Fig. 5.4, the human provoked a fall to the left side. As depicted in the figures, assistive forces on the left and right hand were computed and realized by the robot arms as soon as the y component of the estimated XCOM violated its first phase of the BOS. The obtained z component of the forces to be applied on the

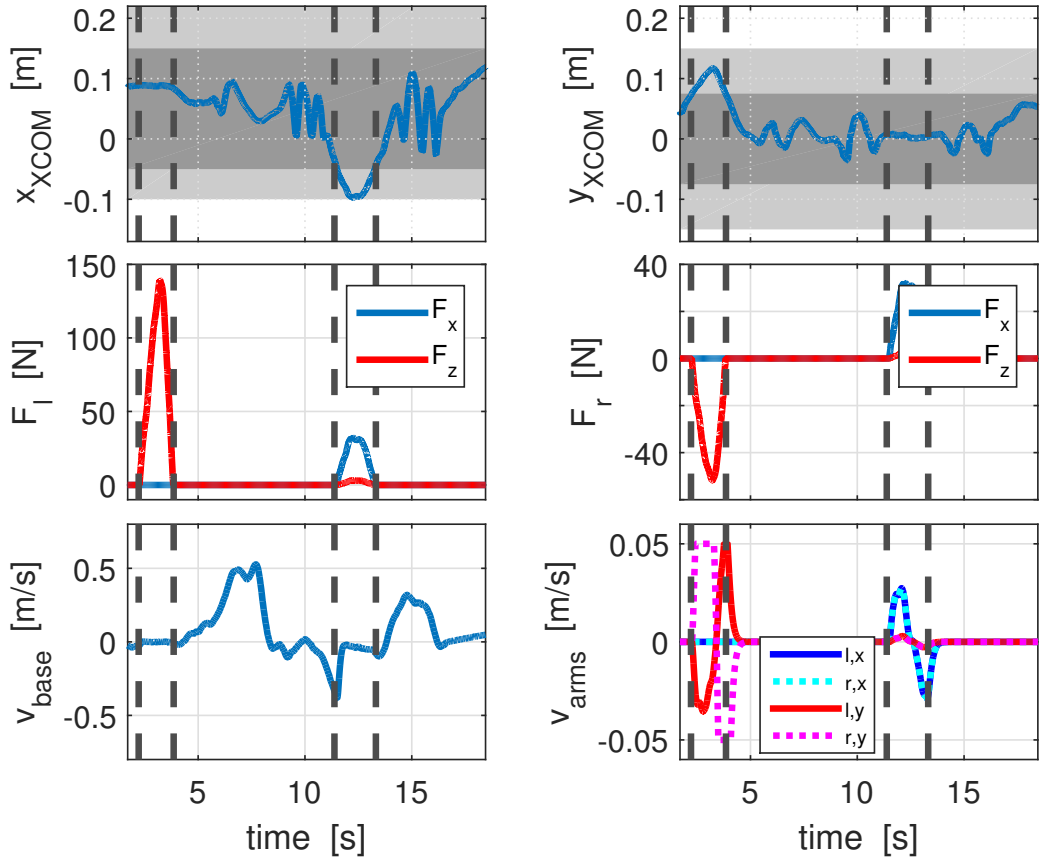

Figure 5.6: Experimental results for provoked sideways and backward human falls. The balance features and their corresponding two phases of the BOS boundaries are depicted by dark and light gray areas in the first row. Assistive forces for the left and right arms and the realized robot base and arm velocities are depicted in the second and third rows, respectively.

two handles are in opposite directions creating a moment on the human COM position against the fall direction. Forces obtained in x direction are zero as they cannot contribute to sideways fall prevention. In the diagonal fall experiment, see Fig. 5.5, the two x and y components of the XCOM position violate their boundaries. The algorithm provides required forces at the right and left handles with opposite directions in their z components, and aligned direction in the x components. In the last experiment the user provoked two falls, one sideways at the beginning of the motion and one backward at the end of motion. Fig. 5.6 presents the obtained results while a series of corresponding snapshots are presented in Fig. 5.3. In all presented experiments, the motion of the robot base was well damped during fall prevention phases. Moreover, the arm configurations are autonomously (but very smoothly) brought back to their initial configurations thanks to the nature of the admittance controller (5.12). This robot behavior allows users to return to their balance state and safely continue their normal task. Moreover, please note that in all presented results the arm motions are smoothly realized, see the plot related to the arm's velocities.

5.4 Summary and Discussion

Human falls while interacting with a MAR is a critical event and needs to be prevented. Available approaches for human fall prevention have been mainly developed for passive platforms without actuated arms. Moreover, only braking strategies were realized for fall prevention. The approach presented in this chapter, for the first time, proposes optimal solutions for human fall prevention. Although the COM was typically used as the human's fall detection measure in MARs, this chapter proposes to evaluate the user's Extrapolated Center of Mass (XCOM) (which is faster in fall detection than the COM) in order to determine the required supportive forces to be provided to the user for fall prevention. The human was modeled as a 3D-LIP while the assistive forces were applied at two interaction points between human and robot arms. Finally, a compliant robot controller was proposed to realize the required forces for fall prevention. Applicability and performance of the proposed approach were evaluated in experiments on the robotic platform supporting a subject provoking falls in different directions.

The main restriction of the presented approach is the required online estimation of the user's COM and its derivative. These can be performed by online evaluation of vision data, such as camera or Kinect sensors. Therefore, future research may be directed towards the development of reliable algorithms for articulated tracking of the users interacting with MARs, and the estimation of required information such as the COM position. Such algorithms can also help developing more sophisticated assistive strategies for human fall prevention by providing further information on human states and positions of the body segments, e.g. hand or leg configurations.

This thesis so far focused on different human safety aspects in the control design for each mode of operation. Human safety was considered in chapter 3, by considering the balance criteria aiming at avoiding human falls during STS transfers, in chapter 4 by developing an as passive as possible assistive strategy, and in this chapter by proposing an optimal human fall prevention approach. The safety aspect is emphasized even further in the next chapter by realizing a general safety supervisory controller that aims at supervising the behavior of the specific control unit in the specified mode of operation and reshaping the robot's behavior to enhance the user's safety if an unsafe situation is about to happen.

6 Energy-Based Supervisory Control for Safety Enhancement

Enhancing safety of the human is a critical issue to be addressed for every collaborative robot system, especially assistance robots that interact with the elderly or patients. So far, this thesis has focused on different aspects of human safety in the control design for each specific mode of operations. In this chapter, a complementary control system is proposed to further emphasize the safety aspect of the collaborative robots. The novelty of this chapter is to realize a general safety supervisory controller that can supervise the behavior of the specific control unit in the specified mode of operation and reshapes the robot's behavior to enhance the user's safety if an unsafe situation is about to happen. The safety approach presented in this chapter is general and can be applied not only to assistance devices, but also to other collaborative robots, with multiple potential applications, e.g. robot co-workers in industry. Therefore, the proposed concept in this chapter goes beyond the specific application of MARs and is discussed for a general case of physical Human-Robot Collaboration (pHRC).

Realization of pHRI requires proper hardware and software components so as to enhance the safety of the user. Intrinsically safe mechanisms as well as lightweight and compliant designs have been proven to increase robot safety [200–203]. Nowadays, a variety of motion planning and reactive control methods exist that are able to prevent human-robot collisions, using sensors to monitor the workspace, and to reduce contact-related injuries, see e.g. [204–209].

In many tasks, however, there is a need of establishing intentional, continuous, and often multiple contacts between human and robot(s). This is a typical collaboration phase for assistance robots when the user is in continuous contact with the robot platform through multiple contact points (e.g. by two hands gripping two robot arms). Such a pHRC comes with a series of new challenges for modeling the overall dynamical system and for the design of safe robot control. A human and one or more robots may in fact interact directly or even indirectly (e.g. via a carried object), at a single point or over several interaction ports, with multiple, changing and intermittent contact situations, resulting in a very complex dynamical system which is difficult to model. In addition, safety-related control issues have to be redefined for continuous pHRC since behaviors such as collision avoidance and reactive escape control [205] are no longer representative ones.

Since pHRC can be seen as an exchange of force and motion signals over contact points, an energy and port-based approach provides a very powerful tool for both modeling and control design. While several researchers have already used the concept of energy and power for robot collision detection [207] and safe reaction control [210], a systematic energy-based modeling and control approach to pHRC tasks involving continuous contact and a varying number and location of contact points is missing so far. The Port-Hamiltonian (PH) formalism, which is a domain-independent concept, has proven to be very successful for

modeling complex systems [211, 212]. It provides a framework to describe a system in terms of energy variables and interconnection of sub-systems by means of power ports. So far, it was adopted to model the dynamical behavior of robots with rigid or flexible links [213], hybrid hopping robots [214], underactuated aerial vehicles [215], soft finger manipulation [216], as well as for the control of bipedal walking robots [217].

The major contribution in this chapter is the development of an energy monitoring and control system that observes energy flows among the different subsystems involved in pHRC, and shaping them to improve human safety according to selected metrics. Port-Hamiltonian formalisms are used to model each sub-system and their interconnection. Each sub-system is modeled independently using the power port concept, and then interconnected to form the overall system. This allows us to also include, without essential model changes, transition events from contact to non-contact and vice versa, or changes in the overall system dynamics, e.g., when adding a further collaborative robot to the picture. Based on this model, an energy monitoring system is defined that continuously observes the energy flows between all components, but especially over the interaction port with the human. Finally, a novel safety-enhancing controller is proposed that shapes the energy exchanged with the human whenever a harmful energy flow or human fatigue is observed.

The chapter starts with a brief introduction to the port-based modeling in section 6.1. In section 6.2, the energy and port-based modeling is presented for a general cooperative task of jointly manipulating an object by human-robot teams. Then, section 6.3 formulates the safety metrics in human-robot cooperation and shows how the proposed port-based modeling is used for establishing a supervision-based safety controller. Validity of the modeling and control approach are further illustrated in section 6.4 by means of different simulations.

6.1 Background

This section provides a brief overview of the basic components of the port-based modeling framework including the Dirac structure, the Port-Hamiltonian formalism and screw theory. The reader is referred to [218–220] for details.

6.1.1 Port-based Modeling Framework

Energy is the underlying concept for the port-based modeling. Each sub-system interacts with the others through the rate of change of energy, namely power, as a dual product of the two power-conjugate port variables, *flow* f and *effort* e. The interconnection between sub-systems is described by a network topology called *Dirac structure* $\mathcal{D}$, which mathematically represents how the power flows among the ports of the structure. With $\mathcal{F}$ being the linear space of flows ($f \in \mathcal{F}$) and $\mathcal{F}^*$ the dual linear space of efforts ($e \in \mathcal{E}$), the Dirac structure is expressed in the space $\mathcal{F} \times \mathcal{F}^*$ as

$$\mathcal{D} = \{(f, e) \in \mathcal{F} \times \mathcal{F}^* | Ff + Ee = 0\} \tag{6.1}$$

with F and E two specific mappings imposing the power-conservation in the whole system.

Elements in the network are characterized by their energetic behavior and are grouped into energy storage ports (f_S, e_S), resistive ports (f_R, e_R) for energy dissipation, control ports (f_C, e_C) and interaction ports (f_I, e_I).

6.1.2 PH Formulation

The PH formulation represents the input/output relation of a port-based model. Considering the Hamiltonian function H of the total system energy, the standard representation of a PH system is given by:

$$\begin{cases} \dot{\boldsymbol{x}} = & [\boldsymbol{J}(\boldsymbol{x}) - \boldsymbol{R}(\boldsymbol{x})]\frac{\partial H}{\partial \boldsymbol{x}} + \boldsymbol{G}(\boldsymbol{x})\boldsymbol{u} \\ \boldsymbol{y} = & \boldsymbol{G}^T(\boldsymbol{x})\frac{\partial H}{\partial \boldsymbol{x}} \end{cases} \tag{6.2}$$

where $\boldsymbol{J}(\boldsymbol{x})$ is a skew symmetric matrix, $\boldsymbol{R}(\boldsymbol{x}) \geq 0$ is the symmetric dissipation matrix, $\boldsymbol{G}(\boldsymbol{x})$ is a mapping matrix, $\boldsymbol{x}$ is the state associated to the storage elements and $\boldsymbol{u}$, $\boldsymbol{y}$ are the input and output variables, respectively.

A system presented in PH form (6.2) can be easily represented by its underlying Dirac structure:

$$\begin{bmatrix} -\dot{\boldsymbol{x}} \\ \boldsymbol{e}_R \\ \boldsymbol{y} \end{bmatrix} = \begin{bmatrix} -\boldsymbol{J}(\boldsymbol{x}) & -\boldsymbol{G}_R(\boldsymbol{x}) & -\boldsymbol{G}(\boldsymbol{x}) \\ \boldsymbol{G}_R^T(\boldsymbol{x}) & 0 & 0 \\ \boldsymbol{G}^T(\boldsymbol{x}) & 0 & 0 \end{bmatrix} \begin{bmatrix} \frac{\partial H}{\partial \boldsymbol{x}} \\ \boldsymbol{f}_R \\ \boldsymbol{u} \end{bmatrix}$$

with $\boldsymbol{R}(\boldsymbol{x}) = \boldsymbol{G}_R(\boldsymbol{x})\boldsymbol{Y}_R\boldsymbol{G}_R^T(\boldsymbol{x})$ for a linear admittance relation $\boldsymbol{f}_R = -\boldsymbol{Y}_R\boldsymbol{e}_R$.

6.1.3 Twists and Wrenches

In physical systems, a *twist* is the relative instantaneous motion of a body with frame Ψ_i with respect to a body with frame Ψ_j expressed in frame Ψ_0 and is mathematically given by ${}^0\boldsymbol{T}_i^j = [\boldsymbol{\omega}, \boldsymbol{v}]^T$ where $\boldsymbol{\omega}$ and $\boldsymbol{v}$ are the angular and translational velocities. The coordinate transformation of a twist is defined by ${}^0\boldsymbol{T}_i^j = \boldsymbol{A}_l^0\, {}^l\boldsymbol{T}_i^j$ in which

$$\boldsymbol{A}_l^0 = \begin{bmatrix} \boldsymbol{R}_l^0 & 0 \\ \boldsymbol{p}_l^{0*}\boldsymbol{R}_l^0 & \boldsymbol{R}_l^0 \end{bmatrix}, \tag{6.3}$$

$\boldsymbol{R}_l^0$ the rotation matrix, and $\boldsymbol{p}_l^{0*}$ the skew-symmetric matrix form for the displacement between frames Ψ_0 and Ψ_l.

The *wrench* applied to the body with frame Ψ_i acting on frame Ψ_j is an element of the dual space to the twist vector space and is represented as ${}^0\boldsymbol{W}_i^j = [\boldsymbol{m}, \boldsymbol{f}]^T$ with torques $\boldsymbol{m}$ and forces $\boldsymbol{f}$. The coordinate transformation of a wrench is then defined as ${}^0\boldsymbol{W}_i^j = \boldsymbol{A}_l^{0T}\, {}^l\boldsymbol{W}_i^j$.

6.2 PH Modeling of HRC

In this section, we present an energy and port-based modeling approach for the collaborative task of jointly manipulating a rigid bulky object by a human-robot team, see a general

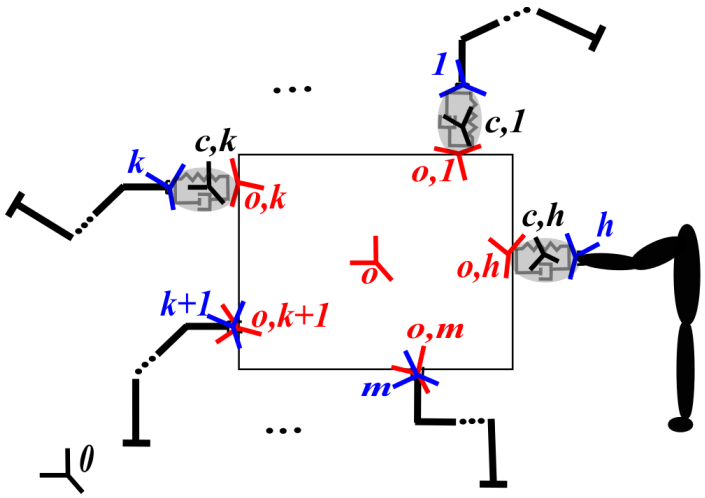

Figure 6.1: An example scenario of object transportation by a human and m collaborative robots and possible associated frame definition.

example in Fig. 6.1. We believe that the selected scenario is representative for modeling different HRC scenarios, which include physical contact between different sub-systems. This example decided to cover one of the most complex HRI scenarios, not only covering the direct physical interaction, but also indirect interaction through an object. However, the first case (direct physical interaction that is often the case for assistance robotics applications) can be considered a subclass of the first problem by simply removing the object in all of the following proposed approaches. Therefore, the safety approach presented here can be easily applied to all the control modes presented in the last three chapters of this thesis.

The mathematical representation of each sub-system including robot(s), human as well as contacts (e.g. between human and object or object and robot) are introduced first, then the whole system is described by the interconnection of the different sub-systems through their interaction ports. For each sub-system we present only its underlying Dirac structure while their transformation to PH formulation is very straightforward, and is thus not reported explicitly. The overall system is finally presented in PH form, which is more convenient for the control of the system.

6.2.1 PH Modeling of the Robot

For each robot r among m collaborative robots, $r \in \{1, 2, \ldots, m\}$, having n_r degrees of freedom (DoF), generalized coordinates $\mathbf{q}_r = (q_1, \ldots, q_{n_r})^T$, and symmetric, positive definite inertia matrix $\boldsymbol{M}_r(\boldsymbol{q}_r)$, the energy ports for storing potential and kinetic energies, the control ports, as well as the interaction ports have to be defined.

Considering the robot r, the Hamiltonian function and state variables for the storage port describing the potential energy $\langle \dot{\boldsymbol{q}}_r, \frac{\partial H_r}{\partial \boldsymbol{q}_r} \rangle$ are defined based on the robot gravitational energy $U_r(\boldsymbol{q}_r)$ and the robot configuration vector $\boldsymbol{q}_r$. The Hamiltonian function and state variables for the storage port describing the kinetic energy are given by $\frac{1}{2}\boldsymbol{p}_r^T \boldsymbol{M}_r^{-1}(\boldsymbol{q}_r)\boldsymbol{p}_r$ and are defined with the help of the vector of generalized momenta $\boldsymbol{p}_r = (p_1, ..., p_{n_r})^T$, where

$\boldsymbol{p}_r = \boldsymbol{M}_r(\boldsymbol{q}_r)\dot{\boldsymbol{q}}_r$.

The resistive port $\langle \boldsymbol{e}_{R,r}, \boldsymbol{f}_{R,r} \rangle$ describes the dissipative behavior of the robot, e.g. due to friction in joints or transmissions. The port variables are related by $\boldsymbol{f}_{R,r} = -\boldsymbol{D}_r \boldsymbol{e}_{R,r}$ where $\boldsymbol{f}_{R,r}$ means the flow variable representing the dissipative joint torques, $\boldsymbol{e}_{R,r}$ the effort variable representing the joint velocities and $\boldsymbol{D}_r$ the dissipation matrix.

Finally, the control $\langle \dot{\boldsymbol{q}}_r, \boldsymbol{\tau}_r \rangle$ and interaction ports $\langle {}^0\boldsymbol{T}^0_r, {}^0\boldsymbol{W}^r_{o,r} \rangle$ describe the robot behavior with respect to its actuation as well as the interaction with the environment. In the considered scenario this means the robot interaction with the object. The flow variable ${}^0\boldsymbol{T}^0_r$ thus, describes the instantaneous motion of the robot end-effector, while the effort variable ${}^0\boldsymbol{W}^r_{o,r}$ describes the interaction forces and torques that can be measured between object and end-effector of the robot r at their contact point. For the sake of simplicity both flow and effort variables for each robot are expressed in the world reference frame, see Fig. 6.1.

The total Hamiltonian of the robot is then given by

$$H_r = \frac{1}{2}\boldsymbol{p}_r^T \boldsymbol{M}_r^{-1}(\boldsymbol{q}_r)\boldsymbol{p}_r + U_r(\boldsymbol{q}_r), \tag{6.4}$$

while the underlying Dirac structure of the robot can be formulated following the Hamiltonian principle (see [218])

$$\begin{bmatrix} \dot{\boldsymbol{p}}_r \\ \dot{\boldsymbol{q}}_r \\ \boldsymbol{e}_{R,r} \\ {}^0\boldsymbol{T}^0_r \\ \dot{\boldsymbol{q}}_r \end{bmatrix} = \begin{bmatrix} \boldsymbol{0}_{n_r \times n_r} & -\boldsymbol{N}_r \\ \boldsymbol{N}_r^T & \boldsymbol{0}_{(3n_r+6)\times(3n_r+6)} \end{bmatrix} \begin{bmatrix} \frac{\partial H_r}{\partial \boldsymbol{p}_r} \\ \frac{\partial H_r}{\partial \boldsymbol{q}_r} \\ -\boldsymbol{f}_{R,r} \\ -{}^0\boldsymbol{W}^r_{o,r} \\ -\boldsymbol{\tau}_r \end{bmatrix} \tag{6.5}$$

$$\boldsymbol{N}_r = [\boldsymbol{I}_{n_r}, \boldsymbol{I}_{n_r}, \boldsymbol{J}_r^T(\boldsymbol{q}_r), \boldsymbol{I}_{n_r}]$$

with robot Jacobian $\boldsymbol{J}_r$ and identity matrix $\boldsymbol{I}_{n_r}$ of order n_r.

6.2.2 PH Modeling of the Object

The dynamics of the object with total mass M_o and body inertia matrix $\boldsymbol{I}_o$ is described by interaction ports and storing ports taking into account the potential energy and linear and angular kinetic energy.

The number of interaction ports depends on the number of contacts between the object and the human or collaborative robot(s). Each interaction port includes the flow variable ${}^0\boldsymbol{T}^0_{o,t}$, which describes the instantaneous motion of the object at the contact point with element t, either with the human or with the robots $t \in \{h, 1, \cdots, m\}$, and the effort variable ${}^0\boldsymbol{W}^{o,t}_t$, which describes the wrenches applied by the element t to the object at the specific contact point, both expressed in frame 0. Given the position vector ${}^o\boldsymbol{P}_{o,t}$ of each contact point between the object and the element t expressed in the object frame, the input matrix $\boldsymbol{G}_t$ for each interaction port can be written as follows

$$\boldsymbol{G}_t = \begin{bmatrix} \boldsymbol{I}_3 & \boldsymbol{0}_{3\times3} \\ ({}^o\boldsymbol{P}_{o,t})^* & \boldsymbol{I}_3 \end{bmatrix}^T \tag{6.6}$$

with identity matrix $\boldsymbol{I}_3$, and 3×3 skew-symmetric matrix $({}^o\boldsymbol{P}_{o,t})^*$ associated to the displacement vector ${}^o\boldsymbol{P}_{o,t}$.

The position $\boldsymbol{x}_o$ of the center of mass of the object is the state variable for the storage port $\langle \dot{\boldsymbol{x}}_o, \frac{\partial H_o}{\partial \boldsymbol{x}_o} \rangle$ describing the gravitational energy with the Hamiltonian function $H_o = M_o \boldsymbol{g}^T \boldsymbol{x}_o$ and $\boldsymbol{g} = [0, -g_0, 0]^T$ the gravity vector.

The storage ports for the linear kinetic energy $\langle \dot{\boldsymbol{p}}_o, \frac{\partial H}{\partial \boldsymbol{p}_0} \rangle$ and angular kinetic energy $\langle \dot{\boldsymbol{l}}_o, \frac{\partial H}{\partial \boldsymbol{l}_o} \rangle$ are characterized by their state variables $\boldsymbol{p}_o = M_o \boldsymbol{v}_o$ for the object's linear momentum and $\boldsymbol{l}_o = \boldsymbol{I}_o \boldsymbol{\omega}_o$ for the object's angular momentum. Corresponding Hamiltonian functions for aforementioned storage ports are presented as $\frac{1}{2}\boldsymbol{p}_o^T M_o^{-1} \boldsymbol{p}_o$ and $\frac{1}{2}\boldsymbol{l}_o^T \boldsymbol{I}_o^{-1} \boldsymbol{l}_o$. In above formulas, $\boldsymbol{v}_o$ is the linear velocity of the object, $\boldsymbol{\omega}_o$ the angular velocity, and $\boldsymbol{I}_o$ the inertia tensor of the object. Please note that assigning two storage ports is performed to be able to explicitly analyse linear and angular motions of the object independently, although these two ports could be also combined into one as done e.g. in section 6.2.1.

The total Hamiltonian function of the object is given by

$$H = \frac{1}{2}\boldsymbol{p}_o^T M_o^{-1} \boldsymbol{p}_o + \frac{1}{2}\boldsymbol{l}_o^T \boldsymbol{I}_o^{-1} \boldsymbol{l}_o + (-M_o \boldsymbol{g}^T \boldsymbol{x_o}). \tag{6.7}$$

Following the Hamiltonian principle this results in the following formulation of the corresponding Dirac structure

$$\begin{bmatrix} \begin{bmatrix} \dot{\boldsymbol{p}}_o \\ \dot{\boldsymbol{l}}_o \end{bmatrix} \\ \dot{\boldsymbol{x}}_o \\ {}^0\boldsymbol{T}^0_{o,1} \\ \vdots \\ {}^0\boldsymbol{T}^0_{o,m} \\ {}^0\boldsymbol{T}^0_{o,h} \end{bmatrix} = \begin{bmatrix} \boldsymbol{0}_{6\times 6} & -\boldsymbol{N}_o \\ \boldsymbol{N}_o^T & \boldsymbol{0}_{(6m+9)\times(6m+9)} \end{bmatrix} \begin{bmatrix} \begin{bmatrix} \frac{\partial H}{\partial \boldsymbol{p}_o} \\ \frac{\partial H}{\partial \boldsymbol{l}_o} \end{bmatrix} \\ \frac{\partial H}{\partial \boldsymbol{x}_o} \\ -{}^0\boldsymbol{W}^{o,1}_1 \\ \vdots \\ -{}^o\boldsymbol{W}^{o,m}_m \\ -{}^o\boldsymbol{W}^{o,h}_h \end{bmatrix}. \tag{6.8}$$

$$\boldsymbol{N}_o = [\boldsymbol{I}_3, \boldsymbol{0}_{3\times 3}, \boldsymbol{G}_1, \cdots, \boldsymbol{G}_m, \boldsymbol{G}_h]$$

6.2.3 PH Modeling of the Human

Since the number of degrees of freedom does not affect the procedure of modeling based on the PH formalism, without loss of generality we consider a n_h DOF human arm structure, which can e.g. include flexion-extension movements in the shoulder, elbow and wrist. The visco-elasticity of the human skin (or even arm) can also be considered within the compliant contact model as detailed in section 6.2.4.

Similar to section 6.2.1, an energy storage port corresponding to the arm's potential energy, an interaction port representing the dynamical behavior due to the contact between human and object, and a control port for the joint torques generated by human muscles are considered. The final PH formulation results in the same structure as (6.2).

6.2.4 Physical Contacts

The physical contact between human, object and robot(s) are established using rigid or compliant contacts. Thus, two physical contact models are formulated using port variables.

Rigid Contact

In this case, the physics of contact is described by a kinematic constraint imposed on the relative motion of two connected sub-systems i and j, which imposes the relative twist ${}^{b}\boldsymbol{T}_{i}^{j}$ to belong to a specific subspace of $se(3)$, which includes only feasible directions of motion.

Thus, kinematic constraints of zero relative twist between component i and component j are introduced by setting ${}^{0}\boldsymbol{T}_{i}^{j} = {}^{0}\boldsymbol{T}_{i}^{0} - {}^{0}\boldsymbol{T}_{j}^{0} = \boldsymbol{0}_{6}$. Zero rate of change of ${}^{0}\boldsymbol{T}_{i}^{j}$ is used to compute the imposed wrenches ${}^{0}\boldsymbol{W}_{j}^{i}$ and ${}^{0}\boldsymbol{W}_{i}^{j}$, which are a consequence of the kinematic constraints[1].

Compliant Contact

Compliant contacts are modeled as a coupling of an elastic and a dissipative element [221, 222]. Elasticity in the contact is modeled by a storage port with state variable $\boldsymbol{s}$ and Hamiltonian function $H_{\boldsymbol{s}} = \frac{1}{2}\boldsymbol{s}^{T}\boldsymbol{K}_{s}\boldsymbol{s}$, with $\boldsymbol{K}_{s}$ the stiffness matrix. Moreover, damping effects are considered by a dissipative port with related variables $\boldsymbol{f}_{R,c} = -\bar{\boldsymbol{D}}_{c}\boldsymbol{e}_{R,c}$ with $\boldsymbol{f}_{R,c}$ the dissipative wrench applied on the bodies i and j expressed in the contact frame, $\boldsymbol{e}_{R,c}$ the corresponding twist, and $\bar{\boldsymbol{D}}_{c}$ the damping coefficient matrix for the contact c. The overall Dirac structure for compliant contacts can be written as follows:

$$\begin{bmatrix} {}^{0}\boldsymbol{W}_{c}^{i} \\ {}^{0}\boldsymbol{W}_{c}^{j} \\ \boldsymbol{e}_{R,c} \\ \dot{\boldsymbol{s}} \end{bmatrix} = \begin{bmatrix} \boldsymbol{0}_{12\times12} & -\boldsymbol{A}_{tot} \\ \boldsymbol{A}_{tot}^{T} & \boldsymbol{0}_{12\times12} \end{bmatrix} \begin{bmatrix} {}^{0}\boldsymbol{T}_{i}^{0} \\ {}^{0}\boldsymbol{T}_{j}^{0} \\ -\boldsymbol{f}_{R,c} \\ -\frac{\partial H_{s}}{\partial \boldsymbol{s}} \end{bmatrix}, \tag{6.9}$$

with $\boldsymbol{A}_{tot} = \begin{bmatrix} \boldsymbol{A} & -\boldsymbol{A} \\ \boldsymbol{A} & -\boldsymbol{A} \end{bmatrix}^{T}$ and $\boldsymbol{A}$ a mapping of the form (6.3).

6.2.5 Overall PH Modeling

In this section we finally formulate the PH equations of the whole system describing the joint object handling performed by a human and m collaborative robots. Compliant contact is assumed for the connection of the object with the human and the first k robots, while rigid contact is assumed for the rest of the connections, see Fig. 6.2 which details the interconnections between subsystems, clarifies the definition of each port variable used in each subsystem, and represents the port-based principle of the whole system.

The interconnection of all sub-systems results in a PH formulation of form (6.2) with

[1] Please note that ${}^{0}\boldsymbol{W}_{j}^{i} = -{}^{0}\boldsymbol{W}_{i}^{j}$ due to the power-conserving nature of the connection.

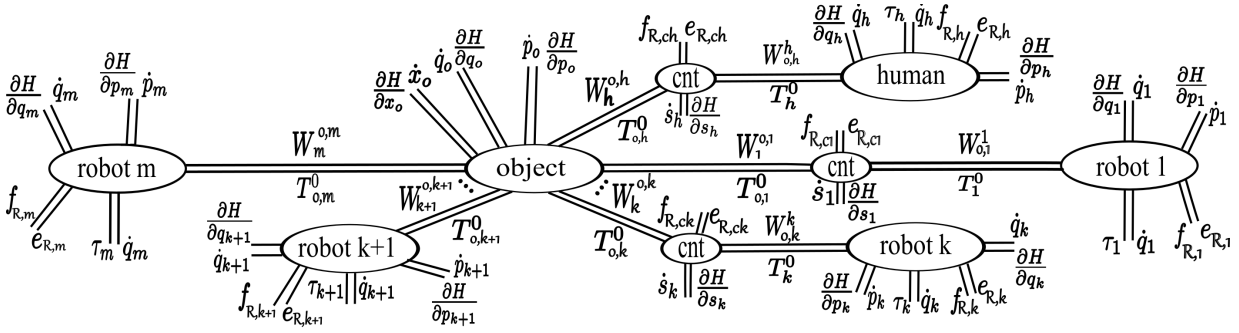

Figure 6.2: Port-based representation of collaborative transportation of an object by a human and m robots, each with either rigid contact (direct connection) or compliant contact (represented by (cnt)).

state vector

$$\begin{aligned} \boldsymbol{x} &= \left[\boldsymbol{P}_o, \boldsymbol{X}_o, \boldsymbol{P}_a, \boldsymbol{Q}_a, \boldsymbol{S}_a\right]^T, \quad \text{and} \\ \boldsymbol{P}_o &= \left[\boldsymbol{p}_o; \boldsymbol{l}_o\right]^T, \quad \boldsymbol{X}_o = \left[\boldsymbol{x}_o\right]^T, \quad \boldsymbol{P}_a = \left[\boldsymbol{p}_h; \boldsymbol{p}_1; \cdots; \boldsymbol{p}_m\right]^T, \\ \boldsymbol{Q}_a &= \left[\boldsymbol{q}_h; \boldsymbol{q}_1; \cdots; \boldsymbol{q}_m\right]^T, \quad \boldsymbol{S}_a = \left[\boldsymbol{s}_h; \boldsymbol{s}_1; \cdots; \boldsymbol{s}_k\right]^T, \end{aligned} \tag{6.10}$$

$\boldsymbol{J}(\boldsymbol{x})$ and $\boldsymbol{R}(\boldsymbol{x})$ matrices as reported in (6.11) and (6.12),

$$\boldsymbol{J} = \begin{bmatrix} \boldsymbol{0} & -\tilde{\boldsymbol{I}} & \boldsymbol{0} & \boldsymbol{0} & -\boldsymbol{B} \\ \tilde{\boldsymbol{I}}^T & \boldsymbol{0} & \boldsymbol{0} & \boldsymbol{0} & \boldsymbol{0} \\ \boldsymbol{0} & \boldsymbol{0} & \boldsymbol{0} & -\boldsymbol{E} & -\boldsymbol{F} \\ \boldsymbol{0} & \boldsymbol{0} & \boldsymbol{E}^T & \boldsymbol{0} & \boldsymbol{0} \\ \boldsymbol{B}^T & \boldsymbol{0} & \boldsymbol{F}^T & \boldsymbol{0} & \boldsymbol{0} \end{bmatrix}, \tag{6.11}$$

$$\begin{aligned} \tilde{\boldsymbol{I}} &= [\boldsymbol{I}_3\, \boldsymbol{0}_{3\times 3}]^T, \\ \boldsymbol{B} &= [-z_h \boldsymbol{G}_h^T \boldsymbol{A}_h^T, -z_1 \boldsymbol{G}_1^T \boldsymbol{A}_1^T, \cdots, -z_k \boldsymbol{G}_k^T \boldsymbol{A}_k^T, 0, \cdots, 0], \\ \boldsymbol{E} &= \boldsymbol{I}_{(n_h + \sum_{r=1}^m n_r)}, \\ \boldsymbol{F} &= \mathrm{diag}(-z_h \boldsymbol{J}_h^T \boldsymbol{A}_h^T,\, -z_1 \boldsymbol{J}_1^T \boldsymbol{A}_1^T, \cdots,\, -z_k \boldsymbol{J}_k^T \boldsymbol{A}_k^T), \end{aligned}$$

$$\boldsymbol{R} = \begin{bmatrix} z_h \boldsymbol{G}_h^T \boldsymbol{A}_h^T \bar{\boldsymbol{D}}_h \boldsymbol{A}_h \boldsymbol{G}_h + \sum_{r=1}^k z_r \boldsymbol{G}_r^T \boldsymbol{A}_r^T \bar{\boldsymbol{D}}_r \boldsymbol{A}_r \boldsymbol{G}_r & 0 & \boldsymbol{L} & 0 & 0 \\ \boldsymbol{0} & \boldsymbol{0} & \boldsymbol{0} & \boldsymbol{0} & \boldsymbol{0} \\ \boldsymbol{L}^T & \boldsymbol{0} & \boldsymbol{V} & \boldsymbol{0} & \boldsymbol{0} \\ \boldsymbol{0} & \boldsymbol{0} & \boldsymbol{0} & \boldsymbol{0} & \boldsymbol{0} \\ \boldsymbol{0} & \boldsymbol{0} & \boldsymbol{0} & \boldsymbol{0} & \boldsymbol{0} \end{bmatrix}, \tag{6.12}$$

$$\begin{aligned} \boldsymbol{L} &= \begin{bmatrix} z_h \boldsymbol{G}_h^T \boldsymbol{A}_h^T \bar{\boldsymbol{D}}_h \boldsymbol{A}_h \boldsymbol{J}_h & z_1 \boldsymbol{G}_1^T \boldsymbol{A}_1^T \bar{\boldsymbol{D}}_1 \boldsymbol{A}_1 \boldsymbol{J}_1 & \cdots & z_k \boldsymbol{G}_k^T \boldsymbol{A}_k^T \bar{\boldsymbol{D}}_k \boldsymbol{A}_k \boldsymbol{J}_k \end{bmatrix} \\ \boldsymbol{V} &= \mathrm{diag}(\boldsymbol{D}_h,\, \boldsymbol{D}_1,\, \cdots, \boldsymbol{D}_m), \end{aligned}$$

mapping matrices (6.13) for control and interaction ports

$$\boldsymbol{G}_C = \begin{bmatrix} \mathbf{0} \\ \mathbf{0} \\ \boldsymbol{I}_{(n_h+\sum_{r=1}^{k} n_r)} \\ \mathbf{0} \\ \mathbf{0} \end{bmatrix}, \quad \boldsymbol{G}_I = \begin{bmatrix} \begin{bmatrix} z_{k+1}\boldsymbol{G}_{k+1} & \cdots & z_m\boldsymbol{G}_m \end{bmatrix} \\ \mathbf{0} \\ \begin{bmatrix} \mathbf{0} & \cdots & \mathbf{0} \\ \vdots & \ddots & \vdots \\ z_{k+1}\boldsymbol{J}_{k+1} & \cdots & \mathbf{0} \\ \mathbf{0} & \cdots & \mathbf{0} \\ \mathbf{0} & \cdots & z_m\boldsymbol{J}_m \end{bmatrix} \\ \mathbf{0} \\ \mathbf{0} \end{bmatrix}, \tag{6.13}$$

as well as $\boldsymbol{u}_I$ the wrenches acting on the interaction ports $\boldsymbol{u}_I = \begin{bmatrix} {}^0\boldsymbol{W}_{o,k+1}^{k+1} & \cdots & {}^0\boldsymbol{W}_{o,m}^{m} \end{bmatrix}^T$, with $\boldsymbol{A}_t$ of form (6.3), $\boldsymbol{J}_i$ the Jacobians of the robots or human, $\bar{\boldsymbol{D}}_t$ the damping coefficient for the contact point t and $\boldsymbol{D}_i$ the dissipation matrix for the robot(s) or human. The constraint for the rigid contact points can be described by: ${}^0\boldsymbol{T}_i^0 - {}^0\boldsymbol{T}_{o,i}^0 = \mathbf{0}_6$ for $i \in \{k+1, \cdots, m\}$.

Finally, changes in the interconnection of subsystems can be simply modelled by binary variables z_t to manipulate e.g. the contact behavior of each sub-system, i.e. z_t = Identity if the sub-system is connected to the rest of the system over contact point t and z_t = Zero if not.

6.3 Safety-Enhancing Energy Shaping Control

The proposed model connects all sub-systems via power ports and thus, allows to easily install a flow-based energy monitoring system that observes energy flows between all sub-systems, especially the port connecting the human to the rest of the system. We propose safety metrics and a supervision-based controller to shape the energy exchanged with the human, whenever a harmful or fatiguing energy flow over the human/robot interaction (HRI) port is observed.

6.3.1 Safety Metrics for HRC

In literature several metrics for the risk assessment of unintended and hazardous contacts between humans and robots exist. They mostly specify injury-related limits for mechanical hazards such as collisions. The most frequently investigated quantities in this context are transferred energy, force, and pressure observed at the collision points [223].

However, hardly any safety metrics related to continuous physical HRC are available in state-of-the-art literature. Inspired by the main injury-related factors known to be the total amount of discharged energy, the rate of discharge and the area over which energy is released, we defined the following safety principles to enhance user's safety during continuous physical collaboration with robots:

a. The maximum possible energy to be exchanged with the human and its rate of change should not violate a pre-defined safe threshold.

b. The pre-defined safe threshold should be adaptive based on user fatigue to decrease the risk of muscle injury.

Hazardous situations during HRC can be the consequence of unpredictable robot behavior resulting from e.g. false sensor readings or actuator failures. They may lead to a fast change of total energy or rate of change of energy exchanged with the human. Therefore, keeping the total energy in the system below an acceptable limit ($H_{tot} < H_{max}$) is a first step to improve safety. Such upper safety limits are the results of experimental energy-related injury analyses performed in literature, see [224, 225] for collision-based results on cranial bones and neck bones. Also the rate of change of energy, namely power, passing through the HRI port should be bounded ($P_h < P_{max}$). As currently ONLY metrics for safety evaluation during impacts are available, we use P_{max} found in impact studies, see e.g. [223, 226].

Finally, human fatigue can be considered a further risk factor as muscle injuries may result from over-straining (see [227–230]). Therefore, we propose the aforementioned upper thresholds for energy and power to be not only functions of injury-related measures, but also of user fatigue.

6.3.2 Control Design

The safety controller is represented as an independent PH system that operates on the basis of energetic information and energy flows in the system. The controller should interfere as little as possible with the execution of the task (e.g. transporting an object from an initial to a final position), while implementing the aforementioned safety principles without explicit knowledge of the human sub-system. Then the controller is designed based on the information provided from the port-based modeling of the system interacting with the human.

Nominal Controller

As the coordination of multiple robots is beyond the scope of this thesis and our aim is to illustrate the main principle of the proposed safety controller, without loss of generality we reduced the control problem to the tracking of pre-determined trajectories starting at an initial and ending at a final robot configuration. The desired equilibrium state for robot r is considered $(\boldsymbol{x}_r, \boldsymbol{P}_r) = (\boldsymbol{x}_{des,r}, \boldsymbol{0})$, where $\boldsymbol{x}_{des,r}$ is the desired robot configuration. As controller we chose

$$\boldsymbol{u}_r = \boldsymbol{K}_{p,r}\boldsymbol{x}_{e,r} + \boldsymbol{K}_{d,r}\dot{\boldsymbol{x}}_{e,r} \tag{6.14}$$

with a global and unique minimum at the desired equilibrium and $\boldsymbol{x}_{e,r} = \boldsymbol{x}_{des,r} - \boldsymbol{x}_r$ the robot configuration error. The stiffness $\boldsymbol{K}_{p,r}$ connects the desired equilibrium and the current robot configuration, while the additional damping factor $\boldsymbol{K}_{d,r}$ helps stabilizing the controlled PH system.

Safety-Enhancing Adaptive Controller

A safe system behavior during HRC is achieved by proper tuning of the parameters $\boldsymbol{K}_p$ and $\boldsymbol{K}_d$ of the nominal controller for all robots based on safety principles defined in section 6.3.1.

The controlled system interacting with the human includes m robots and the object with a total energy of

$$H_{tot} = \sum_{r=1}^{m} \frac{1}{2} \boldsymbol{x}_{e,r}^T \boldsymbol{K}_{p,r} \boldsymbol{x}_{e,r} + \sum_{r=1}^{m} H_r + H_o \tag{6.15}$$

where $K_{p,r}$ is a diagonal matrix representing the stiffness factor in the controller of robot r, and H_r and H_o are the Hamiltonian functions of the robot r and the object, respectively. Considering H_{max} to be the upper safe value of H_{tot}, (6.15) can be re-written as follows:

$$H_{\mathit{eff}} = \boldsymbol{Q}\boldsymbol{K}_p = H_{max} - \sum_{r=1}^{m} H_r - H_o \tag{6.16}$$

where $\boldsymbol{Q} = [\boldsymbol{x}_{e,1}^T \boldsymbol{x}_{e,1}, ..., \boldsymbol{x}_{e,m}^T \boldsymbol{x}_{e,m}]$ and $\boldsymbol{K}_p = [\boldsymbol{K}_{p,1}, ..., \boldsymbol{K}_{p,m}]^T$. Thus, considering H_{max} to be the limit of the total energy, the stiffness factors for each robot controller are selected as follows:

$$\boldsymbol{K}_p = \begin{cases} \boldsymbol{K}_p & H_{tot} \leq H_{max} \\ \boldsymbol{Q}^{\#} H_{\mathit{eff}} & H_{tot} > H_{max} \end{cases} \tag{6.17}$$

with $\boldsymbol{Q}^{\#}$ the Pseudoinverse of $\boldsymbol{Q}$. Please note that also a weighted Pseudoinverse could be used instead.

Next, the upper limit for the rate of change of the energy flow needs to be guaranteed. The power conservation property of the Dirac structure implies that the change in the stored energy of a system equals the sum of the power provided by the external ports and dissipative ports:

$$\boldsymbol{e}_R^T \boldsymbol{f}_R + \boldsymbol{e}_C^T \boldsymbol{f}_C + \boldsymbol{e}_I^T \boldsymbol{f}_I = -\boldsymbol{e}_S^T \boldsymbol{f}_S = \dot{H}. \tag{6.18}$$

Applying this logic to the system, the total power transferred over the HRI port is written as:

$$\begin{aligned} P_h &= -\sum_{r=1}^{m} P_{c,r} + \sum_{r=1}^{m} \dot{H}_r + \dot{H}_o, \quad \text{with} \\ P_{c,r} &= (\boldsymbol{K}_{p,r} \boldsymbol{x}_{e,r} - \boldsymbol{K}_{d,r} \dot{\boldsymbol{x}}_{e,r})^T \dot{\boldsymbol{x}}_{e,r} \end{aligned} \tag{6.19}$$

where $P_{c,r}$ is the power injected by the controller of robot r. Considering the maximum power applied to the human to be P_{max} we finally get

$$P_{\mathit{eff}} = \boldsymbol{V}\boldsymbol{K}_d = P_{max} + \sum_{r=1}^{m} \boldsymbol{x}_{e,i}^T \boldsymbol{K}_{p,r} \dot{\boldsymbol{x}}_{e,r} - \sum_{r=1}^{m} \dot{H}_r - \dot{H}_o \tag{6.20}$$

with $\boldsymbol{V} = [\dot{\boldsymbol{x}}_{e,1}^T \dot{\boldsymbol{x}}_{e,1}, ..., \dot{\boldsymbol{x}}_{e,m}^T \dot{\boldsymbol{x}}_{e,m}]$ and $\boldsymbol{K}_d = [\boldsymbol{K}_{d,1}, ..., \boldsymbol{K}_{d,m}]^T$. In order to consider the upper and lower limits for power exchange between the human and the rest of the system, the sign of P_{max} is selected as follows

$$P_{max} = \begin{cases} -P_{max} & P_h \leq -P_{max}, \\ P_{max} & P_h > P_{max}. \end{cases} \tag{6.21}$$

The damping factors for each robot controller are finally tuned to avoid unsafe rates of change of energy to be discharged over the HRI port, resulting in:

$$\boldsymbol{K}_d = \begin{cases} \boldsymbol{K}_d & |P_h| \leq |P_{max}|, \\ \boldsymbol{V}^{\#} P_{\mathit{eff}} & \text{else}, \end{cases} \tag{6.22}$$

with $\boldsymbol{V}^{\#}$ the Pseudoinverse of $\boldsymbol{V}$.

Please note that the values of $\boldsymbol{K}_p$ will never become negative and thus, result in instability, as long as H_{max} is reasonably chosen. This can be easily checked by analyzing (6.17), where $\boldsymbol{Q}$ is positive definite and thus, only a negative value of H_{eff} can lead to a negative $\boldsymbol{K}_p$. However, H_{eff} is computed based on (6.16), which will never become negative as long as H_{max}, is larger than the two other terms in (6.16). This is always the case because a reduction of H_{eff} would result in a reduction of $\boldsymbol{K}_p$, which again would reduce $\sum_{r=1}^{m} H_r$ and thus, would increase H_{eff} again. A similar logic can also be applied for the adaptation of the $\boldsymbol{K}_d$ gain.

Overloading muscles may result in muscle pain, or even strain injury. Thus, apart from preventing dangerous robot behavior, we further aim at reducing the risk of muscle injury through adaptation of the power applied to the human based on estimation of the fatigue. Taking into account relations of fatigue and work, see [231, 232], a probability for human muscle fatigue is derived by integrating the energy flow over the HRI port,

$$p_{\mathit{fatigue}} = \frac{\int P_h \, dt}{W_{h,max}}, \tag{6.23}$$

with $W_{h,max}$ the total performed work at which human muscle fatigue starts to be observed [231–233].

To take fatigue into account in the controller design, we control the energy flow over the HRI port by online adapting the value of P_{max} according to the level of muscle fatigue:

$$P_{max} = p_{\mathit{fatigue}} \tilde{P}_{min} + (1 - p_{\mathit{fatigue}}) \tilde{P}_{max}, \tag{6.24}$$

with $\tilde{P}_{min}$ and $\tilde{P}_{max}$ being the minimum and, respectively, the maximum human contribution to the task.

Passive Implementation

While in the previous sections we discussed few aspects of stability of the proposed safety-enhancing control system, here we introduce an energy-based procedure for a passive implementation of the controller (6.14) with variable damping and stiffness terms. As the human is a complex and time-varying dynamic system, it's difficult to be studied directly within an overall system stability analysis requiring accurate human models. We propose an approach that guarantees passivity of the system interacting with the human. This ensures that the system interacting with the human will not lead to an unstable situation due to the behavior of the robot controller at least as far as it is interacting with other passive systems (assuming here that the human will behave passively). Currently, the variation of the damping term in the proposed controller in section 6.3.2 may result in the violation

of passivity by internal production of energy. This can be formally solved by including a virtual energy storage element, called *energy tank* system [234, 235], that allows us keep tracking of the energy dissipated by the controller because of the damping terms. The energy stored in this reservoir can be used without violating the passivity in the system. Therefore, this ensures that only a bounded level of energy can be injected to the plant, and thus guarantees passivity (see [236] for further information on requirements of passivity).

Thus, the complete system (excluding the human) is passive by design as it has bounded energy levels due to the fact that it consists of energy transferring elements (mainly from the tank to the plant) and intrinsically passive mass and spring elements (in the plant). In the following we introduce how such a tank-based approach can be realized.

Considering an energy tank element being modeled as a spring with stiffness constant of 1, its port behavior is described by

$$\begin{cases} \dot{s}_T = & f_C \\ y_C = & \frac{\partial H_T}{\partial s_T} \end{cases} \tag{6.25}$$

where H_T is a lower bounded Hamiltonian function corresponding to the stored energy and (y_C, f_C) the power port through which the tank exchanges energy. Interconnecting the energy storage tank with the plant allows to install a power flow modulator to influence the amount of power allowed to flow between the storage element and the plant. Considering that the flow modulator tunes a modulating factor z, then the complete isolation of the storage tank and the plant (no energy exchanges between them) is realized by $z = 0$. Therefore, for a robot r, with the controller (6.14) and state $\boldsymbol{x}_r \in \mathbf{R}^b$, b energy tanks can be considered corresponding to the dimensions of the state. A power-preserving feedback interconnection of b energy tanks to the controller considering the modulating factors is established as follows:

$$\begin{aligned} \dot{\boldsymbol{s}}_T &= \boldsymbol{Z}\dot{\boldsymbol{x}}_r \\ \boldsymbol{u}_r &= -\boldsymbol{Z}\boldsymbol{s}_T \end{aligned} \tag{6.26}$$

where the transmission ratio is presented by the diagonal matrix $\boldsymbol{Z}$ with elements $(z_1, ...z_b)$, and the spring-like storage elements by the state vector $\boldsymbol{s}_T = [s_1, ...s_b]^T$. With reference to (6.26), the desired control input $\boldsymbol{u}_r$ (from (6.14)) can be calculated by the modulating factor $\boldsymbol{Z} = -\boldsymbol{s}_T^{\#}\boldsymbol{u}_r$.

Finally, in order to ensure energetic passivity of the controller, it is necessary to avoid a singularity when a tank state tends to zero, i.e. the tank is empty. This requires that the power flows from each storage tank to the plant only if there is a minimum available energy remaining in the tank. This is ensured by the adaptation of $\boldsymbol{Z}$, e.g. if the energy in a storage tank is below a threshold (ϵ), the controller isolates the storage tank and the plant by setting the transmission ratio for the corresponding tank to zero. Thus, for every specific tank T_i with the Hamiltonian $H_{Ti} = 0.5{s_{Ti}}^2$, the modulating factor z_{Ti} is finally implemented as

$$z_{Ti} = \begin{cases} 0 & (H_{Ti} < \epsilon) \wedge (P_{c,r_i} > 0) \\ i^{th} \text{ element of } \boldsymbol{Z} = -\boldsymbol{s}_T^{\#}\boldsymbol{u}_r & \text{otherwise} \end{cases} \tag{6.27}$$

where ϵ is the minimum energy threshold considered for tank i and P_{c,r_i} the power flowing from the controller to the plant related to the state that the tank is specified for (that can be calculated similar to (6.19)).

To avoid an excess of energy stored in the tanks that would allow implementation of practically unstable behaviors in the system, see the reasons reported in [237], it is wise to disable the charging of the tanks when their energies are bigger than a suitable upper bound. This bounded level of energy in the tanks should be defined specific to each application and task to be accomplished as well as a possible estimation of the maximum energy that can be injected by subsystems (e.g. considering the possible force that can be applied by the human).

6.4 Results

We present simulation results for the port-Hamiltonian model of the considered HRC task, including also the proposed energy-based safety controller.

6.4.1 Simulation of the HRC Model

Validation of the modeling approach was performed on an academic test scenario considering the collaborative object manipulation by a 2 DOF serial robot manipulator with revolute joints and a 2 DOF human arm with shoulder and elbow joints moving in the vertical plane. The total mass and inertia tensor of the object were considered to be $M_o = 5$ kg and $I_o = \text{diag}(0.006, 0.04, 0.04)$ [kgm^2] respectively, while the dynamic and geometric parameters of the robot were assumed as follows: link lengths $l_{1,r} = l_{2,r} = 1$ m, mass and inertia of the segments $m_{1,r} = m_{2,r} = 1$ kg and $I_{1,r} = I_{2,r} = 0.084$ kgm^2. The friction in the joints was neglected for the sake of simplicity. For the human arm the following values were assumed for simulation: $m_{1,h} = 1.4$, $m_{2,h} = 1.1$ kg, $l_{1,h} = 0.3$, $l_{2,h} = 0.33$ m, and $I_{1,h} = 0.025$, $I_{2,h} = 0.045$ kgm^2 and $\boldsymbol{K}_{p,h} = \text{diag}(100, 100)$ [N/m], $\boldsymbol{K}_{d,h} = \text{diag}(10, 10)$ [N·s/m].

Figure 6.3 illustrates the energetic behavior of each sub-system during the experiment. Four different phases were considered: (a) non-contact initial condition from initial to time equal to 1 s, (b) approaching the object between 1 s and 4.8 s and, (c) establishing contact at 4.8 s and keeping the current configuration to 5 s, (d) transporting the object to the desired position from 5 s to the end. Constant stiffness and damping factors $\boldsymbol{K}_p = \text{diag}(2000, 2000)$ [N/m] and $\boldsymbol{K}_d = \text{diag}(100, 100)$ [N·s//m] were considered. In phase (c) contact between human-object and robot-object is established by simply activating the corresponding contact variables. The three top plots show a good trajectory tracking performance since the reference positions, which are defined for human and robot independently, are well followed using the aforementioned controller. The Hamiltonian of each sub-system, as well as the power exchanged between them, is monitored thanks to the port-based modeling. For example, the transferred powers P_h and P_r are zero before establishing connection, while their value after connection to the object represents their injected or absorbed power during task execution. The value of the power exchanged over the robot-object interaction point (P_r) is almost three times bigger than the power exchanged over the human-object

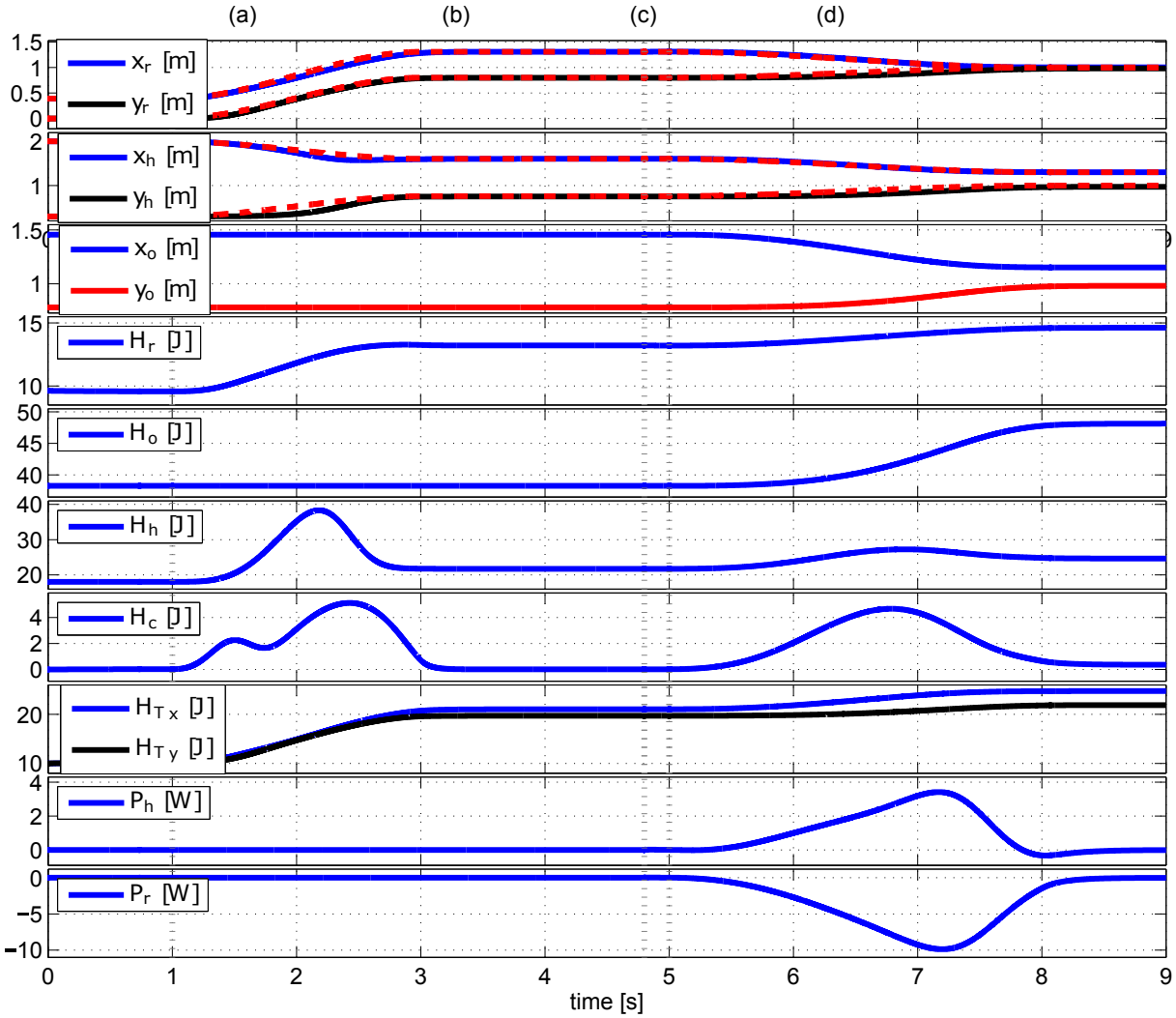

Figure 6.3: Evaluation of the energy-based HRC model. In the first two top plots, dashed red lines show the reference positions and solid lines show obtained values. The four phases (a), (b), (c) and (d) are separated by dotted gray lines.

interaction port (P_r) and thus, indicates a larger contribution of the robot than the human to the execution of the task. Please consider that the positive value for the human power corresponds to the power transferred from the object to the human. The initial change in the Hamiltonian of the robot and human during phase (b) is due to movements towards the obstacle, while further changes during phase (d) are because of transporting the object. Moreover, the behavior of the tank energies (H_{Tx}, H_{Ty}) over time shows their recharging due to the dissipated power of the controller. The charging of tanks mainly happens in two time intervals of (a) and (d) when parts of the energy of the robot controller are dissipated due to its damping terms. The tank energies were neither discharged nor depleted (no decrease of energy is found in the energy profiles), thus confirming passivity of the control system, which is expected when the controller uses constant values for its damping and stiffness parameters. Finally, slow gradual changes in the Hamiltonian of the object can be explained by changes of its potential energy since it was transferred to a higher position.

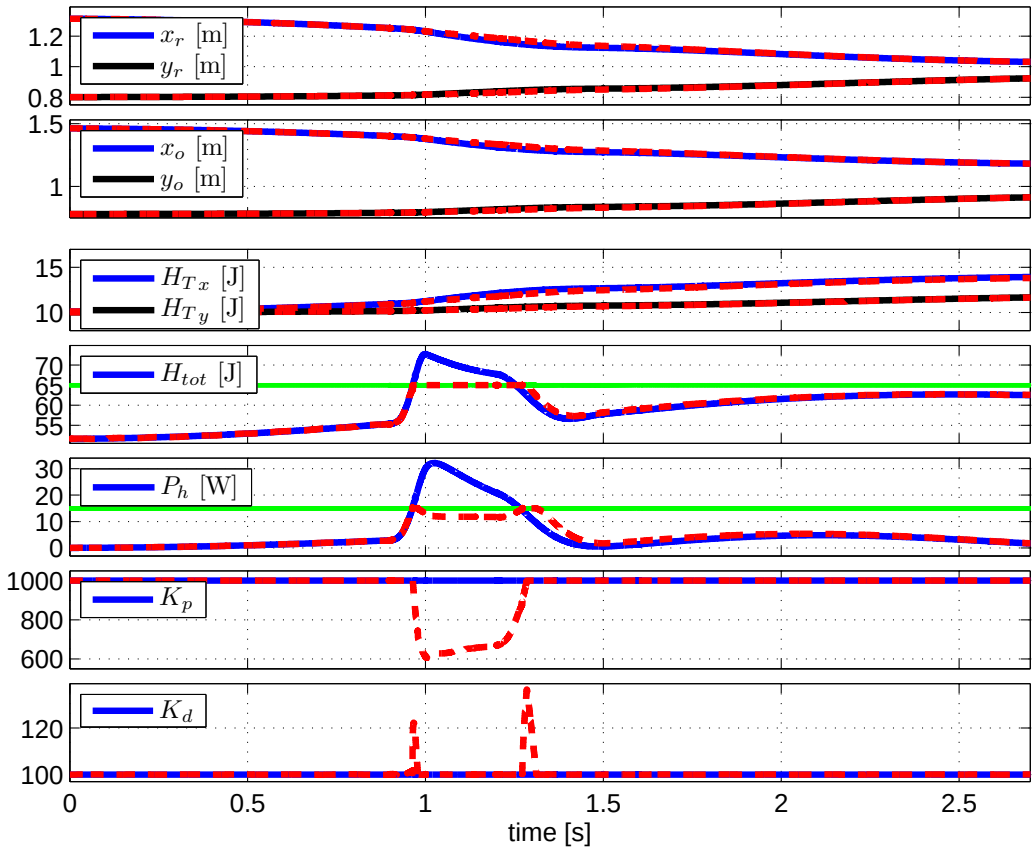

Figure 6.4: Validation of energy-based adaptive shared controller. Solid blue and black lines show signals using nominal controller, dashed red lines show signals using safety-enhancing adaptive controller and green lines in the two middle plots show the considered safety thresholds.

6.4.2 Validation of the Safety-Enhancing Control Approach

A trajectory tracking task was considered, and the following two scenarios were studied to validate the safety-enhancing controller design proposed in previous sections. In the first scenario, we evaluate the robot behavior while satisfying aforementioned safety criteria, and in the second scenario we focus on the adaptation of the robot actions based on the estimated human fatigue.

Scenario I

The human and the robot transport the object from an initial to a final configuration, while the robot avoids a dynamic obstacle placed very close to the path and suddenly appearing at time 0.8 s to 1.3 s.[2] The system performance for cases with and without safety controller is depicted in Fig. 6.4 with $H_{max} = 65$ J, $P_{max} = 15$ W, $\boldsymbol{K}_p = \text{diag}(1000, 1000)$ [N/m] and $\boldsymbol{K}_d = \text{diag}(100, 100)$ [N·s/m]. Looking at the results for the case without safety

[2]Please note that collision avoidance during HRC is out of focus of this thesis and the case of a suddenly appearing obstacle is used as representative example of many other unpredictable and hazardous situations that can happen during HRC.

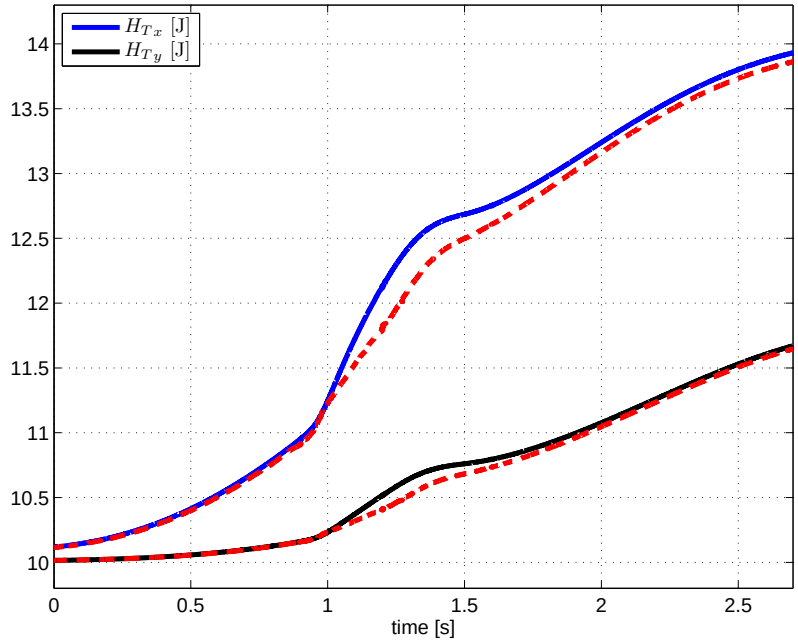

Figure 6.5: Behavior of the energy tanks. Solid blue and black lines show signals using nominal controller, dashed red lines show signals using safety-enhancing adaptive controller.

controller, it can be seen that the robot reaction to avoid collision with the obstacle results in violating constraints for the maximum power to be allowed to be exchanged with the human, i.e. $P_h > P_{max}$ as well as a potential harmful increase of the total energy of the system interacting with the human, i.e. $H_{tot} > H_{max}$. The two top plots in Fig. 6.4 show that the actual trajectory minimally deviates from the desired one as a consequence of the safety controller adjusting its parameters $\boldsymbol{K}_p$ and $\boldsymbol{K}_d$ to prevent violation of safety constraints. Please note that the energy tanks are only charged over time. This is due to the behavior of the controller that only results in a further energy dissipation rather than generation, e.g. the value of the damping factor is always positive and bigger than the considered constant value. [3] The tank energy profiles follow a similar pattern as shown in Fig. 6.3 for both controllers, while a very slightly lower level of stored energy is found for the case with safety controller, see Fig. 6.5 that shows the zoomed plot of energy tanks. Before appearance of the obstacle (at time 0 to 0.8 s), the energy profiles are similar for both cases (with and without the safety controller). The tank's energy when using the safety controller increases with a lower rate than using the nominal controller at time 0.8 to 1.3 s. This is mainly due to reduction of the robot velocity by increasing the damping and reducing the stiffness factors. Afterward, from 1.3 s to the end, again the behavior of the two controllers gradually become similar and therefore the energy tanks are charged more similarly. Please note that, an arbitrary initial value has been considered for the tanks to avoid starting the simulation with the singularity case discussed in section 6.3.2.

[3] As explained in section 6.3.2, a proper upper boundary can be defined to disable overcharging of the tanks. However, in the simulations in this chapter, we decided to show the results without such a boundary to show the difference of the tanks behavior for both controllers.

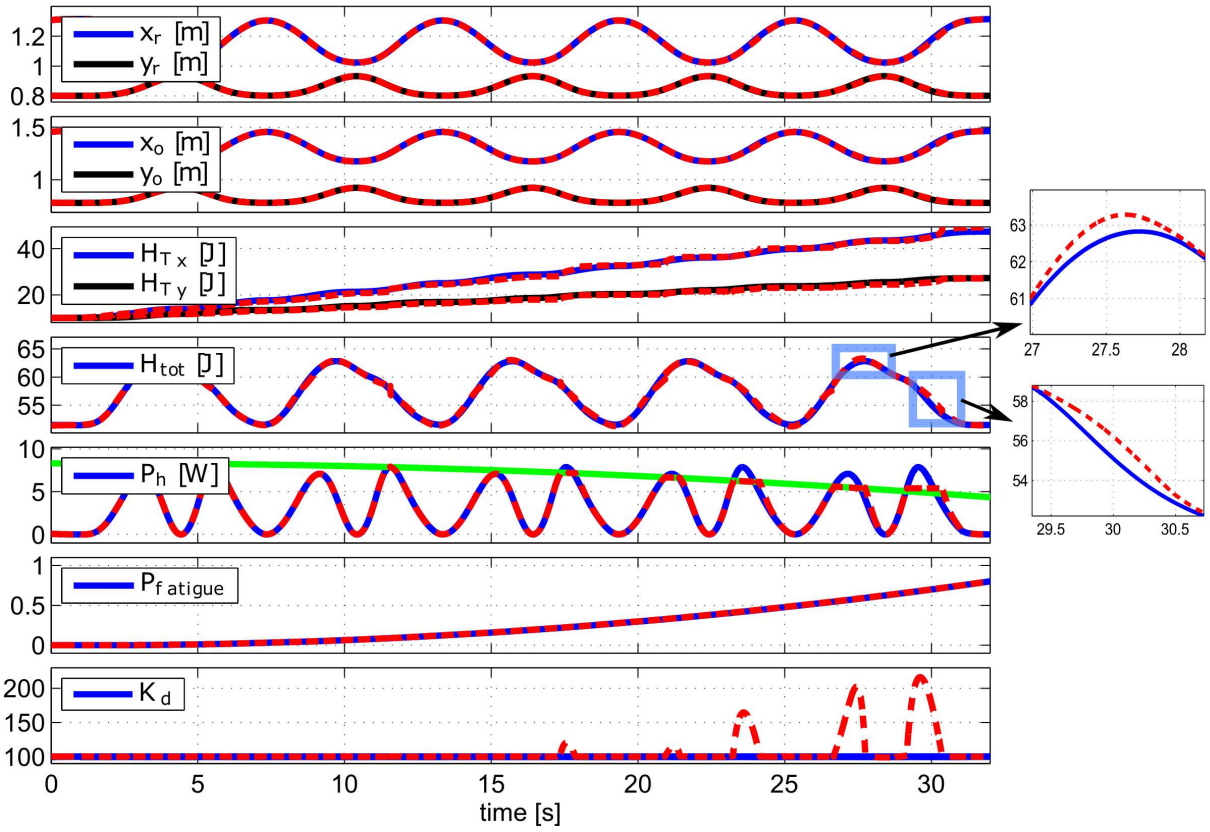

Figure 6.6: Validation of energy-based adaptive shared controller for user's fatigue reduction. Solid blue and black lines show signals using nominal controller, dashed red lines show signals using the safety-enhancing adaptive controller and the green line in the fourth plot shows the considered adaptive safety threshold.

Scenario II

A repetitive task of object transportation is studied, which allows to observe an increasing level of human fatigue. We considered $P_{high} = 8.3$ W and $P_{low} = 5$ W. As can be observed in Fig. 6.6, the control parameters are adjusted automatically to prevent extra power applied to the human if the estimated user's fatigue increases. In both cases, with and without safety controller, the system tracks well the desired trajectory as depicted in the two top plots. While this results in similar profiles for the total energy H_{tot}, their differences have been illustrated by two zoomed plots corresponding to the instances that the adaptation law is activated. In these instances, H_{tot} is slightly bigger for the case of using the safety-enhancing controller since the robot system takes over parts of the task of the human (the power exchanged in the human port is decreased, see P_h profile, while the object is following the same trajectory). Moreover, with increasing user's fatigue, the maximum allowed power to be transferred over the human-object interaction port is reduced, which results in an increase of $\boldsymbol{K}_d$ to prevent the violation of safety constraints. For illustration purposes, a relatively low value for $W_{h,max} = 1200$ J was considered, which resulted in a rather fast increase of fatigue. The energy tanks also behave similarly to the previous simulations and keep storing the dissipated energy of the controller.

6.5 Summary and Discussion

Robotics research is progressing towards physical interaction between humans and robots, with multiple potential applications not only in rehabilitation and assistive robotics, but also in industry (e.g. robot co-workers). Close interaction of a human with robots demands for proper control approaches so as to enhance the safety of the user. However, while collision detection and contact-related injury reduction in physical human-robot interaction has been studied intensively, safety issues in physical human-robot collaboration (pHRC) with continuous coupling of human and robot(s) (which is a common case of assistance robots) has received little attention so far. This chapter for the first time proposes an energy monitoring and control system that supervises energy flows among the different subsystems involved in pHRC and shapes them to improve human safety whenever an unsafe situation is about to happen. A general pHRC task is considered and further described using bond graphs and energy flows through ports to cover the different, continuous and time-varying contact situations that arise in such scenarios. Moreover, a novel monitoring system was designed that observes energy flows between sub-systems, with a compliance controller that shapes these flows so as to enhance human safety.

While a priori information was used for the object dynamics within the considered pHRC task, in particular, an on-line identification scheme would be more appropriate which can be considered as a possible future direction for practical implementation as well as experiments with real robots. Nonetheless, the proposed approach relies on power and energy flows and only required to monitor and bound such physical quantities, rather than canceling dynamic terms by control. In this sense, the presented controller is intrinsically more robust to uncertainties. However, dependence of accurate dynamic models of the sub-systems (except the human as its direct usage has been excluded in the design of the safety-enhancing controller) is the main restriction of the proposed approach.

As currently, only metrics for safety evaluation during impacts are available, in this work the thresholds for maximum exchangeable power and energy were specified from impact studies. However, future research can focus on deriving proper new thresholds for continuous interaction taking the specific human configuration into account. Finally, investigation of other safety metrics that consider the continuous nature of tasks and the actual configuration of bodies can be studied in future.

The proposed safety-enhancing concept in this chapter can be considered complementary to any of the developed controllers presented in the last three chapters, e.g. to shape the energy applied to the human and to keep its magnitude and rate of change within safe boundaries during STS or fall prevention. However, an immediate future work can extend the proposed modeling and control approaches for a mobility assistance robot including actuated arms.

7 Conclusion and Future Work

7.1 Summary and Concluding Remarks

Mobility problems can impede independent living and are prevalent in the elderly population. Mobility assistance robots (MARs) can help in overcoming this situation by incorporating features like sit-to-stand assistance, walking and navigation assistance in indoor and outdoor environments, posture control and fall prevention. However, they also come with challenges in terms of acceptability by the users, adaptability to users and environment as well as safety due to their close interaction with humans, more specifically the elderly or patients with cognitive and/or physical impairments. This thesis has proposed approaches to design novel and human-inspired controllers for mobility assistance robots. Achieving safe, natural, and user and environment-adaptive robot behavior were considered to be the main challenges in the control design.

The research directions of this thesis were formulated based on an overview of the current state of the art MAR functionalities presented in chapter 2. This literature review of a total number of 27 rollator-type MARs showed that most available systems are active, based on four wheels and having a non-holonomic kinematics. Moreover, main functionalities of MARs were identified as sit-to-stand (STS) and stand-to-sit transfer assistance, walking assistance and health monitoring. This thesis therefore focused on the development of the control approaches for three commonly demanded modes of STS and walking as well as human's fall prevention due to its crucial importance.

In terms of STS transfer assistance, chapter 3 proposed biologically-inspired and optimal assistance approaches to be provided by MARs. This chapter extended the state of the art on STS assistance with respect to the following aspects: i) mathematical modeling of the human's STS transfers and exploiting their underlying principles, ii) extension of the obtained models to derive optimal and biologically-inspired assistive strategies to be provided to the users, and iii) intensive evaluation by real end-users. Modeling of assisted and unassisted human STS transfers were formulated as an optimal feedback control formulation. Compared to previous work based on SQP approaches, we based our optimization on Differential Dynamic Programming that has been shown to be a powerful tool in studying biological movements. It has allowed us to obtain an optimal solution with respect to a defined cost function and considers the nonlinearity of human biomechanics as well as physical constraints, which are naturally incorporated into the optimization framework. It further showed potential for future online implementation. The model was extended with external forces and torques. Optimal assistive STS transfer strategies were determined considering two types of assistance classes and weaknesses. The resulting optimal assistive trajectories were calculated and implemented on a robotic mobility assistant. The assistive STS transfer approach was finally evaluated within an intensive user-study of elderly subjects. Results showed a high user satisfaction as well

as excellent success rate for all participants indicating the effectiveness of the proposed assistance optimization approaches.

The control design of MARs during walking (as the second considered operational mode) was studied in chapter 4. The novelty of this chapter focuses on two aspects: i) to develop an integrated shared control approach that helps the user by providing sensorial, cognitive and physical assistance, and ii) to employ the human's decision making mechanism as the key component in the adaptation laws of the robot controller. The integrated shared control architecture distinguishes between short-term adaptations providing a) cognitive assistance to support the user to follow a desired path towards a predefined destination and b) sensorial assistance to avoid collisions with obstacles and to allow for an intentional approach of them. Furthermore, it considered a long-term adaptation of c) the overall assistance based on long-term user performance and observed fatigue. To achieve an intuitive and human-like adaptation policy of the provided assistance, a decision-making model explored in cognitive science, the Drift-Diffusion model, was employed. The effectiveness of the proposed architecture evaluated by means of technical experiments as well as a user-study with elderly people. Obtained results indicated that the required functionalities can be realized with the proposed decision-making algorithm showing a general high potential of the proposed adaptive shared control architecture for MARs.

Human balance recovery and fall prevention was discussed in chapter 5, where for the first time a fall prevention approach was proposed for a mobility assistance robot equipped with a pair of actuated arms. The algorithm evaluated the user's Extrapolated Center of Mass (XCOM) and determined the required supportive forces to be provided to the user for fall prevention. Moreover, a compliant robot controller was proposed to realize the required forces for fall prevention. Results of this chapter revealed that the use of XCOM is an appropriate choice for human's balance determination and fall prevention control design as its computation is easier than the ZMP or COP, and its reaction to human's fall is faster than COM. The later allows for a faster robot reaction and therefore prevention of the human's falls as soon as it is about to happen.

Safety aspects are the crucial requirement in the control design and were considered for each mode of operation. In chapter 3 it was focused on by considering the balance criteria aiming at avoiding human's fall during STS transfers, in chapter 4 by developing as passive as possible assistive strategies, and in chapter 5 by developing an optimal human fall prevention approach. Moreover, the safety aspect was further emphasized in chapter 6 by the realizing of a general and complementary controller that aimed to supervise the behavior of the specific control unit in the specified mode of operation and reshape the robot's behavior to enhance the user's safety if an unsafe situation is about to happen. The safety approach presented in this chapter is general and can be applied not only to assistance devices, but also to other collaborative robots, with multiple potential applications, e.g. robot co-workers in industry.

A major contribution here was to develop an energy-flow and port-based model for a general pHRC scenario taking the different and time-varying contact situations that are typical for such a scenario into account. Based on this model, a novel energy monitoring and adaptive controller was proposed that observes energy flows between all sub-systems and that shapes them accordingly to guarantee human safety. Safety metrics were defined

considering the maximum energy that is allowed to be exchanged with humans and the maximum rate of change of it, along with measures that take human fatigue into account.

In summary, the ideas, concepts and approaches developed in this dissertation significantly advance the state of the art in the control design of assistance robots taking into account safety, intuitiveness and acceptability as well as user and environment-adaptation.

7.2 Perspectives

The research field of mobility assistance robots is of a highly interdisciplinary nature. By combining the research fields of cognitive science and motor control, with computer science and robotics engineering, the work in this thesis provides a solid ground for future interdisciplinary research for the further advancement of the control design of MARs. The topics addressed in this dissertation also motivate a number of interesting future research directions, as drafted in the following:

- **Developement of systems and functionalities of mobility assistance robots**: Important points for the future development of rollator-type mobility assistance robots will be to advance the robots not only from a hardware perspective, but also from a software, and thus, functionality perspective. In terms of hardware and system design, sensors like GPS, Kinect, 3D laser, and tactile sensors could be further explored along with independent actuation systems for handles providing STS transfer assistance. In terms of functionalities, more weight could be given to STS transfer support, fall prevention, health monitoring, and extra functionalities involving more advanced human-system interfaces. Although explored human-machine interfaces are so far mainly limited to touch-screens and speech interfaces, nonverbal interaction via gesture and mimics with the systems can be a target for future advancements. Though these human-machine systems are generally an interesting research topic, their benefits in the context of mobility assistance robots for the elderly has still to be proven as cognitive disabilities typically may reduce the capability of the elderly to communicate via gestures and mimics.

- **Unified control system for different operational modes**: Different phases of human motion and robot operational modes call for different robot controllers to be implemented, as considered in this thesis for three main modes. Automatic switching between the control modes was out of focus of this thesis and has received very little attention in literature. So far, only hard switching between different controllers has been performed by either using some predefined thresholds in measurement data, or evaluating user inputs provided via touch screens or voice interfaces. However, intelligent mechanisms for switching the robot controllers can be investigated. This could advance the development of a sophisticated MAR providing assistance in different modes of operation based on the user state and needs. In case of multiple switching between controllers, this can also be studied from a control theory perceptive to prove the overall stability of the hybrid and switched systems.

- **Sit-to-stand transfers modeling and optimal assistance**: While in this thesis a basic human biomechanical model has been studied, future work can focus on considering more complex three-dimensional human dynamic models, even with direct muscle control. This could result in a deeper understanding of the underlying principles. Moreover, it will allow to better understand the contribution of the human muscles and thus, to better address muscle weaknesses during STS transfers allowing to take muscle weaknesses into account through personalized user assistance.

- **Human articulated tracking for walking and fall prevention assistance**: Advanced robot controllers require information about the actual human posture and thus, articulated tracking functionalities have to be implemented on the robot. Although in literature basic approaches for articulated tracking were proposed with the help of a small number of laser scanners that scanned the user at different heights of the body and thus, allowed us to only roughly estimate the actual human posture, further investation on available sensors like 3D laser scanners and Kinect may help for a better human posture determination. This could provide more sophisticated information and therefore improve the development of the user-adaptive approaches for both walking and human fall prevention assistance.

- **Safety**: Safety will become one of the critical factors to bring MARs on the market and suitable for daily usage by the end-users. In this thesis, safety was considered during walking by concentration on passive support, while it was evaluated mainly in terms of posture stability measures for STS transfers and human fall prevention assistance. In this respect, a more elaborate safety analysis that goes beyond classical posture stability measures and includes the definition of posture-dependent safe states and safe robot behaviors can be investigated. Moreover, this thesis particularly considered the allowed energy exchange between user and robot and proposed approaches to limit the energy of the robots and the power transferred to the human to enhance the safety of the system. Future directions could further investigate other factors such as environmentally constrained configurations of the human body next to constraints originating from the task itself in order to eliminate possibilities of injuries in HRC. Moreover, investigation of other safety metrics and requirements that consider the continuous nature of collaborative and assistive tasks and the actual configuration of bodies can be studied in future.

The main idea and individual concepts of this thesis are also expected to motivate further developments towards user-oriented, biologically-inspired and context-specific assistive approaches that consider user's safety as well as natural and adaptive robot behavior.

A Anthropomorphic Data of Participants in STS Model Evaluations

Two tables reporting the body measurements of the healthy and elderly participants in the validation of the STS transfer model are reported as follows.

Table A.1: Anthropometric data of healthy subjects participating in the STS model validation

subject	age	weight $[kg]$	height $[m]$
S1	26	74	1.72
S2	25	80	1.80
S3	29	70	1.83

Table A.2: Anthropometric data, cognitive and motor impairment level of elderly subjects participating in the STS model validation.

subject	age	weight $[kg]$	height $[m]$	Cognitive impairment level	Motor impairment level
S1	80	64	1.53	no impairment	moderate
S2	77	60	1.59	no impairment	moderate
S3	77	69	1.75	no impairment	moderate
S4	80	89	1.64	moderate	moderate
S5	85	56	1.49	no impairment	moderate
S6	80	70	1.40	severe	moderate
S7	75	74	1.56	no impairment	moderate
S8	85	85	1.70	moderate	moderate
S9	81	61	1.78	moderate	moderate

B Optimal Feedback Control

Complementary information for Differential dynamic programming (DDP) approach is presented in this section. DDP first proposed in [137] and recently reformulated by [138] is used to solve the optimal control problem cast in the chapter 3. DDP iteratively and quadratically approximates the costs and the nonlinear system dynamics around the current trajectory where an approximately optimal control law in affine form is considered for the approximated system that enforces formulated control constraints. The algorithm starts an initial guess of the control sequence (in our specific STS transfer problem we consider pure gravity compensating forces), which is then iteratively improved with respect to the formulated cost function. The iterative approach is implemented as describes followings.

First, the cost function is time-discretized

$$\boldsymbol{c}(\boldsymbol{x}(k), \boldsymbol{\tau}(k)) = \sum_{k=0}^{N-1} \Big(\sum_{i=1}^{6} \boldsymbol{C}_i(\boldsymbol{x}(k), \boldsymbol{\tau}(k)) \Big) \Delta t \tag{B.1}$$

with $N = T/\Delta t$. Then, each iteration starts with an open loop control sequence $\hat{\boldsymbol{\tau}}_k$ that is applied to the deterministic nonlinear and discretized forward dynamics $\hat{\boldsymbol{x}}_{k+1} = \hat{\boldsymbol{x}}_k + \Delta t f(\hat{\boldsymbol{x}}_k, \hat{\boldsymbol{\tau}}_k)$ using standard Euler integration at sample k. Then, the dynamics and the cost function are quadratically approximated in the vicinity of the current trajectory. Both aforementioned approximations are expressed in terms of state and control deviations, i.e. $\delta \boldsymbol{x}_k = \boldsymbol{x}_k - \hat{\boldsymbol{x}}_k$ and $\delta \boldsymbol{\tau}_k = \boldsymbol{\tau}_k - \hat{\boldsymbol{\tau}}_k$, and are computed as follows,

$$\begin{aligned} \delta \boldsymbol{x}_{k+1} &= (\mathbf{I} + \Delta t \boldsymbol{f}^{\boldsymbol{x}}) \delta \boldsymbol{x}_k + \Delta t (\boldsymbol{f}^{\boldsymbol{\tau}} \delta \boldsymbol{\tau}_k + \delta \boldsymbol{\tau}_k^T \boldsymbol{f}^{\boldsymbol{\tau x}} \delta \boldsymbol{x}_k) \\ &\quad + 0.5 \Delta t (\delta \boldsymbol{x}_k^T \boldsymbol{f}^{\boldsymbol{xx}} \delta \boldsymbol{x}_k + \delta \boldsymbol{\tau}_k^T \boldsymbol{f}^{\boldsymbol{\tau\tau}} \delta \boldsymbol{\tau}_k) \qquad \text{(B.2)} \\ \boldsymbol{c}(\delta \boldsymbol{x}, \delta \boldsymbol{\tau}) &= \delta \boldsymbol{x}_k^T \boldsymbol{c}^{\boldsymbol{x}} + \delta \boldsymbol{\tau}_k^T \boldsymbol{c}^{\boldsymbol{\tau}} + \delta \boldsymbol{\tau}_k^T \boldsymbol{c}^{\boldsymbol{\tau x}} \delta \boldsymbol{x}_k \\ &\quad + 0.5 (\delta \boldsymbol{x}_k^T \boldsymbol{c}^{\boldsymbol{xx}} \delta \boldsymbol{x}_k + \delta \boldsymbol{\tau}_k^T \boldsymbol{c}^{\boldsymbol{\tau\tau}} \delta \boldsymbol{\tau}_k) \qquad \text{(B.3)} \end{aligned}$$

with $\texttt{func}^{\texttt{vars}}$ the partial derivative of function `func` with respect to variables ordered by `vars` and all the partial derivatives are obtained at $(\hat{\boldsymbol{x}}_k, \hat{\boldsymbol{\tau}}_k)$.

At each moment k, the cost for the optimal control of the system from the current state $\boldsymbol{x}_k$ to the final state $\boldsymbol{x}_N$ is defined by:

$$\boldsymbol{v}(\boldsymbol{x}_k) = \boldsymbol{\phi}_{final}(\boldsymbol{x}_N) + \boldsymbol{c}_k(\boldsymbol{x}_i, \boldsymbol{\tau}_i^*), \tag{B.4}$$

where $\boldsymbol{\tau}_i^*$ is the optimal control decision. This local approximation of the original optimal control problem can then be efficiently solved by evaluating the Hamilton-Jacobi-Bellman

equation

$$\begin{aligned} \boldsymbol{v}_k(\delta\boldsymbol{x}) = \delta\boldsymbol{x}_k^T\boldsymbol{P}_k + \frac{1}{2}\delta\boldsymbol{x}_k^T\boldsymbol{Q}_k\delta\boldsymbol{x}_k + \delta\boldsymbol{\tau}_k^{*T}\boldsymbol{R}_k \\ + \frac{1}{2}\delta\boldsymbol{\tau}_k^{*T}\boldsymbol{S}_k\delta\boldsymbol{\tau}_k^* + \delta\boldsymbol{\tau}_k^{*T}\boldsymbol{T}_k\delta\boldsymbol{x}_k \end{aligned} \tag{B.5}$$

where

$$\begin{aligned} \boldsymbol{P}_k &= \Delta t\, \boldsymbol{c}^{\boldsymbol{x}} + (I + \Delta t \boldsymbol{f}^{\boldsymbol{x}})\boldsymbol{v}_{k+1}^{\boldsymbol{x}} \\ \boldsymbol{R}_k &= \Delta t\, (\boldsymbol{c}^{\boldsymbol{\tau}} + \boldsymbol{f}^{\boldsymbol{\tau}}\boldsymbol{v}_{k+1}^{\boldsymbol{x}}) \\ \boldsymbol{Q}_k &= \Delta t\, \boldsymbol{c}^{\boldsymbol{xx}} + (I + \Delta t \boldsymbol{f}^{\boldsymbol{x}})\boldsymbol{v}_{k+1}^{\boldsymbol{xx}}(I + \Delta t(\boldsymbol{f}^{\boldsymbol{x}})^T) \\ &\quad + \Delta t \boldsymbol{f}^{\boldsymbol{xx}}\boldsymbol{v}_{k+1}^{\boldsymbol{x}} \\ \boldsymbol{S}_k &= \Delta t\, (\boldsymbol{c}^{\boldsymbol{\tau\tau}} + \boldsymbol{f}^{\boldsymbol{\tau}}\boldsymbol{v}_{k+1}^{\boldsymbol{xx}}(\boldsymbol{f}^{\boldsymbol{\tau}})^T) + \Delta t \boldsymbol{f}^{\boldsymbol{\tau\tau}}\boldsymbol{v}_{k+1}^{\boldsymbol{x}} \\ \boldsymbol{T}_k &= \Delta t\, \boldsymbol{c}^{\boldsymbol{\tau x}} + (\Delta t(\boldsymbol{f}^{\boldsymbol{\tau}})^T)\boldsymbol{v}_{k+1}^{\boldsymbol{xx}}(I + \Delta t(\boldsymbol{f}^{\boldsymbol{x}})^T) \\ &\quad + \Delta t \boldsymbol{f}^{\boldsymbol{\tau x}}\boldsymbol{v}_{k+1}^{\boldsymbol{x}}. \end{aligned}$$

Minimizing the right side of (B.5) with respect to $\delta\boldsymbol{\tau}_k$ determines the optimal control policy as follows,

$$\delta\boldsymbol{\tau}_k^* = -\boldsymbol{S}_k^{-1}\boldsymbol{R}_k - \boldsymbol{S}_k^{-1}\boldsymbol{T}_k\delta\boldsymbol{x}_k. \tag{B.6}$$

The resulting control law is of affine form $\delta\boldsymbol{\tau}_k^* = \mathbf{l}_k + \mathbf{L}_k\delta\boldsymbol{x}_k$with an open loop term ($\mathbf{l}_k = -\boldsymbol{S}_k^{-1}\boldsymbol{R}_k$) and a feedback term ($\mathbf{L}_k\delta\boldsymbol{x}_k = -\boldsymbol{S}_k^{-1}\boldsymbol{T}_k\delta\boldsymbol{x}_k$). Additional control constraints are taken into account by enforcing the open loop terms to lie inside of a constrained boundary. If the control constraint is violated, the open loop term is determined to either guide the optimal control inside of the boundary or at least to stay within it by considering,

$$\boldsymbol{l}_k = min(max(\boldsymbol{\tau}_{max},\, \boldsymbol{\tau}_k + \boldsymbol{l}_k),\, \boldsymbol{\tau}_{min}). \tag{B.7}$$

For each iteration i the approximate optimal control sequence $\hat{\boldsymbol{\tau}}_k^{(i+1)}$is finally obtained by adding the newly calculated corrective control term and the control term of the last iteration $\hat{\boldsymbol{\tau}}_k^{(i+1)} = \delta\boldsymbol{\tau}_k^{(i)} + \hat{\boldsymbol{\tau}}_k^{(i)}$, and then the new nominal state and control trajectories are computed using the dynamic equations of the system. [1]

[1] [138, 238] proposed different improvements to the iterative LQG method including the invertability problem of $\boldsymbol{S}_k$ that have been also considered in the above-mentioned DDP implementation, but are not explicitly mentioned here because of space limitations.

Bibliography

[1] UN Report. United nations report: World population prospects, the 2015 revision. *Analytical Report, United Nations New York, http : //esa.un.org/unpd/wpp/publications/files/key_findings_wpp_2015.pdf*, 2015.

[2] E. McAuley, J.F. Konopack, R.W. Motl, K.S. Morris, S.E. Doerksen, and K.R. Rosengren. Physical activity and quality of life in older adults: influence of health status and self-efficacy. *Ann. Behav. Med.*, 1(31):99–103, 2006.

[3] W.W. Spirduso and D.L. Cronin. Exercise dose-response effects on quality of life and independent living in older adults. *Med. Sci. Sports Exerc.*, 6(33):598–608, 2001.

[4] J.S. Brach, J.E. Berlin, J.M. VanSwearingen, A.M. Newman, and S.A. Studenski. Too much or too little step width variability is associated with a fall history in older persons who walk at or near normal gait speed. *NeuroEngineering and Rehabilitation*, 2005.

[5] K. Delbaere, J.C. Close, J. Heim, P.S. Sachdev, H. Brodaty, M.J. Slavin, N.A. Kochan, and S.R. Lord. A multifactorial approach to understanding fall risk in older people. *Am. Geriatr. Soc.*, 9(58):1679–1685, 2010.

[6] Maria M Martins, Cristina P Santos, Anselmo Frizera-Neto, and Ramón Ceres. Assistive mobility devices focusing on smart walkers: Classification and review. *Robotics and Autonomous Systems*, 60(4):548–562, 2012.

[7] Solenne Page, Ludovic Saint-Bauzel, Pierre Rumeau, and Viviane Pasqui. Smart walkers: an application-oriented review. *Robotica*, pages 1–20.

[8] *Rehabilitation and Health Care Robotics*, pages 1223–1251. Handbook of Robotics. Springer, 2008.

[9] A. Frizera, R. Ceres, J. L Pons, A. Abellanas, and R. Raya. The smart walkers as geriatric assistive device. In *6th International Conference of the International Society for Gerontechnology*, pages 1–6, 2009.

[10] Christian Werner, Phoebe Koepp, Milad Geravand, Angelika Peer, and Klaus Hauer. Evaluation studies of robotic rollators by the user perspective: A systematic review. *Gerontology - International Journal of Experimental, Clinical, Behavioural and Technological Gerontology*, 2016.

[11] N. Nejatbakhsh and K. Kosuge. User-environment based navigation algorithm for an omnidirectional passive walking aid system. In *International Conference on Rehabilitation Robotics*, Chicago, USA, 2005.

[12] Y. Hirata, S. Komatsuda, and K. Kosuge. Fall prevention control of passive intelligent walker based on human model. In *IEEE/RSJ International Conference on Intelligent Robots and Systems*, Nice, France, 2008. IROS.

[13] Y. Hirata, A. Muraki, and K. Kosuge. Motion control of intelligent walker based on renew of estimaton parameters fo user state. In *IEEE/RSJ International Conference on Intelligent Robots and Systems*, Beijing, China, 2006. IROS.

[14] Y. Hirata, A. Muraki, and K. Kosuge. Motion control of intelligent passive-type walker for fall-prevention function based on estimation of user state. In *IEEE International Conference on Robotics and Automation*, Orlando, USA, 2006. ICRA.

[15] Y. Hirata, A. Hara, and K. Kosuge. Motion control of passive-type walking support system based on environment information. In *IEEE International Conference on Robotics and Automation*, Barcelona, Spain, 2005. ICRA.

[16] Y. Hirata, A. Muraki, and K. Kosuge. Standing up and sitting down support using intelligent walker based on estimation of user states. In *IEEE International Conference on Mechatronics and Automation*, Luoyang, China, 2006.

[17] O. Chuy Jr., Y. Hirata, and K. Kosuge. Environment feedback for robotic walking support system control. In *IEEE International Conference on Robotics and Automation*, Rome, Italy, 2007. ICRA.

[18] J. Higuchi S. Taghvaei and K. Kosuge. Control of a passive walker using a depth sensor for user state estimation. In *2nd IEEE/RAS-EMBS International Conference on Robotics and Biomimetics*, Thailand, 2011. RoBio.

[19] O. Chuy Jr., Y. Hirata, Z. Wang, and K. Kosuge. A control approach based on passive behaviour to enhance user interaction. *IEEE Transaction on Robotics*, 23(5), Oct. 2007.

[20] Y. Hirata, O. Chuy Jr, A. Hara, and K. Kosuge. Human-adaptive motion control of active and passive type walking support system. In *IEEE Workshop on Advanced Robotics and its Social Impacts*, 2005.

[21] O. Chuy Jr., Y. Hirata, Z. Wang, and K. Kosuge. Approach in assisting a sit-to-stand movement using robotic walking support system. In *IEEE/RSJ International Conference on Intelligent Robots and Systems*, Beijing, China, 2006. IROS.

[22] O. Chuy Jr., Y. Hirata, Z. Wang, and K. Kosuge. A new control approach for a robotic walking support system in adapting user characteristics. *IEEE Transactions on Systems, Man, and Sybernetics part C: Applications and Reviews*, 36(6), Nov. 2006.

[23] G. Wasson, P. Sheth, M. Alwan, K. Granata, A. Ledoux, and C Huang. User intent in a shared control framework for pedestrian mobility aids. In *IEEE/RSJ International Conference on Intelligent Robots and Systems*, 2003.

[24] G. Wasson, J. Gunderson, S. Graves, and R. Felder. Effective shared contol in cooperative mobility aids. In *American Association for Artificial Intelligence*, 2000.

[25] G Wasson and J Gunderson. Variable autonomy in a shared control pedestrian mobility aid for the elderly. In *Proceedings of the IJCAI 01 Workshop on Autonomy, Delegaiton, and Control*, 2001.

[26] G. Wasson, J. Gunderson, S. Graves, and R. Felder. An assistive robotic agent for pedestrian mobility. In *International Conference on Autonomous Agents*, 2001.

[27] M. Alwan, P. J. Rajendran, A. Ledoux, C. Huang, G. Wasson, and P. Sheth. Stability margin monitoring in steering-controlled intelligent walkers for the elderly. In *AAAI Fall 2005 Symposium (EMBC)*, 2005.

[28] V. Kulyukin, A. Kutiyanawala, E. LoPresti, J. Matthews, and R. Simpson. iwalker: Toward a rollator-mounted wayfinding system for the elderly. In *International Conference on RFID*, 2008.

[29] Ulises Cortés, Antonio Martínez-Velasco, Cristian Barrué, Toni Benedico, Fabio Campana, Carlo Caltagirone, and Roberta Annicchiarico. A share-it service to elders mobility using the i-walker. volume 7, page 95, 2008.

[30] Takehito Kikuchi, Toshimasa Tanaka, Sosuke Tanida, Keigo Kobayashi, and Kazuhisa Mitobe. Basic study on gait rehabilitation system with intelligently controllable walker (i-walker). In *IEEE International Conference on Robotics and Biomimetics*, 2010.

[31] C. Huang, G. Wasson, M. Alwan, P. Sheth, and A. Ledoux. Shared navigational control and user intent detection in an intelleginet walker. In *AAAI Fall 2005 Symposium (EMBC)*, 2005.

[32] R. Schraft, C. Schaeffer, , and T. May. Care-o-bot: The concept of a system for assiting elderly or disabled persons in home environements. In *IECON: IEEE 24th Annual Conference*, 1998.

[33] B. Graf. Reactive navigation of an intelligent robotic walking aid. In *IEEE international Workshop on Robot and Human Interactive Communication*, 2001.

[34] J. Manuel, H. Wandosell, and B. Graf. Non-holonomic navigation system of a walking-aid robot. In *IEEE international Workshop on Robot and Human Interactive Communication*, Berlin, Germany, 2002.

[35] M. Hans and W Baum. Concept of a hybrid architecture for care-o-bot. In *ROMAN*, pages 407–411, 2001.

[36] B. Graf, A. Hans, J. Kubacki, and R.D. Schraft. Robotic home assistant care-o-bot ii. In *IEEE EMBS/BMES Conference*, TX, USA, 2002.

[37] S. MacNamara and G. Lacey. A smart walker for the frail visually impaired. In *IEEE International Conference on Robotics and Automation*, San Frandsco. CA, USA, 2000.

[38] G. Lacey and K. M. Dawson-Howe. The application of robotics to a mobility aid for the elderly blind. In *IEEE International Conference on Robotics and Automation*. ICRA, 1998.

[39] D. Rodriguez-Losada, F. Matia, A Jimenez, R. Galan, and G. Lacey. Implementing map based navigation in guido, the robotic smartwalker. In *IEEE International Conference on Robotics and Automation*, Barcelona, Spain, 2005.

[40] J. Glover, D. Holstius, M. Manojlovich, K. Montgomery, A. Powers, J. Wu, S. Kiesler, J. Matthews, and S. Thrun. A robotically-augmented walker for older adults. 2003.

[41] Aaron Morris. A robotic walker that provide guidance. In *IEEE International Conference on Robotics and Automation*, Taipei, Taiwan, 2003.

[42] N. Roy, G. Baltus, D. Fox, F. Gemperle, J. Goetz, T. Hirsch, D. Magaritis, M. Montemerlo, J. Pineau, N. Roy, J. Schulte, and S. Thrun. Towards personal service robots for the elderly. In *Workshop on Interactive Robots and Entertainment*, 2000.

[43] M. E. Pollack, S. Engberg, J. T. Matthews, S. Thrun, L. Brown, D. Colbry, C. Orosz, B. Peintner, S. Ramakrishnan, J. Dunbar-Jacob, C. McCarthy, M. Montemerlo, J. Pineau, and N. Roy. Pearl: A mobile robotic assistant for the elderly. In *AAAI Workshop on Automation as Eldercare*, Aug. 2002.

[44] Michael Montemerlo, Joelle Pineau, Nicholas Roy, Sebastian Thrun, and Vandi Verma. Experiences with a mobile robotic guide for the elderly. In *AAAI/IAAI*, pages 587–592, 2002.

[45] Haoyong Yu, Matthew Spenko, and Steven Dubowsky. An adaptive shared control system for an intelligent mobility aid for the elderly. *Autonomous Robots*, 15(1):53–66, 2003.

[46] S. Dubowsky, F. Genot, S.Godding, H. Kozono, A. Skwersky, H. Yu, and L. S. Yu. Pamm - a robotic aid to the elderly for mobility assistance and monitoring: A "helping-hand" for the elderly. In *IEEE International Conference on Robotics and Automation*, 2000.

[47] M. Spenko, H. Yu, and S. Dubowsky. Robotic personal aids for mobility and monitoring for the elderly. *IEEE Trans. on Neur. Syst. and Rehabil. Eng.*, 14(3):344–351, 2006.

[48] Yi-Che Huang, Hsiang-Ping Yang, Chun-Hsu Ko, and Kuu-Young Young. Human intention recognition for robot walking helper using anfis. In *8th Asian Control Conference*, Kaohsiung, Taiwan, 2011. ASCC.

[49] Chun-Hsu Ko and Sunil K. Agrawal. Walk-assist robot: A novel approach to gain selection of a braking controller using differential flatness. In *American Control Conference*, Baltimore, MD, USA, 2010. ACC.

[50] Wei-Hao Mou, Ming-Fang Chang, Chien-Ke Liao, Yuan-Han Hsu, Shih-Huan Tseng, and Li-Chen Fu. Context-aware assisted interactive robotic walker for parkinsons disease patients. In *IEEE/RSJ International Conference on Intelligent Robots and Systems*, Vilamoura, Algarve, Portugal, 2012. IROS.

[51] Kuan-Ting Yu, Chi-Pang Lam, Ming-Fang Chang, Wei-Hao Mou, Shi-Huan Tseng, and Li-Chen Fu. An interactive robotic walker for assisting elderly mobility in senior care unit. In *IEEE workshop on advanced robotics and its social impact*, 2010.

[52] Fei Shi, Qixin Cao, Chuntao Leng, and Hongbing Tan. Based on force sensing-controlled human-machine interaction system for walking assistant robot. In *8th World Congress on Intelligent Control and Automation*, Jinan, China, 2010.

[53] Kai-Tai Song and Chen-Yang Lin. A new compliant motion control design of a walking-help robot based on motor current and speed measurment. In *IEEE Int. Conf. on Intell. Robo. and Syst.*, 2009.

[54] Kai-Tai Song and Sin-Yi Jiang. Force-cooperative guidance design of an omni-directional walking assistive robot. In *IEEE Int. Conf. on Mechatr. and Autom.*, 2011.

[55] G. Lee, T. Ohnuma, and N. Y. Chong. Design and control of jaist active robotic walker. *Journal of Intelligent Service Robotics*, 3(3), 2010.

[56] Geunho Lee, Eui-Jung Jung, Takanori Ohnuma, Nak Young Chong, and Byung-Ju Yi. Jaist robotic walker control based on a two-layered kalman filter. In *IEEE International Conference on Robotics and Automation*, Shanghai, China, 2011.

[57] Takanori Ohnuma, Geunho Lee, , and Nak Young Chong. Particle filter based feedback control of jaist active robotic walker. In *20th IEEE International Symposium on Robot and Human Interactive Communication*, Atlanta, GA, USA, 2011.

[58] S. McLachlan, J. Arblaster, D.K. Liu, J Vallas Miro, and L. Chenoweth. A multi-stage shared control method for an intelligent mobility assistant. In *9th International Conference on Rehabilitation Robotics*, Chicago, IL, USA, 2005.

[59] Hideo Mori, Shinji Kotani, and Noriaki Kiyohiro. A robotic travel aid hitomi. In *Intelligent Robots and Systems' 94.'Advanced Robotic Systems and the Real World', IROS'94. Proceedings of the IEEE/RSJ/GI International Conference on*, volume 3, pages 1716–1723. IEEE, 1994.

[60] M. Martins, A. Frizera-Neto, E. Urendes, C. dos Santos, R. Ceres, and T. Bastos-Filho. A novel human-machine interface for guiding: The neoasas smart walker. In *Biosignals and Biorobotics Conference*, 2012.

[61] A. Frizera Neto, R. Ceres, E. Rocon, and JL Pons. Empowering and assisting natural human mobility: The simboisis walker. *INTECH: Int. J. Adv. Robotics, Special Issue Assistive Robotics*, pages 34 – 50, 2011.

[62] Anselmo Frizera Neto, Juan A Gallego, Eduardo Rocon, José L Pons, and Ramón Ceres. Extraction of users navigation commands from upper body force interaction in walker assisted gait. *Biomedical engineering online*, 9:37, 2010.

[63] P. Médéric, V. Pasqui, F. Plumet, and Ph. Bidaud. Design of a walking-aid and sit to stand transfer assisting device for elderly people. In *15th CISM-IFToMM Symposium on Robot Design, Dynamics and Control*, St Hubert, Canada, 2004.

[64] Mdŕic P., V. Pasqui, F. Plumet, and Ph. Bidaud. Sit to stand transfer assisting by an intelligent walking-aid. In *7th International Conference on Climbing and Walking Robots*, Madrid,Espagne, 2004.

[65] P. Médéric, V. Pasqui, F. Plumet, Ph. Bidaud, and J.C. Guinot. Elderly people sit to stand transfer experimental analysis. In *8th Int. Conf. on Climbing and Walking Robots (Clawar'05)*, pages 953–960, Londres,Royaume-Uni, 2005. Actes sur CD-RoM de Clawar'05 : 8th Int. Conf. on Climbing and Walking Robots.

[66] V. Pasqui, L. Saint-Bauzel, and O. Sigaud. Characterization of a least effort user-centered trajectory for sit-to-stand assistance user-centered trajectory for sit-to-stand assistance. In *Symposium on Dynamics modeling and interaction control in virtual and real environments*, pages 197–204. IUTAM, june 2010.

[67] V. Pasqui, L. Saint-Bauzel, and Ph. Bidaud. Postural stability control for robot-human cooperation for sit-to-stand assistance. In *10th International Conference on Climbing and Walking Robots and the Supporting Technologies for Mobile Machines*, pages 409–416, Singapore, 2007. CLAWAR'07.

[68] Viviane Pasqui, Didier Marin, Ludovic Saint-Bauzel, Pierre Rumeau, and Blandine Boudet. Description of robuwalker. Technical report, Institut des Systemes Intelligent et de Robotique(ISIR), 2013.

[69] D. Chugo, K. Kawabata, H. Okamoto, H. Kaetsu, H. Asama, N. Miyake, and K. Kosuge. Force assistance system for standing-up motion. *Industrial Robot: The International journal of industrial and service robotics*, 34(2):128–134, 2007.

[70] D. Chugo, W. Matsuoka, and K. Takase S. Jia. Rehabitation walker system for standing-up motion. In *IEEE/RSJ International Conference on Intelligent Robots and Systems*, San Diego, USA, 2007. IROS.

[71] D. Chugo, T. Asawa, T. Kitamura, S. Jia, and K. Takase. A rehabilitation walker with standing and walking assistance. In *IEEE/RSJ International Conference on Intelligent Robots and Systems*. IROS, 2008.

[72] D. Chugo, T. Asawa, T. Kitamura, J. Songmin, and K. Takase. A motion control of a robotic walker for continuous assistance during standing, walking and seating operation. In *IEEE/RSJ International Conference on Intelligent Robots and Systems*, St. Louis, USA, 2009. IROS.

[73] D. Chugo, Y. Sakaida, S Yokota, and K. Takase. Sitting motion assistance on a rehabitation robotics walker. In *IEEE Int. Conf. on Robotics and Biomimetics*, Phuket, Thailand, 2011.

[74] D. Chugo, Y. Morita, Y. Sakaida, S Yokota, and K. Takase. A robotic walker for standing assistance with realtime estimation of patients load. In *12Â ´th IEEE Int. W. on Advanced Motion Control*, Sarajevo, Bosnia and Herzegovina, 2012.

[75] Hyeon-Min Shim, Eung-Hyuk Lee, Jae-Hong Shim, Sang-Moo Lee, and Seung-Hong Hong. Implementation of an intelligent walking assistant robot for the elderly in outdoor environment. In *IEEE 9th International Conference on Rehabilitation Robotics*, Chicago, IL, USA, 2005.

[76] Hyeon-Min Shim, Chi Youn Chung, Eung-Hyuk Lee, Hong ki Min, and Hong Seung-Hong. Silbo: Development walking assistant robot for the elderly based on shared control strategy. *IJCSNS International Journal of Computer Science and Network Security*, 6(9A), 2006.

[77] H-G. Jun, Y-Y. Chang, B-J. Dan, H. Yang, W-K.Song, and J. Kin. Walking and sit-to-stand support system for elderly and disabled. In *IEEE Int. Conf. on Rehabilitation Robotics*, Zurich, Switzerland, 2011.

[78] I. Kim, W. Cho, G. Yuk, B-R. Jo, and B-H Min. Kinematic analysis of sit-to-stand assistive device for the elderly and disabled. In *IEEE International Conference on Rehabilitation Robotics*, ETH Zurich, Switzerland, 2011.

[79] Christian Buhler, Helmut Heck, Janus Nedza, and Rainer Wallbruch. Evaluation of the mobil walking and lifting aid. *Assistive Technology Added Value to the Quality of Life*, pages 210 – 215, 2001.

[80] Angelo M. Sabatini, Vincenzo Genovese, and Elena Pacchieotti. A mobility aid for the support to walking and object transportation of people with motor impairments. In *IEEE Conference on Intelligent Robots and Systems*, EPFL, LAusanne, Switzerland, 2002.

[81] Khai-Long Ho Hoang and Katja D Mombaur. Optimal design of a physical assistive device to support sit-to-stand motions. In *Robotics and Automation (ICRA), 2015 IEEE International Conference on*, pages 5891–5897. IEEE, 2015.

[82] Milad Geravand, Wolfgang Rampeltshammer, and Angelika Peer. Control of mobility assistive robot for human fall prevention. In *IEEE International Conference on Rehabilitation Robotics (ICORR),*, pages 882–887. IEEE, 2015.

[83] Milad Geravand, Peter zeno Korondi, Christian Werner, Klaus Hauer, and Angelika Peer. Human sit-to-stand transfer modeling towards intuitive and biologically-inspired robot assistance. 2016.

[84] Gerard Lacey and Diego Rodriguez-Losada. The evolution of guido. *IEEE Robotics and Automation Magazine*, 15:75–83, 2008.

[85] B. Graf, M. Hans, and D.S. Rolf. Care-o-bot ii- development of a next generation robotic home assistant. In *IEEE/RSJ International Conference on Intelligent Robots and Systems*, 2004.

[86] C-Y Lee, K-H Seo, C-H Kim, S-K Oh, and J-J Lee. A system for gait rehabitation: Mobile manipulator approach. In *IEEE International Conference on Robotics and Automation*, Washington, DC, May, 2002.

[87] Y. Hirata, A. Hara, and K. Kosuge. Passive-type intelligent walking support system rt walker. In *IEEE/RSJ International Conference on Intelligent Robots and Systems*, Nice, France, 2008. IROS.

[88] Ulrich Reiser, Theo Jacobs, Georg Arbeiter, Christopher Parlitz, and Kerstin Dautenhahn. Care-o-bot® 3–vision of a robot butler. In *Your virtual butler*, pages 97–116. Springer, 2013.

[89] Christopher Parlitz, Winfried Baum, Ulrich Reiser, and Martin Hägele. Intuitive human-machine-interaction and implementation on a household robot companion. In *Human Interface and the Management of Information. Methods, Techniques and Tools in Information Design*, pages 922–929. Springer, 2007.

[90] Joelle Pineau, Michael Montemerlo, Martta Pollak, Nicholas Roy, , and Sebastian Thrun. Towards robotic assistants in nursing homes : challenge and results. *Robotics and Autonomous Systems*, 2003.

[91] K. F. Lee. Automatic speech recognition: The development of the SPHINX system. *Kluwer Publishers*, 1989.

[92] N. Nejatbakhsh and K. Kosuge. A human adaptive pass tracking method for omnidirectional passive walking aid system. In *IEEE/RSJ International Conference on Intelligent Robots and Systems*, Alberta, Canada, 2005. IROS.

[93] B. Graf, M. Hans, and R.D Schraft. Mobile robot assistants - issues for dependable operation in direct cooperation with humans. *IEEE Robotics and Automation Magazine*, 11(2):67–77, 2004.

[94] Birgit Graf and Rolf D. Schraft. Behavior-based path modification for shared control of robotic walking aids. In *IEEE 10th International Conference on Rehabilitation Robotics*, Noordwijk, Netherlands, 2007.

[95] B. Graf. An adaptive guidance system for robotic walking aids. *Journal of Computing and Information Technology - CIT*, (1):109–120, 2009.

[96] Chun-Hsu Ko, Kuu-Young Young, Yi-Che Huang, and Sunil Kumar Agrawal. Active and passive control of walk-assist robot for outdoor guidance. *IEEE/ASME Transactions on Mechatronics*, 2012.

[97] Gerard Lacy and Shane MacNamara. Context-aware shared control of a robot mobility aid for the elderly blind. 19(11):1054 – 1065, 2000.

[98] L. Saint-Bauzel, V. Pasqui, and I. Monteil. A reactive robotized interface for lower limb rehabilitation: clinical results. *IEEE Transaction on Robotics*, 25(3):583–592, 2009.

[99] V. Pasqui and P. Bidaud. Natural trajectory generation for robot-human cooperation for sit-to-stand assistance. pages 246–251, Brussels, Belgium.

[100] Milad Geravand, Peter zeno Korondi, and Angelika Peer. Human sit-to-stand transfer modeling for optimal control of assistive robots. In *IEEE/RAS-EMBS International Conference on Biomedical Robotics and Biomechatronics*, Brazil, 2014.

[101] Milad Geravand and Angelika Peer. Safety constrained motion control of mobility assistive robots. In *IEEE/RAS-EMBS International Conference on Biomedical Robotics and Biomechatronics*, Brazil, 2014.

[102] Milad Geravand, Christian Werner, Klaus Hauer, and Angelika Peer. An integrated decision making approach for adaptive shared control of mobility assistive robots. *submitted to: International Journal of Social Robotics*, 2016.

[103] Miomir Vukobratović and Branislav Borovac. Zero-moment point thirty five years of its life. *International Journal of Humanoid Robotics*, 1(01):157–173, 2004.

[104] T. Flash and N. Hogan. The coordination of arm movements: an experimentally confirmed mathematical model. *The journal of Neuroscience*, 5(7):1688–1703, 1985.

[105] T. Nakamura and K. Kosuge. Model-based walking support system with wearable walking helper. In *12th Robot and Human Interactive Communication*. RO-MAN, 2003.

[106] V. M. Zatsiorsky. Kinetics of human motion. *Human Kinetics*, 2002.

[107] M. Schenkman, R. A. Berger, P. O. Riley, R. W. Mann, and W. A. Hodge. Whole-body movements during rising to standing from sitting. *Physical Therapy*, 70(10):638–648, 1990.

[108] D. Chugo, K. Kawabata, H. Kaetsu, N. Miyake, E. Okada, H. Asama, and K. Kosuge. Force assistance control for standing-up motion. In *IEEE International Conference on Robotics and Biomimetics*, 2006.

[109] J. Huang, P. Di, K. Wakita, T. Fukuda, and K. Sekiyama. Study of fall detection using intelligent cane based on sensor fusion. In *IEEE Int. Symp. Micronanomechatron. Human Sci*, 2008.

[110] Y. Hirata, A. Hara, and K. Kosuge. Motion control of passive intelligent walker using servo brakes. *IEEE Transaction on Robotics*, 23(5), Oct. 2007.

[111] P. Aigner and B. McCarragher. Contrasting potential fields and constraints in a shared control task. In *IEEE International Conference on Intelligent Robots and Systems*, pages 140–146, Sep. 1997.

[112] Sean Quinlan and Oussama Khatib. Elastics bands: Connecting path planning and control. *IEEE Transactions on Robotics and Automation*, 1993.

[113] U. Lindemann, H. Claus, M. Stuber, P. Augat, R. Muche, T. Nikolaus, and C. Becker. Measuring power during the sit-to-stand transfer. *European J. of Applied Physiology*, 89(5):466–470, 2003.

[114] A. Kralj, R. J. Jaeger, and M. Munih. Analysis of standing up and sitting down in humans - definitions and normative data presentation. *J. of Biomechanics*, 23(11):1123–1138, 1990.

[115] M. Schenkman, R. A. Berger, P. O. Riley, R. W. Mann, and W. A. Hodge. Whole-body movements during rising to standing from sitting. *Physical Therapy*, 70(10):638–648, 1990.

[116] M. Galli, V. Cimolin, M. Crivellini, and I. Campanini. Quantitative analysis of sit to stand movement: Experimental set-up definition and application to healthy and hemiplegic adults. *Gait and Posture*, 28(1):80–85, 2008.

[117] W. G. M. Janssen, H. B. J. Bussmann, and H. J. Stam. Determinants of the sit-to-stand movement: A review. *Physical Therapy*, 82(9):866–879, 2002.

[118] P. Millington, B. M. Myklebust, and G. M. Shambes. Biomechanical analysis of the sit-to-stand motion in elderly persons. *Arch Phys Med Rehabil.*, 73:09–17, 1992.

[119] T. Kotake, N. Dohi, T. Kajiwara, N. Sumi, Y. Koyama, and T. Miura. An analysis of sit-to-stand movements. *Arch Phys Med Rehabil*, 74:1095–1099, 1993.

[120] E. R. Ikeda, M. L. Schenkman, P. O. Relay, and A. H.Hodge. Influence of age in dynamics of raising from a chair. *Physical Therapy*, 71, 1991.

[121] H. Hirshfeld, M. Thorsteinsdottir, and E. Olsson. Coordinated ground forces exerted by buttocks and feet re adequately programmed for weight transfer during sit-to-stand. *J. of Neurophysiology*, 82:3021–3029, 1999.

[122] W. Mathiyakom, J.L. McNitt-Gray, P. Requejo, and K. Costa. Modifying center of mass trajectory during sit-to-stand tasks redistributes the mechanical demand across the lower extremity joints. *Clinical Biomechanics*, pages 105–111, 2005.

[123] M. W. Rodosky, T.P. Andriachhi, and G.B. Andersson. The influence of chair height on lower limb mechanism during rising. *J. of Orthopedic Research*, 7:66–71, 1989.

[124] S. Yoshioka, A. Nagano, R. Himeno, and S. Fukashiro1. Computation of the kinematics and the minimum peak joint moments of sit-to-stand movements. *BioMedical Engineering OnLine*, 6, 2007.

[125] S. Yoshioka, A. Nagano, D. C. Hay, and S. Fukashiro1. Biomechanical analysis of the relation between movement time and joint moment development during a sit-to-stand task. *BioMedical Engineering OnLine*, 8, 2009.

[126] K. M. Kerr, J. A. Whilte, RAB Mollan, and H. E. Baird. Rising from a chair: a review of the literature. *Physiotherapy*, pages 15–19, 1991.

[127] Asif M Mughal and Kamran Iqbal. A fuzzy biomechanical model for H_∞ suboptimal control of sit-to-stand movement. In *8th Int. IASTED Conf. on Intelligent Systems and Control*, pages 374–379, 2005.

[128] F. Bahrami, R. Riener, P. Jebedar-Maralani, and G. Schmidt. Biomechanical anaylsis of sit-to-stand transfer in healthy and paraplegic subjects. *Clinical Biomechanics*, 15:123–133, 2000.

[129] A. M. Mughal and K. Iqbal. A fuzzy biomechanical model with H_2 optimal control of sit to stand movement. In *American Control Conf.*, pages 3427–3432, 2006.

[130] A. M. Mughal and K. Iqbal. Bipedal modeling with decoupled optimal control design of biomechanical sit-to-stand transfer. In *Int. W. on Robotic and Sensors Environments*, Ottawa, ON, Canada, 2008.

[131] A. M. Mughal and K. Iqbal. Synthesis of angular profiles for bipedal sit-to-stand movement. In *40th Southeastern Symposium on System Theory*, pages 374–379, New Orleans, LA, USA, 2008.

[132] A. M. Mughal, S. Perviaz, and K. Iqbal. LMI based physiological cost optimization for biomechanical sts transfer. In *IEEE Int. Conf. on Systems, Man, and Cybernetics (SMC)*, pages 1508 – 1513, 2011.

[133] Katja Mombaur. Optimization of sit to stand motions of elderly people for the design and control of physical assistive devices. *PAMM*, 14(1):805–806, 2014.

[134] Khai-Long Ho Hoang and Katja D Mombaur. Optimal design of a physical assistive device to support sit-to-stand motions. In *IEEE International Conference on Robotics and Automation (ICRA)*, pages 5891–5897. IEEE, 2015.

[135] J. Kuzelicki, M. Zefran, H. Burger, and T.Bajd. Synthesis of standing-up trajectories using dynamic optimization. *Gait and Posture*, 21:1–11, 2005.

[136] E. Todorov and M. Jordan. Optimal feedback control as a theory of motor coordination. *Nature Neuroscience*, 5:1226–1235, 2002.

[137] David Mayne. A second-order gradiant method of optimizing non-linear discrete time systems. *Int J Control*, 3:85–95, 1966.

[138] Y. Tassa, T. Erez, and E. Todorov. Synthesis and stabilization of complex behaviors through online trajectory optimization. In *In IEEE/RSJ Int. Conf. on Intelligent Robots and Systems*, Vilamoura, Portugal, 2012.

[139] K. Iqbal and A. Roy. Stabilizing PID controllers for a single-link biomechanical model with position, velocity, and force feedback. *ASME Transactions on Biomechanical Engineering*, 126:838–843, 2004.

[140] M. Vukobratovic and B. Borovac. Zero-moment point – thirty five years of its life. *Int. J. of Humanoid Robotics*, 1(1):157–173, 2004.

[141] Yao Li, William S Levine, Yonghong Yang, and Chengqi He. A nonlinear optimal human postural regulator. In *American Control Conference (ACC)*, pages 5420–5425. IEEE, 2011.

[142] Li zhi Liao and Christine A. Shoemaker. Advantages of differential dynamic programming over newton's method for discrete-time optimal control problems. *Cornell University*, 1992.

[143] Katja Mombaur, Anh Truong, and Jean-Paul Laumond. From human to humanoid locomotion - an inverse optimal control approach. *Autonomous robots*, 28(3):369–383, 2010.

[144] O. Dreben. *Introduction to Physical Therapy for Physical Therapist Assistants*, chapter Patient positioning, body mechanics and transfer techniques, pages 217–234. Jones & Bartlett Pub, 2006.

[145] D. Roetenberg, H. Luinge, and P. Slycke. Xsens MVN: Full 6 DOF human motion tracking using miniature inertial sensors. *XSENS TECHNOLOGIES*, APRIL 3, 2013.

[146] Jack M Guralnik, Eleanor M Simonsick, Luigi Ferrucci, Robert J Glynn, Lisa F Berkman, Dan G Blazer, Paul A Scherr, and Robert B Wallace. A short physical performance battery assessing lower extremity function: association with self-reported disability and prediction of mortality and nursing home admission. *Journal of gerontology*, 49(2):M85–M94, 1994.

[147] Marshal F Folstein, Susan E Folstein, and Paul R McHugh. Mini-mental state: a practical method for grading the cognitive state of patients for the clinician. *Journal of psychiatric research*, 12(3):189–198, 1975.

[148] V. Zatsiorsky and V. Seluyanov. The mass and inertia characteristics of the main segments of the human body. *Biomechanics*, IIIB:1152–1159, 1983.

[149] L Schwickert, J Klenk, A Stähler, C Becker, and U Lindemann. Robotic-assisted rehabilitation of proximal humerus fractures in virtual environments. *Zeitschrift für Gerontologie und Geriatrie*, 44(6):387–392, 2011.

[150] Thomas B Sheridan. *Telerobotics, automation, and human supervisory control*. MIT press, 1992.

[151] J. Kofman, X. Wu, T. Luu, and S. Verma. Teleoperation of a robot manipulator using a vision-based human-robot interface. *IEEE Trans. Ind. Electron.*, 52(5):1206–1219, 2005.

[152] J. Borenstein and Y. Koren. Teleautonomous guidance for mobile robots. *IEEE Trans. Syst., Man Cybern.*, 20(6):1437–1443, 1990.

[153] G. Hirzinger, B. Brunner, J. Dietrich, and J. Heindl. Sensor-based space robotics rotex and its telerobotic features. *IEEE Trans. Robot. Autom.*, 9(5):649–661, 1993.

[154] D. J. Bruemmer, D. A. Few, R. L. Boring, J. L. Marble, M. C. Walton, and C. W. Nielsen. Shared understanding for collaborative control. *IEEE Trans. Syst., Man Cybern.*, 19(4), 2005.

[155] Behzad Khademian and Keyvan Hashtrudi-Zaad. Shared control architectures for haptic training: Performance and coupled stability analysis. *The International Journal of Robotics Research*, 2011.

[156] Behzad Khademian, Jacob Apkarian, and Keyvan Hashtrudi-Zaad. Assessment of environmental effects on collaborative haptic guidance. *Presence: Teleoperators and Virtual Environments*, 20(3):191–206, 2011.

[157] Behzad Khademian and Keyvan Hashtrudi-Zaad. Dual-user teleoperation systems: New multilateral shared control architecture and kinesthetic performance measures. *Mechatronics, IEEE/ASME Transactions on*, 17(5):895–906, 2012.

[158] Behzad Khademian and Keyvan Hashtrudi-Zaad. Performance issues in collaborative haptic training. In *Robo. and Auto., 2007 IEEE Int. Conf. on*, pages 3257–3262. IEEE, 2007.

[159] Rory A Cooper. Intelligent control of power wheelchairs. *Engineering in Medicine and Biology Magazine, IEEE*, 14(4):423–431, 1995.

[160] Richard C Simpson. Smart wheelchairs: A literature review. *Journal of rehabilitation research and development*, 42(4):423–436, 2004.

[161] David M Egelman, Christophe Person, and P Read Montague. A computational role for dopamine delivery in human decision-making. *J. of Cognitive Neuroscience*, 10(5):623–630, 1998.

[162] Kohei Wakita, Jian Huang, Pei Di, Kosuke Sekiyama, and Toshio Fukuda. Human-walking-intention-based motion control of an omnidirectional-type cane robot. *IEEE/ASME Trans. on Mechatro.*, 18(1), Feb. 2013.

[163] J. Huang, P. Di, T. Fukuda, and T. Matsuno. Motion control of omnidirectional-type cane robot based on human intention. In *IEEE/RSJ Int. Conf. Intell. Robots Syst*, Nice, France, 2008.

[164] Andrea Nedic, Damon Tomlin, Philip Holmes, Deborah A Prentice, and Jonathan D Cohen. A decision task in a social context: Human experiments, models, and analyses of behavioral data. *Proceedings of the IEEE*, 100(3):713–733, 2012.

[165] Richard J Herrnstein. Rational choice theory: Necessary but not sufficient. *American Psychologist*, 45(3):356, 1990.

[166] Richard J Herrnstein. Experiments on stable suboptimality in individual behavior. *American Economic Review*, pages 360–364, 1991.

[167] Andrew Stewart, Ming Cao, and Naomi Ehrich Leonard. Steady-state distributions for human decisions in two-alternative choice tasks. In *American Control Conference*, pages 2378–2383. IEEE, 2010.

[168] Ming Cao, Andrew Stewart, and Naomi Ehrich Leonard. Convergence in human decision-making dynamics. *Systems & Control Letters*, 59(2):87–97, 2010.

[169] Andrew Stewart, Ming Cao, Andrea Nedic, Damon Tomlin, and Naomi Ehrich Leonard. Towards human–robot teams: Model-based analysis of human decision making in two-alternative choice tasks with social feedback. *Proceedings of the IEEE*, 100(3):751–775, 2012.

[170] Caleb Woodruff, Linh Vu, Kristi A Morgansen, and Damon Tomlin. Deterministic modeling and evaluation of decision-making dynamics in sequential two-alternative forced choice tasks. *Proceedings of the IEEE*, 100(3):734–750, 2012.

[171] Meeko MK Oishi. Assessing information availability for user-interfaces of shared control systems under reference tracking. In *American Control Conference*, pages 3474–3481. IEEE, 2014.

[172] Javier Corredor, Jorge Sofrony, and Angelika Peer. Deciding on optimal assistance policies in haptic shared control tasks. In *IEEE Int. Conf. on Robo. and Autom.*, pages 2679–2684. IEEE, 2014.

[173] John F Schnelle, Maciej S Buchowski, Talat A Ikizler, Daniel W Durkin, Linda Beuscher, and Sandra F Simmons. Evaluation of two fatigability severity measures in elderly adults. *Journal of the American Geriatrics Society*, 60(8):1527–1533, 2012.

[174] Basil A Eldadah. Fatigue and fatigability in older adults. *PM&R*, 2(5):406–413, 2010.

[175] P Read Montague and Gregory S Berns. Neural economics and the biological substrates of valuation. *Neuron*, 36(2):265–284, 2002.

[176] P Read Montague, Peter Dayan, and Terrence J Sejnowski. A framework for mesencephalic dopamine systems based on predictive hebbian learning. *The Journal of neuroscience*, 16(5):1936–1947, 1996.

[177] Raphaela Groten, Daniela Feth, Harriet Goshy, Angelika Peer, David A Kenny, and Martin Buss. Experimental analysis of dominance in haptic collaboration. In *IEEE Int. Symp. on Robo. and Hum. Interac. Communic.*, pages 723–729. IEEE, 2009.

[178] Oussama Khatib. Real-time obstacle avoidance for manipulators and mobile robots. *The international journal of robotics research*, 5(1):90–98, 1986.

[179] Samuele M Marcora, Walter Staiano, and Victoria Manning. Mental fatigue impairs physical performance in humans. *Journal of Applied Physiology*, 106(3):857–864, 2009.

[180] Wallace O Fenn. The relation between the work performed and the energy liberated in muscular contraction. *The Journal of physiology*, 58(6):373–395, 1924.

[181] GA Cavagna and R Margaria. Mechanics of walking. *J Appl Physiol*, 21(1):271–8, 1966.

[182] M. E. Tinetti. Performance-oriented assessment of mobility problems in elderly patients. *J Am Geriatr Soc*, 34(2):119–126, 1986.

[183] JM Guralnik, EM Simonsick, L Ferrucci, RJ Glynn, LF Berkman, DG Blazer, PA Scherr, and RB Wallace. A short physical performance battery assessing lower extremity function: association with self-reported disability and prediction of mortality and nursing home admission. *J Gerontol*, 49(2):387–392, 1994.

[184] Y. Hirata, A. Hara, and K. Kosuge. Motion control of passive intelligent walker using servo brakes. *IEEE Transaction on Robotics*, 23(5), Oct. 2007.

[185] Mirja Hirvensalo, Taina Rantanen, and Eino Heikkinen. Mobility difficulties and physical activity as predictors of mortality and loss of independency in community living older population. *Journal of the American Geriatrics Society*, (48):493–498, 2000.

[186] Yasuhisa Hirata, Asami Muraki, and Kazuhiro Kosuge. Motion control of intelligent passive-type walker for fall-prevention function based on estimation of user state. In *Robotics and Automation, 2006. ICRA 2006. Proceedings 2006 IEEE International Conference on*, pages 3498–3503. IEEE, 2006.

[187] Yasuhisa Hirata, Shinji Komatsuda, and Kazuhiro Kosuge. Fall prevention control of passive intelligent walker based on human model. In *Intelligent Robots and Systems, 2008. IROS 2008. IEEE/RSJ International Conference on*, pages 1222–1228. IEEE, 2008.

[188] Milad Geravand and Angelika Peer. Safety constrained motion control of mobility assistive robots. In *5th IEEE RAS & EMBS International Conference on Biomedical Robotics and Biomechatronics*, pages 1073–1078. IEEE, 2014.

[189] Yi-Chung Pai and James Patton. Center of mass velocity-position predictions for balance control. *Journal of biomechanics*, 30(4):347–354, 1997.

[190] Marko B Popovic, Ambarish Goswami, and Hugh Herr. Ground reference points in legged locomotion: Definitions, biological trajectories and control implications. *The International Journal of Robotics Research*, 24(12):1013–1032, 2005.

[191] AL Hof, MGJ Gazendam, and WE Sinke. The condition for dynamic stability. *Journal of biomechanics*, 38(1):1–8, 2005.

[192] At L Hof, Renske M van Bockel, Tanneke Schoppen, and Klaas Postema. Control of lateral balance in walking: experimental findings in normal subjects and above-knee amputees. *Gait & posture*, 25(2):250–258, 2007.

[193] At L Hof. The equations of motion for a standing human reveal three mechanisms for balance. *Journal of biomechanics*, 40(2):451–457, 2007.

[194] At L Hof. The extrapolated center of mass concept suggests a simple control of balance in walking. *Human movement science*, 27(1):112–125, 2008.

[195] Johannes Englsberger, Christian Ott, Máximo A Roa, A Albu-Schaffer, and Gerhard Hirzinger. Bipedal walking control based on capture point dynamics. In *Intelligent Robots and Systems (IROS), 2011 IEEE/RSJ International Conference on*, pages 4420–4427. IEEE, 2011.

[196] Jerry Pratt, John Carff, Sergey Drakunov, and Ambarish Goswami. Capture point: A step toward humanoid push recovery. In *6th IEEE-RAS International Conference on Humanoid Robots*, pages 200–207. IEEE, 2006.

[197] Twan Koolen, Tomas De Boer, John Rebula, Ambarish Goswami, and Jerry Pratt. Capturability-based analysis and control of legged locomotion, part 1: Theory and application to three simple gait models. *The International Journal of Robotics Research*, 31(9):1094–1113, 2012.

[198] Shuuji Kajita, Fumio Kanehiroand Kenji Kaneko, Kazuhito Yokoi, and Hirohisa Hirukawa. The 3D linear inverted pendulum mode: A simple modeling for a biped walking pattern generation. In *5th IEEE/RSJ International Conference on Intelligent Robots and Systems*. IEEE, 2001.

[199] Stephen J Wright and Jorge Nocedal. *Numerical optimization*, volume 2. Springer New York, 1999.

[200] A. Albu-Schäffer, O. Eiberger, M. Grebenstein, S. Haddadin, Ch. Ott, T. Wimbock, S. Wolf, and G. Hirzinger. Soft robotics. *IEEE Robotics & Automation Mag.*, 15(3):20–30, 2008.

[201] A. Albu-Schäffer, S. Haddadin, Ch. Ott, A. Stemmer, T. Wimböck, and G. Hirzinger. The DLR lightweight robot: Design and control concepts for robots in human environments. *Industrial Robot*, 34(5):376–385, 2007.

[202] A. Bicchi and G. Tonietti. Fast and soft-arm tactics. *IEEE Robotics & Automation Mag.*, 11(2):22–33, 2004.

[203] Y. Yamada, Y. Hirasawa, S.Y. Huang, and Y. Umetani. Fail-safe human/robot contact in the safety space. In *Proc. 5th IEEE Int. Work. on Robot and Human Communication*, pages 59–64, 1996.

[204] S. Haddadin, A. Albu-Schäffer, A. De Luca, and G. Hirzinger. Collision detection and reaction: A contribution to safe physical human-robot interaction. In *Proc. IEEE/RSJ Int. Conf. on Intelligent Robots and Systems*, pages 3356–3363, 2008.

[205] A. De Luca and F. Flacco. Integrated control for pHRI: Collision avoidance, detection, reaction and collaboration. In *Proc. 4th IEEE Int. Conf. on Biomedical Robotics and Biomechatronics*, pages 288–295, 2012.

[206] M. Geravand, F. Flacco, and A. De Luca. Human-robot physical interaction and collaboration using an industrial robot with a closed control architecture. In *Proc. IEEE Int. Conf. on Robotics and Automation*, pages 4000–4007, 2013.

[207] S. Haddadin. *Towards Safe Robots: Approaching Asimov's 1st Law*. Springer, 2013.

[208] M. Geravand and A. Peer. Safety constrained motion control of mobility assistive robots. In *Proc. 5th IEEE Int. Conf. on Biomedical Robotics and Biomechatronics*, pages 1073–1078, 2014.

[209] T.S. Tadele, T.J.A. de Vries, and S. Stramigioli. Combining energy and power based safety metrics in controller design for domestic robots. In *Proc. IEEE Int. Conf. on Robotics and Automation*, 2014.

[210] M. Laffranchi, N.G. Tsagarakis, and D.G. Caldwell. Improving safety of human-robot interaction through energy regulation control and passive compliant design. In M. Inaki, editor, *Human Machine Interaction - Getting Closer*, chapter 8. InTech, 2012.

[211] B.M. Maschke, A.J. van der Schaft, and P.C. Breedveld. An intrinsic Hamiltonian formulation of the dynamics of LC-circuits. *IEEE Trans. on Circuits and Systems I: Fundamental Theory and Applications*, 42(2), 1995.

[212] D. Eberard, L. Lefevre, and B.M. Maschke. Multiscale coupling in heterogeneous diffusion processes: A port-based approach. In *Proc. Int. Conf. on Physics and Control*, pages 543–547, 2005.

[213] A. Macchelli, C. Melchiorri, and S. Stramigioli. Port-based modeling and simulation of mechanical systems with rigid and flexible links. *IEEE Trans. on Robotics*, 25(5):1016–1029, 2009.

[214] M. Ishikawa, A. Neki, J. Imura, and S. Hara. Energy preserving control of a hopping robot based on hybrid port-controlled Hamiltonian modeling. In *Proc. IEEE Conf. on Control Applications*, pages 1136–1141, 2003.

[215] A.Y. Mersha, R. Carloni, and S. Stramigioli. Port-based modeling and control of underactuated aerial vehicles. In *Proc. IEEE Int. Conf. on Robotics and Automation*, pages 14–19, 2011.

[216] F. Ficuciello, R. Carloni, L.C. Visser, and S. Stramigioli. Port-Hamiltonian modeling for soft-finger manipulation. In *Proc. IEEE/RSJ Int. Conf. on Intelligent Robots and Systems*, pages 4281–4286, 2010.

[217] V. Duindam and S. Stramigioli. *Modeling and control for efficient bipedal walking robots*. Springer, 2009.

[218] V. Duindam, A. Macchelli, S. Stramigioli, and H. Bruyninckx. *Modeling and control of complex physical systems*. Springer, 2009.

[219] A. Macchelli. *Port Hamiltonian systems. A unified approach for modeling and control finite and infinite dimensional physical systems.* PhD thesis, DEIS, University of Bologna, 2003.

[220] C. Secchi, S. Stramigioli, and C. Fantuzzi. *Control of interactive robotic interfaces: A Port-Hamiltonian approach*, volume 29 of *STAR*. Springer, 2007.

[221] N. Diolaiti, C. Melchiorri, and S. Stramigioli. Contact impedance estimation for robotic systems. *IEEE Trans. on Robotics*, 21(5):925–935, 2005.

[222] V. Duindam and S. Stramigioli. Modeling the kinematics and dynamics of compliant contact. In *Proc. IEEE Int. Conf. on Robotics and Automation*, volume 3, pages 4029–4034, 2003.

[223] R. Behrens and N. Elkmann. Study on meaningful and verified thresholds for minimizing the consequences of human-robot collisions. In *Proc. IEEE Int. Conf. on Robotics and Automation*, pages 3378–3383, 2014.

[224] J.L. Wood. Dynamic response of human cranial bone. *J. of Biomechanics*, 4(1):1–12, 1971.

[225] N. Yoganandan, F.A. Pintar, D.J. Maiman, J.F. Cusick, A. Sances Jr, and P.R. Walsh. Human head-neck biomechanics under axial tension. *Medical Engineering & Physics*, 18(4):289–294, 1996.

[226] BG/BGIA risk assessment recommendations according to machinery directive: Design of workplaces with collaborative robots. Technical Report U001/2009e, Deutsche Gesetzliche Unfallversicherung, 2011.

[227] S.A. Dugan and W.R. Frontera. Muscle fatigue and muscle injury. *Physical Medicine and Rehabilitation Clinics of North America*, 11(2):385–403, 2000.

[228] A.M. Genaidy et al. Biomechanical tolerance limits for manual lifting tasks: A tool to control back injuries. In *Proc. Int. Conf. of IEEE Engineering in Medicine and Biology Soc.*, pages 803–805, 1989.

[229] K.B. Veiersted, R.H. Westgaard, and P. Andersen. Pattern of muscle activity during stereotyped work and its relation to muscle pain. *International Arch. of Occupational and Environmental Health*, 1990.

[230] S.D. Mair, A.V. Seaber, R.R. Glisson, W.E. Garrett, et al. The role of fatigue in susceptibility to acute muscle strain injury. *American J. of Sports Medicine*, 24(2):137–143, 1996.

[231] M. Hagberg. Work load and fatigue in repetitive arm elevations. *Ergonomics*, 24(7):543–555, 1981.

[232] T. Moritani, A. Nagata, H.A. deVries, and M. Muro. Critical power as a measure of physical work capacity and anaerobic threshold. *Ergonomics*, 24(5):339–350, 1981.

[233] T. Sakurai, M. Toda, S. Sakurazawa, J. Akita, K. Kondo, and Y. Nakamura. Detection of muscle fatigue by the surface electromyogram and its application. In *9th IEEE/ACIS Int. Conf. on Computer and Information Science*, pages 43–47, 2010.

[234] Stefano Stramigioli, Robert Mahony, and Peter Corke. A novel approach to haptic tele-operation of aerial robot vehicles. In *IEEE International Conference on Robotics and Automation (ICRA)*, pages 5302–5308. IEEE, 2010.

[235] Cristian Secchi, Stefano Stramigioli, and Cesare Fantuzzi. Position drift compensation in port-hamiltonian based telemanipulation. In *IEEE/RSJ International Conference on Intelligent Robots and Systems*, pages 4211–4216. IEEE, 2006.

[236] J Wyatt, Leon Chua, Joel Gannett, I Goknar, and Douglas Green. Energy concepts in the state-space theory of nonlinear n-ports: Part i-passivity. *IEEE transactions on Circuits and Systems*, 28(1):48–61, 1981.

[237] Dongjun Lee and Ke Huang. Passive-set-position-modulation framework for interactive robotic systems. *IEEE Transactions on Robotics*, 26(2):354–369, 2010.

[238] W. Li and E. Todorov. Iterative linear quadratic regulator applied to nonlinear biological movement systems. In *1st Int. Conf. on Informatics in Control, Automation and Robotics*, pages 222–229, 2004.

Supervised Students' Theses

[239] Tobias Blume. *Human Sit-to-Stand Synthesis using a Pseudospectral Optimal Control Approach.* Master's thesis, TUM, May 2013.

[240] Li Chao. *Safe and Compliant Motion Control for Mobility Assistant Robots.* M.sc. course, advance project, TUM, 2013.

[241] Peter Zeno Korondi. *Modeling and control of the Human Sit-to-Stand Motion.* Bachelor's thesis, TUM, 2013.

[242] Erfan Shahriari. *Port-based Modeling of Human-Robot Cooperation.* Master's thesis, TUM, 2014.

[243] Navid Zeinali. *Adaptive Shared Control of Active Mobility Assistive Robots.* Bachelor's thesis, TUM, 2014.

[244] Wolfgang Rampeltshammeri. *Control of Mobility Assistive Robots for Human Fall Prevention.* Bachelor's thesis, TUM, 2014.

[245] Andreas Lederhuber. *Robust Invariance Control for Human Balance with Torque Limitation and External Support.* Bachelor's thesis, TUM, 2014.

[246] Peter Zeno Korondi. *Inverse Optimal Control for Modeling of Human's Sit-to-Stand Transfer.* M.sc. course, advance project, TUM, 2015.

[247] Wolfgang Rampeltshammeri. *Human Fatigue Detection by Evaluation of the Human Heart-Rate and Performed Work*. M.sc. course, advance project, TUM, 2015.

Author's Publications

[248] Christian Werner, Phoebe Ullrich, Milad Geravand, A Peer, and K Hauer. A systematic review of study results reported for the evaluation of robotic rollators from the perspective of users. *Disability and Rehabilitation: Assistive Technology*, 2017.

[249] Milad Geravand, Phoebe Koepp, Klaus Hauer, and Aangelika Peer. Mobility assistance robots: A survey. *Submitted to International Journal of Social Robotics*, 2017.

[250] Milad Geravand, Christian Werner, Klaus Hauer, and Angelika Peer. An integrated decision making approach for adaptive shared control of mobility assistance robots. *International Journal of Social Robotics*, pages 1–18, 2016.

[251] Milad Geravand, Erfan Shahriari, Alessandro De Luca, and Angelika Peer. Port-based modeling of human-robot collaboration towards safety-enhancing energy shaping control. In *IEEE International Conference on Robotics and Automation (ICRA)*. IEEE, 2016, Sweden.

[252] Milad Geravand, Peter Zeno Korondi, Christian Werner, Klaus Hauer, and Angelika Peer. Human sit-to-stand transfer modeling towards intuitive and biologically-inspired robot assistance. *Autonomous Robots*, pages 1–18, 2016.

[253] Christian Werner, Phoebe Ullrich, Milad Geravand, A Peer, and K Hauer. Evaluation studies of robotic rollators by the user perspective: A systematic review. *Gerontology*, 2016.

[254] George P. Moustris, Milad Geravand, Costas Tzafestas, and Angelika Peer. User-adaptive shared control in a mobility assistance robot based on human-centered intention reading and decision making scheme. In *IEEE International Conference on Robotics and Automation Workshop: Human-Robot Interfaces for Enhanced Physical Interactions*. Stockholm, Sweden, May 2016.

[255] Milad Geravand, Peter Zeno Korondi, and Angelika Peer. Control of Mobility Assistive Robots for Human Falls Prevention. In *5th IEEE RAS & EMBS International Conference on Rehabilitation Robotics*, Singapore, 2015.

[256] Milad Geravand, Peter Zeno Korondi, and Angelika Peer. Human sit-to-stand transfer modeling for optimal control of assistive robots. In *5th IEEE RAS & EMBS International Conference on Biomedical Robotics and Biomechatronics*, pages 670–676. IEEE, 2014.

[257] Milad Geravand and Angelika Peer. Safety constrained motion control of mobility assistive robots. In *5th IEEE RAS & EMBS International Conference on Biomedical Robotics and Biomechatronics*, pages 1073–1078. IEEE, 2014.

[258] Milad Geravand and Angelika Peer. Human sit-to-stand modelling using optimal feedback control. In *DGR-Tage (DGR-days)*, 2013, Munich, Germany.

[259] Phoebe Kopp, Milad Geravand, Angelika Peer, and Klaus Hauer. Evaluationsstudien zu robotergestützten rollatoren: Systematisches review. In *DGG, Deutsche Gesellschaft für Geriatrie*, September 2013, Germany.